BERICHTE
aus dem Fachbereich Geowissenschaften
der Universität Bremen

No. 248

Wien, K.

ELEMENT STRATIGRAPHY AND AGE MODELS FOR PELAGITES AND GRAVITY MASS FLOW DEPOSITS BASED ON SHIPBOARD XRF ANALYSIS

Berichte, Fachbereich Geowissenschaften, Universität Bremen, No. 248, 100 pages, Bremen 2006

ISSN 0931-0800

Die "Berichte aus dem Fachbereich Geowissenschaften" werden in unregelmäßigen Abständen vom Fachbereich 5, Universität Bremen, herausgegeben.

Sie dienen der Veröffentlichung von Forschungsarbeiten, Doktorarbeiten und wissenschaftlichen Beiträgen, die im Fachbereich angefertigt wurden.

Die Berichte können bei:

Frau Monika Bachur

Forschungszentrum Ozeanränder, RCOM

Universität Bremen

Postfach 330 440

D 28334 BREMEN

Telefon: (49) 421 218-65516

Fax: (49) 421 218-65515

e-mail: MBachur@uni-bremen.de

angefordert werden.

Diejenigen Titel, die nur online verfügbar sind, finden Sie unter:

http://elib3.suub.uni-bremen.de/publications/diss/html

Zitat:
Wien, K.
Element Stratigraphy and Age Models for Pelagites and Gravity Mass Flow Deposits based on Shipboard XRF Analysis.
Berichte, Fachbereich Geowissenschaften, Universität Bremen, No. 248, 100 pages, Bremen 2006.

ISSN 0931-0800

ELEMENT STRATIGRAPHY AND AGE MODELS FOR PELAGITES AND GRAVITY MASS FLOW DEPOSITS BASED ON SHIPBOARD XRF ANALYSIS

Dissertation zur Erlangung
des Doktorgrades in den Naturwissenschaften
im Fachbereich Geowissenschaften
der Universität Bremen

vorgelegt von
Katharina Wien
Bremen, Dezember 2005

Tag des Kolloquiums:

14.02.2006

Gutachter:

Prof. Dr. H.D. Schulz

PD Dr. S. Kasten

Prüfer:

Prof. Dr. G. Bohrmann

Dr. T.J.J. Hanebuth

VORWORT

Die vorliegende Arbeit entstand in dem seit Juli 2001 von der Deutschen Forschungsgemeinschaft der Universität Bremen bewilligten "Forschungszentrum Ozeanränder". Fragestellung und Untersuchungsprogramm waren im Rahmen des Teilprojektes C2 mit dem Titel "Physical transport in high-production systems: Characterisation, age-dating, and balancing" angesiedelt. Dieses Teilprojekt richtete sich auf die Sedimenttransportprozesse am Kontinentalhang vor NW-Afrika, die mit Hilfe von seismo-akustischen, sedimentologischen und geochemischen Methoden untersucht wurden. Die vorliegende Studie konzentriert sich auf den geochemischen Aspekt innerhalb des Teilprojektes und wurde von Professor Dr. Horst D. Schulz und Dr. Martin Kölling betreut.

Ein großer Teil der gewonnenen geochemischen Ergebnisse wurde in vier eigenständigen englischsprachigen Manuskripten für die Publikation in internationalen Fachzeitschriften vorbereitet. Diese Manuskripte wurden zusammen mit einem einleitenden und einem abschließenden Kapitel zu der hier vorliegenden kumulativen Arbeit zusammengefasst und diese im Fachbereich Geowissenschaften an der Universität Bremen als Dissertation eingereicht. Die einzelnen Manuskripte sind als separate Abschnitte mit unabhängiger Nummerierung der Abbildungen und Tabellen zu betrachten. Die verwendete Literatur ist am Ende der vorliegenden Dissertationsschrift in einer Gesamt-Literaturliste aufgeführt. Alle im Rahmen dieser Studie gewonnenen Daten können über die Pangaea-Datenbank abgerufen werden (http://www.wdc-mare.org/PangaVista).

DANKSAGUNG

Mein herzlicher und besonderer Dank gilt Professor Dr. Horst D. Schulz für die Vergabe und Betreuung der vorliegenden Arbeit. Die vielen richtungsweisenden Diskussionen sowie sein stetes Interesse am Fortgang der Arbeit waren mir eine große Hilfe und Unterstützung. Bedanken möchte ich mich ebenso bei Dr. Martin Kölling für die kritische Durchsicht der Manuskripte und die vielen konstruktiven Anregungen und Optimierungen, die ebenfalls einen großen Anteil zum Gelingen dieser Arbeit beitrugen.

PD Dr. Sabine Kasten danke ich für die Übernahme des Zweitgutachtens.

Herzlich bedanken möchte ich mich bei den Kolleginnen und Kollegen des Fachbereichs Geowissenschaften und besonders bei allen Mitgliedern der Arbeitsgruppe Geochemie und Hydrogeologie der Universität Bremen, die mir in diesen drei Jahren eine ausgezeichnete wissenschaftliche Arbeitsumgebung zur Verfügung stellten. Mein großer Dank gilt dabei zunächst Karsten Enneking für seine Unterstützung bei der Arbeit an der RFA, und ebenso Silvana Hessler und Susanne Siemer für ihre Hilfsbereitschaft und Unterstützung bei der Laborarbeit. Ein großes Dankeschön gilt auch den Auszubildenden Yvonne Habenicht und Johanna Littek, die mir im Labor hilfreich, zuverlässig und mit viel guter Laune zur Seite standen, ebenso Dr. Björn Panteleit für das ausgezeichnete Arbeitsklima im gemeinsamen Labor. Den Mitarbeitern der Firma Spectro verdanke ich viele wertvolle Hinweise bei der Einarbeitung in die Röntgenfluoreszenzanalytik und beim Schreiben der ersten Veröffentlichung.

Für die unermüdliche Hilfe bei der Laborarbeit auf FS Meteor, v.a. beim ungeliebten Mörsern der unzähligen und teilweise widerspenstigen Sedimentproben, sei v.a. Karsten Enneking, Silvana Hessler, Dr. Martin Kölling, Simone Pannike, Markus Schmidt, Luzie Schnieders, Professor Dr. Horst D. Schulz und Professor Dr. Rainer Zahn ganz herzlich gedankt, ebenso Andrea Gerriets, Dr. Sebastian Krastel und Dr. Lars Zühlsdorff für die Übernahme der nächtlichen Messungen. Ohne ihre großartige Unterstützung wäre eine Bearbeitung der mehreren tausend Proben nicht möglich gewesen, die die Grundlage für diese Arbeit bildeten.

Ausdrücklich gedankt sei meinen Kollegen Andrew A. Antobreh, Dr. Till J.J. Hanebuth, Dr. Christine Holz, Professor Dr. Katrin Huhn, Dr. Martin Kölling, Dr. Sebastian Krastel und Ingo Kock, denen ich viele wertvolle Anregungen und Hinweise verdanke. Besonders hervorgehoben sei dabei v.a. die hervorragende und freundschaftliche Zusammenarbeit mit Dr. Christine Holz, von deren zahllosen konstruktiven Hinweisen diese Arbeit sehr profitierte.

Meinen engsten Bremer Kollegen Kerstin Plewa und Michael Schweizer danke ich ganz herzlich für die angenehme und freundschaftliche Arbeitsatmosphäre im TAB. Beide waren immer meine

ersten Ansprechpartner bei vielen fachlichen und Rechnerproblemen, hatten aber auch stets ein offenes Ohr für alle Themen außerhalb der Wissenschaft.

Meiner gesamten Trainingsgruppe danke ich für die vielen schönen gemeinsamen und erlebnisreichen Stunden, nicht nur in der Turnhalle, die mir immer den nötigen Ausgleich und Abstand zur Arbeit sowie viel Abwechslung gebracht haben.

Von ganzem Herzen danke ich meinen Eltern, meinen drei Brüdern und Kader, die mich immer vielfältig unterstützt haben, und die mir besonders in diesem Jahr ein großer Rückhalt waren und mich wieder auf die Beine gebracht haben.

KURZFASSUNG

Kontinentalränder spielen eine große Rolle bei der Akkumulation von Sedimenten. Die normale Sedimentation in diesen Gebieten wird im wesentlichen durch das Wechselspiel von mariner Produktivität und terrigenem Eintrag bestimmt. Besonders die Schelfgebiete und die oberen Kontinentalhänge weisen hohe Sedimentationsraten auf, die zur Übersteilung der Hänge führen können. Ausgelöst durch einen Trigger-Mechanismus, z.B. ein Erdbeben, werden Teile der akkumulierten Sedimentmassen episodisch in die tieferen Bereiche der Ozeane umgelagert. Dabei sind vor allem drei verschiedene gravitative Transportprozesse von großer Bedeutung, das sind Rutschungen (engl. *slides*), Schuttströme (engl. *debris flows*) und Trübeströme (eng. *turbidity currents*).

Mit dem Ziel, das Auftreten verschiedener Transportereignisse in der quartären Vergangenheit zu datieren, sollte die Methode der Elementstratigraphie auf Sedimentabfolgen angewandt werden, in denen Ablagerungen solcher Ereignisse enthalten sind. Vor diesem Hintergrund lag ein Schwerpunkt der vorliegenden Arbeit auf der Entwicklung einer Methode, mit der Schwerelot-Sedimentkerne bereits an Bord des FS Meteor hochauflösend beprobt, diese Proben vorbereitet und mit der Röntgenfluoreszenzanalytik (RFA) auf ihre geochemische Zusammensetzung untersucht werden können. Dazu wurde zunächst die analytische Qualität des RFA-Gerätes Spectro Xepos unter stationären Bedingungen im Labor an der Universität Bremen durch Messungen von Standard-Referenzmaterial und einem bereits geochemisch untersuchten Schwerelotkerne bestimmt. Die Methode zur Beprobung und Analyse von Kernmaterial wurde anschließend an drei archivierten Schwerelotkerne entwickelt. Auf diese drei Sedimentkerne wurden Altersmodelle durch Korrelation mit datierten Referenzkernen übertragen, was eine zeitliche Einordnung der Sedimente und somit die Nutzung der geochemischen Daten für Elementstratigraphie ermöglichte.

Erstmals eingesetzt wurde die entwickelte RFA-Methode während der FS Meteor-Ausfahrt M 57-1 in den östlichen Südatlantik. Zunächst wurde die Qualität der Messungen unter den vor-Ort-Bedingungen an Bord im Vergleich zu den vorangegangenen Messungen unter ortsfesten Bedingungen an Land anhand von Standard-Referenzmaterial überprüft. Analysiert wurden weiterhin vier stratigraphisch ungestörte Schwerelotkerne aus dem südlichen Kapbecken sowie ein Schwerelotkern aus dem "Holocene Mudbelt" vor der Küste Südafrikas. Die geochemischen Daten erlaubten bereits während der Expedition die Alterseinstufung dieser Sedimentkerne durch Elementstratigraphie und damit Schlussfolgerungen bezüglich Änderungen des Klimas, der Umweltbedingungen und der Ozeanographie während der Glazial-/Interglazial-Wechsel des Quartärs.

Während der FS Meteor-Ausfahrt M 58-1 zum Kontinentalrand vor NW-Afrika erfolgte der Einsatz der RFA-Methode an Material aus Gebieten, die durch gravitative Sedimenttransportprozesse gekennzeichnet sind und in denen die stratigraphische Abfolge der Sedimente demzufolge gestört ist. Geochemisch untersucht wurden turbiditische Sedimentkerne aus dem während der Expedition entdeckten Cap Timiris Canyon sowie Sedimentkerne aus dem Cape Blanc Debris Flow und dem Mauritania Slide Complex. Altersmodelle wurden von datierten Referenzkernen durch Elementstratigraphie zunächst auf die pelagischen Abschnitte dieser Sedimentkerne übertragen und aus diesen Altersmodellen anschließend der Zeitpunkt der jeweiligen Transportereignisse (Trübeströme, Schuttstrom und Rutschung) abgelesen. Das Auftreten dieser Ereignisse steht in deutlichem Zusammenhang mit klimatisch bedingten Meeresspiegelschwankungen.

TABLE OF CONTENTS

1. GENERAL INTRODUCTION

Continental margins play an important role for the accumulation of sediments and their subsequent downslope transport and redistribution in the ocean basins. Normal sedimentation in these areas is basically controlled by an interplay of marine productivity and terrigenous input. Especially the upper continental slope and shelf regions are often characterised by high sedimentation rates as they result for instance from coastal upwelling and high eolian/fluvial input from the adjacent geological hinterland. As these high sedimentation rates continue the slope eventually oversteepens, and by some trigger such as an earthquake the accumulated sediments are subjected to gravity-driven downslope transport (Fig. 1). Various kinds of mass transport have been active during the Late Pleistocene and Holocene.

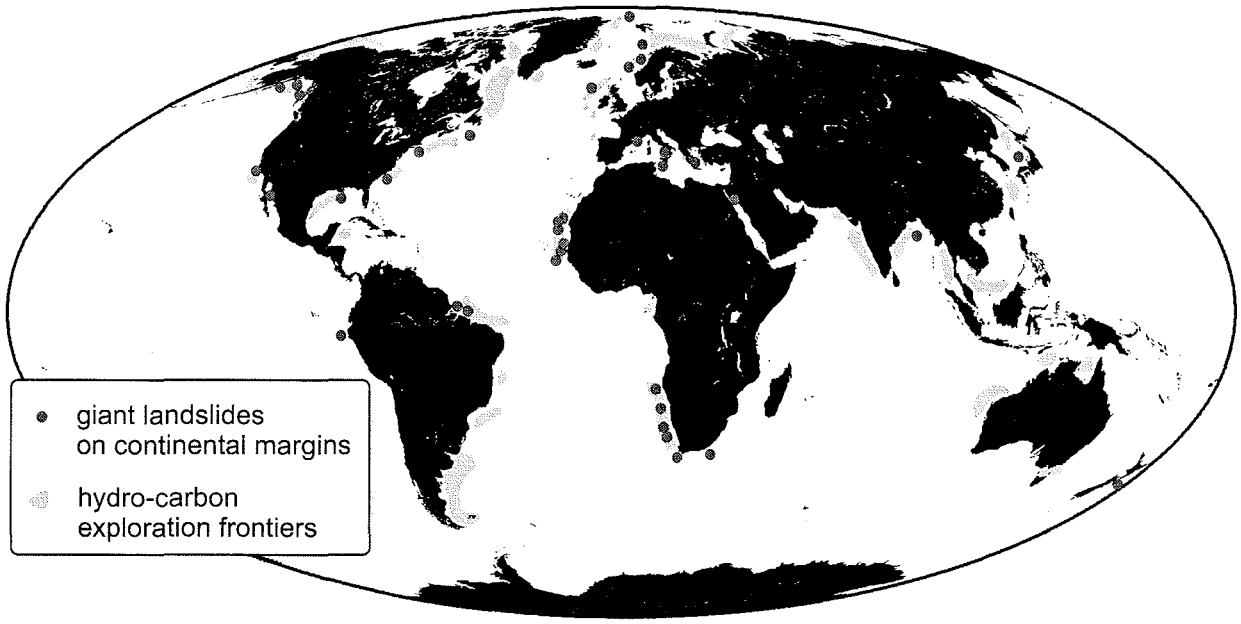

Fig. 1: Global distribution of major submarine gravity mass flow deposits on continental margins and location of hydrocarbon exploration areas. Note that these mass flow deposits coincide with today's exploration activity. From Mienert et al. (2003)

Gravity mass flows are first-order processes in redistributing large amounts of sediment from the shelf and upper continental slope onto the deep-sea abyssal plains. However, their inaccessible nature and rare occurrence when compared to a human life span complicate the observation and study of these processes in operation. There is only indirect evidence for their occurrence, for instance from the damage of submarine communication cables on continental slopes and at the foot of submarine canyons caused by large and fast-moving turbidity currents (e.g. Heezen and Ewing, 1955; Pickering et al., 1989; Nichols, 1999; Einsele, 2000; Khripounoff et al., 2003). By now, the best documented event is the so-called "1929 Grand Banks turbidity current" which was generated by an earthquake in the Laurentian Channel off the coast of Newfoundland on

18 November 1929 and which broke a succession of submarine telegraph cables en route (Heezen and Ewing, 1952; Heezen et al., 1954).

Although the factors controlling the stability of a slope are still not fully understood, it appears that rapid sedimentation, earthquake loading and gas hydrate dissociation are of major importance (e.g. Embley, 1982; Bugge et al., 1988; Einsele et al., 1996; Nichols, 1999; Imbo et al., 2003; Mienert et al., 2003). In order to better understand the possible trigger mechanisms of slope failures and the role of climate-related sea-level changes, it is necessary to reliably age-date their deposits which in marine environments are often well preserved and interbedded with pelagic sediments. However, the more traditional age dating of the over- and underlying pelagites, based for instance on radiocarbon (^{14}C) or oxygen isotope ($\delta^{18}O$) data, is rather time-consuming and the need for dating methods allowing quick and reliable age determination is obvious.

Within this context, the present study was primarily aimed at the assessment of the emplacement times of gravity mass flow deposits which are embedded in pelagic sequences. Age-dating was to be attempted indirectly by element stratigraphy based on a core-to-core correlation of geochemical data on the bracketing pelagites with adequate parameters (e.g. colour, carbonate, elemental data) of dated reference cores. Starting from this point, a XRF technique had to be developed which can be easily applied aboard a research vessel and enables reliable high resolution geochemical analyses of sediment cores, thus allowing for high temporal and high spatial resolution. This technique was initially to be tested on stratigraphically undisturbed pelagic sediment cores from the eastern South Atlantic to prove its general applicability, and then to be employed on continental margin sediments off NW Africa which are interrupted by a variety of redistributed sediments. Age estimates for the sediment transport processes bear valuable information regarding the instability of the NW African continental margin over the Quaternary glacial/interglacial cycles. Especially the studies on the gravity mass flow deposits were done in close cooperation with the seismics and sedimentology working groups at Bremen University.

1.1 Continental margin sediments and element stratigraphy

Sediments along the continental margins mainly consist of fine-grained terrigenous components and biogenic material from planktonic and benthonic organisms. Most abundant among the biogene producers is the calcareous plankton including coccolithophores, foraminifers and pteropods. Less abundant, yet also common in the oceans, are siliceous organisms such as radiolarians and diatoms. The geochemical composition of the terrigenous fraction is partly influenced by the mineralogy in the geological hinterland. Generally, with increasing water depth the marine component increases at the expense of the terrigenous component. The

contribution of terrigenous and biogenic material to the composition of the bulk sediment considerably varied in the geological past, depending especially on climate-related alternations of a system over glacial/interglacial cycles, for instance changes in wind intensity or water mass circulation.

Such changes in the fluvial/eolian input and marine productivity as well as dissolution processes in the water column and diagenetic processes leave their signature in the geochemical record of marine sediments. This element signature can be used to characterise sediment columns, correlate them over long distances and make stratigraphic inferences. This is termed element stratigraphy. Applying this method, the downcore elemental pattern of an age-dated reference core from one investigation area can be fitted to a variety of sediment cores from this area. Especially the contents of the major elements such as Ca, Si, Al, Fe and K are very useful for correlation purposes.

Generally, the various elements in marine sediments may be divided into three major groups; terrigenous, marine/bioactive and diagenetically influenced elements. This classification, of course, is a simplification as no element can solely be confined to one of these categories and elements may also be supplied by other regimes (e.g. volcanogen, hydrothermal, cosmogen). The following paragraphs give a brief overview on the origin of selected elements (cf. Table 1).

Terrigenous elements are for instance Si, Al, K, Fe, Ti, Mn and Rb. Major source are detrital particles derived from weathering of continental rocks which are transported into the ocean by rivers, wind and icebergs. Sand and silt fractions commonly consist of quartz and feldspars and thus, predominantly contribute Si, Al, K, Ca and Na. The clay fraction may comprise micas, kaolinite, illite, smectite and chlorite which, as they mainly derive from weathering of magmatic and metamorphic rocks, likewise contribute Si, Al, Mg, Ca, Na and K. Rb also is a component of the fine clay fraction, particularly illite. Fe is released from mafic silicates such as biotite, pyroxene, amphibole and olivine during weathering. To a minor degree it is incorporated into clay minerals (e.g. vermiculite), however, the major part forms iron oxides, especially goethite and hematite (e.g. Haese, 2000). Mafic silicates also contribute Mg, Ti, Mn and Ca. Less important, yet also significant in the elemental patterns of certain sediment columns and thus for element stratigraphy are volcanic layers such as siliceous ashes which often form distinct isochronous marker beds.

The bioactive elements Ca and Si derive from marine calcareous and siliceous organisms, respectively, which grow calcitic, aragonitic or opaline shells and skeletons. Diverse kinetic and biological factors control variable incorporation of minor amounts for instance of Sr, Mg and Ba by carbonate producers (e.g. Lea and Boyle, 1990; de Villiers, 1999; Stoll et al., 1999; Stoll and Schrag, 2000; Henderson, 2002). Especially Ca and Sr often reveal a strong coherency in continental margin sediments, showing a typical marine signal. By contrast, the marine Si signal

here is superposed by terrigenous input. Marine Si may dominate in areas where siliceous organisms are the main producers (e.g. antarctic circumpolar diatom belt) and in sediments below the calcite compensation depth (cf. Kennett, 1982). Further bioactive elements are P and S which, for example, act as metabolic regulatory in sulfur bacteria (e.g. Schulz and Schulz, 2005). Biogenic barite may be used as indicator for paleoproductivity (e.g. Berger et al., 1989; Elderfield, 1990).

Table 1: Possible sources of selected elements which occur in marine sediments (for references see main text)

Element	Element group	Possible sources
Ca	marine/bioactive	shells and skeletons of calcareous marine organims such as coccolithophores, foraminifers, pteropods; in shelf regions also shill-layers of bivalves
	terrigenous	less abundant; detrital particles from mafic silicates, feldspars, rarely clay minerals
Si	marine/bioactive	shells and skeletons of siliceous marine organism such as radiolarians, diatoms, dinoflagellates
	terrigenous	mainly detrital particles from quartz, feldspars, clay minerals
Sr	marine/bioactive	incorporation into calcareous shells and skeletons of marine organisms such as coccolithophores, foraminifers, corals
Mg	marine/bioactive	incorporation into calcareous shells and skeletons of marine organisms such as foraminifers, corals
	terrigenous	mainly from weathering of mafic silicates
Ba	marine/bioactive	incorporation into calcareous shells and skeletons of marine organisms such as foraminifers, corals
	diagenetically influenced	precipitation slightly above the sulfate/methane transition zone
	terrigenous	main contribution by rivers (particulate, dissolved, incorporated in / adsorbed to alumosilicates)
P	marine/bioactive	metabolic regulatory in sulfur bacteria
	diagenetically influenced	adsorption to Fe/Mn-minerals
S	marine/bioactive	in sulfur bacteria
	diagenetically influenced	fixed as $BaSO_4$ at/above the sulfate/methane transition zone
Al	terrigenous	mainly detrital particles from feldspars, clay minerals
K	terrigenous	mainly detrital particles from feldspars, clay minerals
Ti	terrigenous	mainly from weathering of mafic silicates
Rb	terrigenous	mainly in fine clay fraction, particularly illite
Fe	terrigenous	mainly oxides from weathering of mafic minerals; less abundant in clay minerals
	diagenetically influenced	oxydation fronts in redox-zones
Mn	terrigenous	mainly from weathering of mafic minerals
	diagenetically influenced	oxydation fronts in redox-zones

The distribution of calcareous biogenic sediments in the oceans is largely determined by the calcite compensation depth (CCD). It is the level in the water column where the rate of calcite supply equals the rate of calcite dissolution (both in the water column and in the topmost sediment layer) and below which calcite does not accumulate. Dissolution starts at the lysocline, generally located 500-1000 m above the CCD. The solubility of calcite is largely influenced by deep water currents and, moreover, is favoured by increasing hydrostatic pressure, decreasing temperature and increase of dissolved CO_2. Calcite dissolution recycles Ca as organisms precipitate more $CaCO_3$ than can be supported by terrigenous input of Ca into the oceans.

Approximately 70-80 % of the pelagic carbonate production are estimated to be dissolved in the deep ocean (e.g. Archer, 1996; Schneider et al., 2000).

Postdepositional diagenetic processes either release elements into pore water and sea water or fix them in certain horizons in the sediment column. Mobility and reactivity of Fe and Mn, for example, are strongly influenced by their specific redox-boundaries. Above the respective boundary both elements are present as oxidised species, whereas they occur in their reduced forms below. The boundary is characterised by high pore water concentrations of Fe and Mn unless they are fixed in the solid phase along this boundary by precipitation or adsorption (e.g. Haese, 2000). Selective adsorption/desorption and co-precipitation/release processes are of great relevance for the bounding of P and various trace metals (e.g. Cu, Zn, Pb, Mo, As) to Fe- and Mn-oxides/hydroxides, -sulfides (e.g. FeS) and other Fe-bearing minerals (e.g. Froehlich et al., 1982; Dietrich et al., 1992; Haese, 2000). Ba may diagenetically be fixed as barite ($BaSO_4$) slightly above the sulfate/methane transition zone owing to an upward migration of Ba^{2+} from sulfate-depleted to sulfate-rich pore water. Dissolution of barite occurs below this zone under conditions of sulfate reduction (e.g. von Breymann et al., 1992; McManus et al., 1994; 1998; Torres et al., 1996; Dickens, 2001).

Geochemical multi-element analysis and element stratigraphy have been frequently applied to stratigraphically undisturbed sediments and are highly important for instance in studies of palaeoclimate, palaeoenvironment and palaeoceanography (e.g. Kuhlmann et al., 2004). However, especially on continental margins the sediments are subjected to a variety of gravity-driven transport processes which redistribute thousands of km^3 of sediments. An originally intact stratigraphic column can thus be disturbed to various degrees either by addition or removal and by internal perturbance of the sediments, thus complicating element stratigraphy or making it even impossible.

1.2 Gravity-driven sediment transport processes on continental margins and oceanic islands

The numerous processes how sediments are transported downslope from source to sink can be classified into three principal groups (e.g. Mulder and Cochonat, 1996; Einsele, 2000; Figs. 2 and 3):

1) gravitational transport (e.g. *creeps*, *avalanches*, *slides*, *slumps*)
2) plastic flow (transport due to fluid but laminar motion; *debris flows*, *fluidized flows*, *liquefied flows*)
3) turbulent flow (*turbidity currents*).

They distinguish mainly by flow velocity, motion (laminar or turbulent), internal architecture and shape of the failure surface. Once initiated, the mode of mass movement is not invariable but

may transform continuously in shape and dynamics between triggering and final deposition. The degree of disaggregation of the transported material thereby increases with flow velocity.

The following text will focus only on slides, avalanches, debris flows and turbidity currents. Although flow velocities are as yet subject of speculation especially for slides and debris flows, they are agreed to be slowest ("creeping") for slides and increasing via debris flows and debris avalanches to turbidity currents (e.g. 10-15 m/s). The travel distance of the mass flows also varies significantly, being lowest (several tens of km) for debris avalanches and increasing via slides (tens to hundreds of km) and debris flows (several hundreds of km) to the long run-outs of turbidity currents (up to 1000 km) (Fig. 4; e.g. Mulder and Cochonat, 1996; Urgeles et al., 1997; Nichols, 1999; Einsele, 2000). Emplacement times of recent mass flows may be determined from non-steady-state conditions in pore-water profiles as was done for a slide from the outer Zaire deep-sea fan which was deposited about 300 yr ago (Zabel and Schulz, 2001) and for sedimentary events in the western Argentine Basin on timescales between years and thousands of years (Hensen et al., 2003). Some main characteristics of the above mentioned transport processes and the resulting sediment types are briefly outlined below.

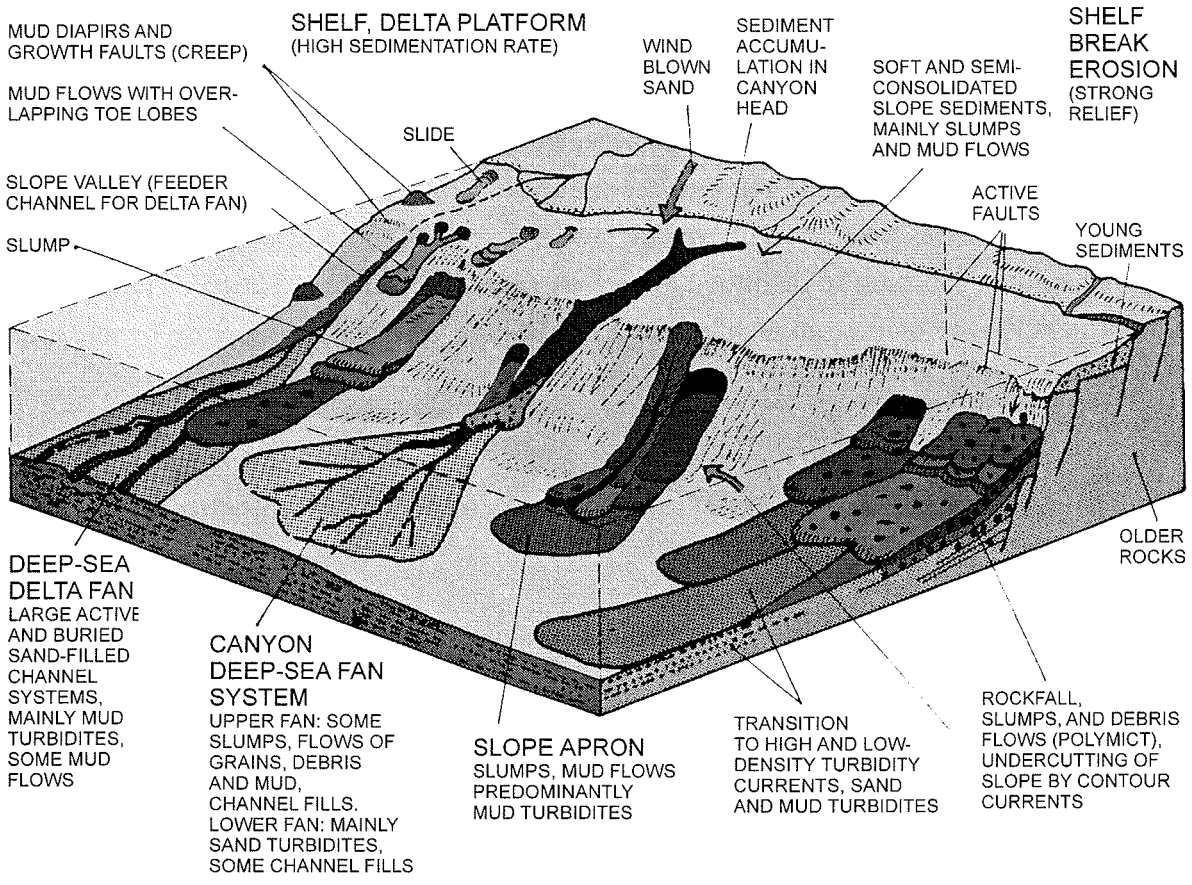

Fig. 2: Overview of gravity-driven depositional environments on a passive continental margin. From Einsele (2000), modified

1.2.1 Slides and their deposits

Slides are coherent masses of semi-consolidated sediment moving down a slope by gravity. They are bounded on all sides by failure planes which usually follow the stratification of the sediments. During transport the internal structure of the removed material remains largely undisturbed (cf. Fig. 3). Slides can be either simple or complex. In the first case, the main slide body does not generate other significant failures whereas in the second case, the motion of the main slide body causes instabilities in adjacent areas. Large-scale slides are for instance the Storegga Slide (Bugge et al., 1988; Evans et al, 1996; Haflidason et al., 2004) and Trænadjupet Slide offshore Norway (e.g. Laberg and Vorren, 2000; Laberg et al., 2002), the Gebra Slide in the Antarctic (e.g. Imbo et al., 2003) and slides on the Atlantic continental margin (e.g. Embley, 1982).

1.2.2 Debris avalanches and their deposits

A debris avalanche is a gravity-driven large-scale event generated by catastrophic failure when the flank of a volcano or mountain collapses. It leaves a well-defined escarpment or amphitheater at its head and is characterised by a hummocky topography in the lower parts. Debris avalanches often result from slope instabilities (cold avalanches) or from volcanic activity (e.g. volcanic earthquakes or injection of magma causing slope instability; hot avalanches). Debris avalanches may transform into debris flows (e.g. Voight et al., 1983; Siebert, 1984; Moore et al., 1989; Mulder and Cochonat, 1996; Urgeles et al., 1997; Hungr and Evans, 2004). Large-scale debris avalanches are known from Augustine Volcano (Alaska; e.g. Siebert et al., 1995), Bandai-san (Japan; e.g. Sekiya and Kikuchi, 1889; Brantley and Glicken, 1986), Mount St. Helens (Washington; e.g. Brantley and Glicken, 1986) and the Canary Islands (e.g. Masson, 1996; Urgeles et al., 1997, 1999; Gee et al., 2001; Krastel et al., 2001; Watts and Masson, 2001).

1.2.3 Debris flows and debrites

A debris flow is a dense, viscous mixture of sediment in water. It is characterised by partial disaggregation of the transported material which may comprise the whole spectrum from clay-sized particles up to large boulders of several meters in diameter (cf. Fig. 3). Only little or no dynamic sorting into different sizes occurs en route, effecting a very poor sorting and conglomeratic appearance of the deposit. Debris flows are plastic flows and usually result from the gravitational movement of underconsolidated masses of sediments down a slope. They are frequent on continental slopes and commonly leave scarps in their source area which influence the shape of the margin. Once a debris flow has started a slope angle of approximately 1° is sufficient to overcome friction. By contrast, when the internal friction exceeds a critical value the flow freezes and the transported material is deposited as debrite (e.g. Mulder and Cochonat, 1996; Urgeles et al., 1997; Nichols, 1999). Examples for large debris flows are the Saharan Debris Flow (e.g. Embley, 1976; Masson et al., 1993; Gee et al., 1999, 2001) and Canary Debris Flow off NW Africa (Simm and Kidd, 1983; Kidd et al., 1985; Masson, 1996;

Masson et al., 1997, 1998; Urgeles et al., 1997) and debris flows related to the 1929 "Grand Banks" earthquake (Piper et al., 1999).

1.2.4 Turbidity currents and turbidites

A turbidity current is the rapid influx of sediment-laden water into a larger water body down a slope (cf. Fig. 3). The suspended sediment effects a higher density of the turbidity current with respect to the surrounding clearer water into which it flows. Moving downslope, the turbidity current accelerates and forms a turbulent undercurrent transporting its load into deeper water. On arriving at the base of the continental slope and on the abyssal plain, the density contrast becomes insufficient to maintain momentum, causing the flow to decelerate. At lower velocities the capacity of the turbidity current to transport dense, coarse material decreases and the load is deposited as turbidite which can be preserved as Bouma sequence. The Bouma sequence results from different settling velocities of the transported particles and is characterised by graded bedding with coarse layers at the bottom gradually turning into finer laminae at the top. Turbidity currents commonly evolve from slope failures by an uptake of water and frequently occur on continental slopes of passive margins (e.g. Bouma, 1962, 2000; Bouma et al., 1985; Mulder and Cochonat, 1996; Nichols, 1999; Einsele, 2000). Large turbidite deposits are known for instance from the Madeira Abyssal Plain off NW Africa (e.g. Weaver and Kuijpers, 1983; Weaver and Rothwell, 1987; Rothwell et al., 1992; Weaver et al., 1992; Masson, 1994) and the Mediterranean Sea (e.g. Reeder et al., 2000; Rothwell et al., 1998, 2000).

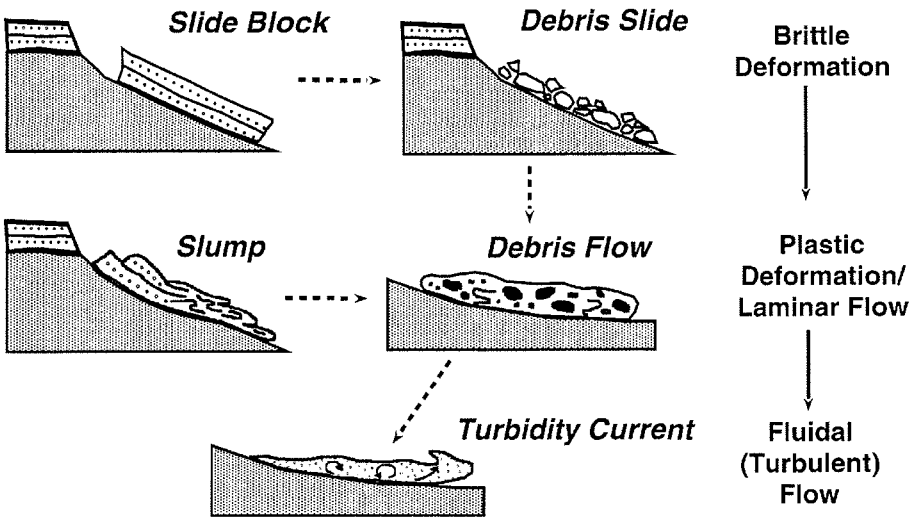

Fig. 3: Types of gravity-driven mass transport processes on continental margins. From McHugh et al. (2002)

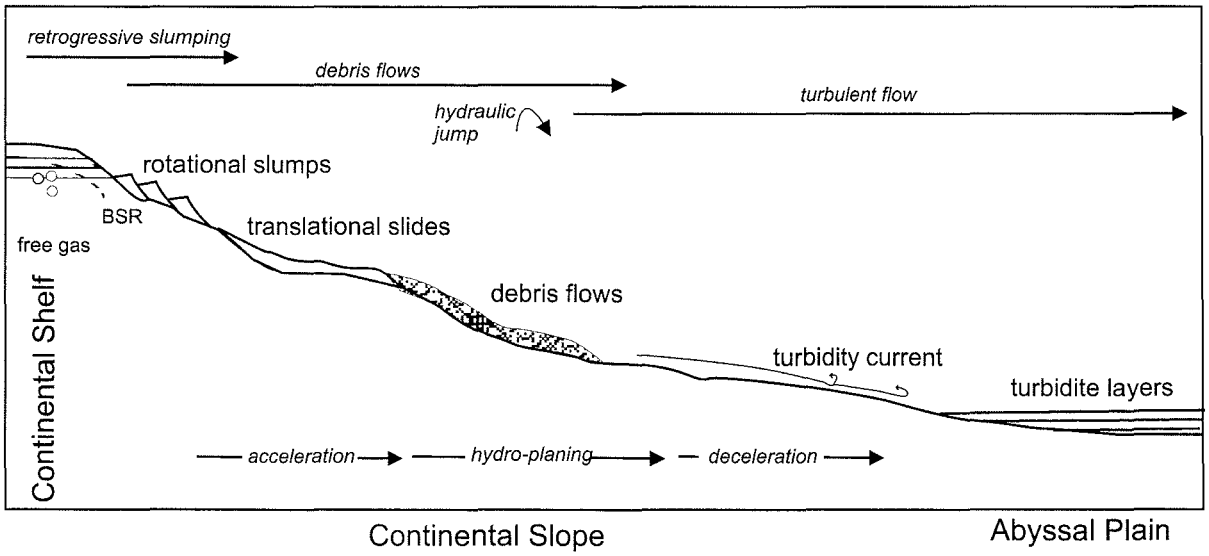

Fig. 4: Schematic illustration of gravity-driven mass transport processes on continental margins, also with regard to their travel distance. From Mienert et al. (2003)

All these gravity-driven transport processes occur widespread on the NW African continental margin (Fig. 5). Despite intensive research, however, the mechanisms of their initiation and the controls on the mode of failure are to date poorly understood. A variety of factors may generally contribute to the triggering of slope failures including sea-level change, oversteepening of the slope, underconsolidation of the sediment due to high accumulation rates, gas build-up or gas hydrate decomposition, external loading for instance by earthquakes, wave loading, bottom currents and occurrence of slope-parallel weak layers within bedded sequences (e.g. Mulder and Cochonat, 1996; Masson et al., 1998). Within this context, efforts to reliably age-date deposits of gravity-driven mass transport will therefore provide valuable information on the timing of slope instability in the geological past.

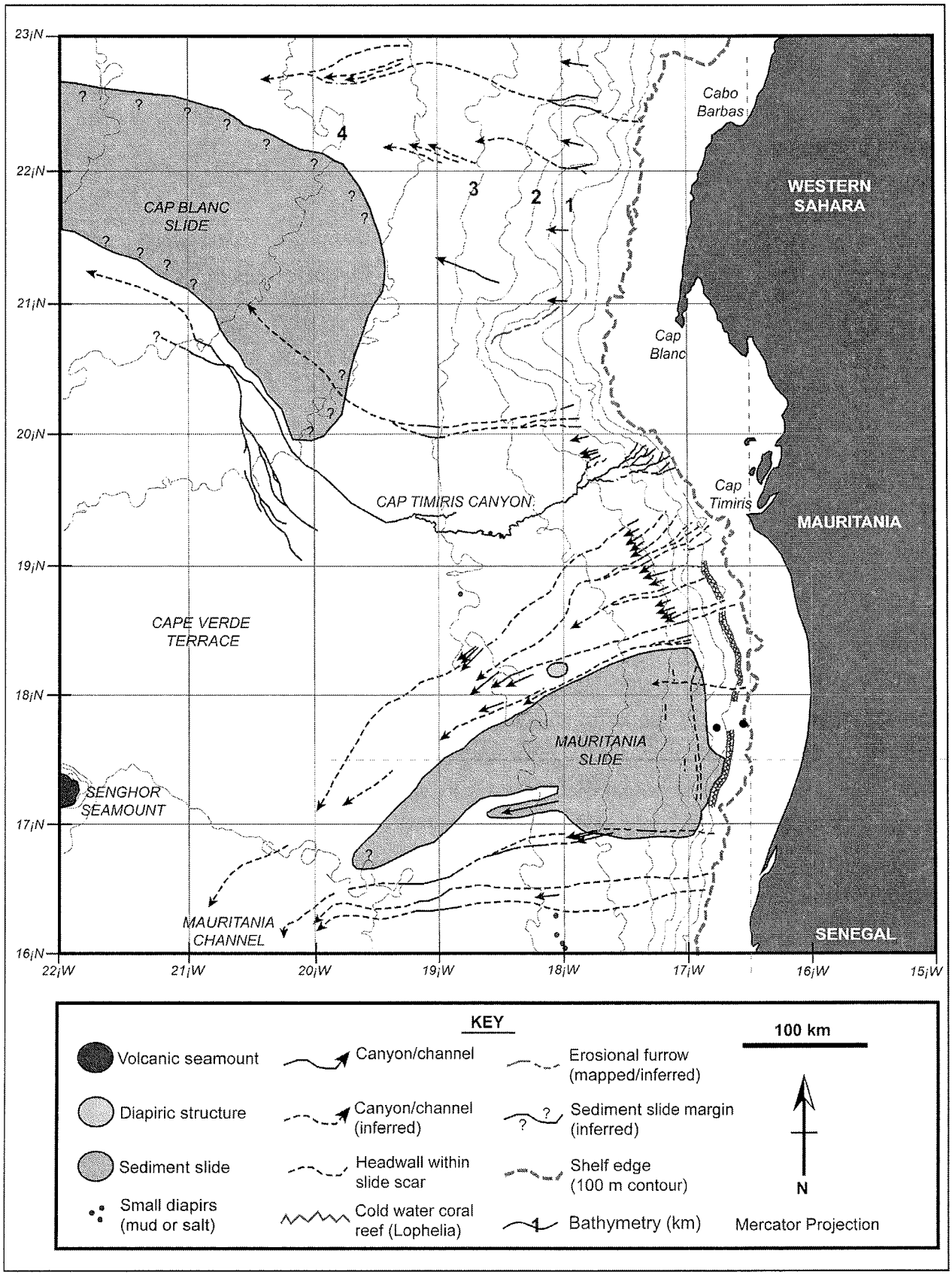

Fig. 5: Sedimentary processes and sedimentary features on the NW African continental margin. From Krastel et al. (subm.), modified

1.3 Outline of this thesis

A main part of the results gathered during the PhD work at Bremen University is presented in four chapters of this thesis which correspond to manuscripts published in (manuscripts 1 and 2), accepted for publication in (manuscript 3) and submitted to (manuscript 4) international journals. A brief outline of each manuscript is given below. They are all based on own investigations and were composed by myself as first author. In addition, the abstracts of two publications as co-author (Abstracts 1 and 2) are likewise listed.

Manuscript 1

Fast application of X-ray fluorescence spectrometry aboard ship: how good is the new portable Spectro Xepos analyser?
Katharina Wien, Dirk Wissmann, Martin Kölling and Horst D. Schulz

A XRF technique which allows fast high-resolution analysis of sediments from gravity cores already aboard a research vessel was developed and tested. The sample preparation technique is described in detail along with instrument parameters. The quality of measurements performed in the non-stationary laboratory aboard ship is evaluated, as well as the consistency with more conventional measurements under stationary conditions onland. It is shown that the geochemical data can successfully be used for element stratigraphy.

Manuscript 2

Close correlation between Sr/Ca ratios in bulk sediments from the southern Cape Basin and the SPECMAP record
Katharina Wien, Martin Kölling and Horst D. Schulz

Sr/Ca ratios as obtained from XRF analyses on sediments from five gravity cores from the southern Cape Basin, South Atlantic Ocean, reveal close correlation with the SPECMAP record. Based on literature data, possible causes for the observed variations in the Sr/Ca patterns are suggested. It is shown that the relationship between Sr/Ca ratios and the SPECMAP record allows an easy fit of age models to all studied cores.

Manuscript 3

Age models for pelagites and turbidites from the Cap Timiris Canyon off Mauritania
Katharina Wien, Christine Holz, Martin Kölling and Horst D. Schulz

Age models were fitted to turbiditc sediments from four gravity cores from the Cap Timiris Canyon offshore Mauritania by correlating downcore XRF data on the interbedded pelagic sequences to carbonate and elemental data on dated reference cores. The method for core-to-core correlation of stratigraphically disturbed sediment cores is introduced in detail. The age models allowed to determine the emplacement times of all turbidites in the study cores and allowed inferences regarding the relationship between turbidite activity in the canyon system and climate-related sea-level variations over the Quaternary glacial/interglacial cycles.

Manuscript 4

Age models for the Cape Blanc Debris Flow and the Mauritania Slide Complex in the Atlantic Ocean off NW Africa
Katharina Wien, Martin Kölling and Horst D. Schulz

High-resolution XRF analyses were performed on sediments from altogether five gravity cores from the Cape Blanc Debris Flow, the Mauritania Slide Complex and a levee of the Mauritania Canyon. Age models for the emplacement of all mass flow deposits were obtained by element stratigraphy and allow the assessment of slope instability on the NW African continental margin with respect to climate-related sea-level variations during the Quaternary. It is shown that downslope sediment transport is frequently coupled to periods of climatic changes at stage boundaries.

Abstract 1

Late Quaternary sedimentation within a submarine channel-levee system offshore Cap Timiris, Mauritania

Christine Holz, Katharina Wien and Rüdiger Henrich

This study combines three sediment records of Cap Timiris Canyon, a submarine meandering system at the western African continental margin offshore Mauritania. Investigated sediment cores have been recovered from the proximal and distal levee as well as from the canyon itself and indicate superior sedimentary processes being active for the canyon and levee deposition. Late Pleistocene to Holocene sedimentation history and the variability in sediment supply related to the climatic situation of presently arid Saharan Africa are discussed on the results of detailed grain-size analysis of the silt fraction and geochemistry data. Dominant transport processes for the terrigenous input to the Atlantic Ocean have been modelled by grain-size distributions of the carbonate-free silt fraction. During the late Pleistocene hemipelagic sedimentation has been consistent through time, while the impact of the African continent was decreasing from the proximal to the distal part of Cap Timiris Canyon. Predominantly coarse-grained particles, which are interpreted as windborne dust, and an enhanced aeolian dust export characterise glacial dry climate conditions with a low sea level and extended sand seas that reach onto the exposed continental shelf of Mauritania. Principal particle fining and the abrupt decrease in terrigenous supply is attributed to humid climate conditions and dune stabilisation on the adjacent African continent with the onset of the Holocene warm period.

Abstract 2

Cap Timiris Canyon: A Newly Discovered Channel System offshore of Mauritania

Sebastian Krastel, Till J.J. Hanebuth, Andrew A. Antobreh, Rüdiger Henrich, Christine Holz, Martin Kölling, Horst D. Schulz, Katharina Wien and Russell B. Wynn

Intensive research over the past decades has greatly improved our understanding of processes operating in the deep ocean. There has been a particular focus on continental margins, as sediments deposited in these areas can provide a high-resolution record of past climatic changes, as well as serve to host some of the world's major hydrocarbon reservoirs. However, the exploration and understanding of the deep ocean remains one of the great challenges of the 21st century [Stow and Mayall, 2000], and many fascinating features still wait to be found. The potential for new deep-water discoveries was recently highlighted during Meteor cruise M58/1 (depart Dakar, Senegal, 21 April 2003, return Las Palmas, Spain, 12 May 2003) of the Research Center Ocean Margins at the Universität Bremen in Germany. A spectacular 400-km-long submarine meandering channel system was discovered off Mauritania. In this article, the system is called the Cap Timiris Canyon (Figure 1). Although a series of incisional gullies at the shelf

break and uppermost slope have been described before [e.g., Rust and Wienecke, 1973], the enormous size and complex morphology of this submarine channel system were previously unknown.

This discovery appears to be the first channel system of this scale – several hundreds of kilometers long and ~ 300 m deep – to be described from offshore of a desert region. Commonly, large-scale submarine channels occur offshore of major river mouths and form large fan complexes (e.g., the Amazon, Mississippi, Zaire and Indus Fans),whereas the isolated Cap Timiris Canyon is located offshore of the Sahara Desert within an arid climatic zone. By studying how the morphology and sediment fill of Cap Timiris Canyon have evolved potentially in response to climatic variations, we may be able to better understand how the adjacent desert region has evolved through the past hundreds of thousands of years.

An additional incentive for this study is that flow processes operating in deep-water meandering channels are poorly understood. Most previous studies have assumed that turbidity currents are the dominant means of transporting sediment through these long-distance conduits [Peakall et al., 2000], although studies of distal sections of some meandering channels have revealed that debris flows may also be important [Schwab et al., 1996]. This article uses geophysical imagery of Cap Timiris Canyon, illustrating plan form morphology and vertical evolution, as well as sediment information, to provide insights into the flow processes responsible for generating and maintaining the channel system.

2 RESULTS

2.1 Fast application of X-ray fluorescence spectrometry aboard ship: how good is the new portable Spectro Xepos analyser?

KATHARINA WIEN, [a] DIRK WISSMANN, [b] MARTIN KÖLLING [a] AND HORST D. SCHULZ [a]

[a] *Department of Earth Sciences (FB 5), University of Bremen, P.O. Box 330440, 28359 Bremen, Germany*

[b] *Spectro Analytical Instruments, Boschstrasse 10, 47533 Kleve, Germany*

Abstract

A technique for onsite application of X-ray fluorescence (XRF) spectrometry to samples from sediment cores aboard a research vessel was developed and tested. The method is sufficiently simple, precise, and fast to be used routinely for high-resolution analyses of depth profiles as well as surface samples. Analyses were performed with the compact high-performance energy-dispersive polarisation X-ray fluorescence (EDPXRF) analyser Spectro Xepos. Contents of the elements Si, Ti, Al, Fe, Mn, Mg, Ca, K, Sr, Ba, Rb, Cu, Ni, Zn, P, S, Cl and Br were simultaneously determined on 200 to 225 samples of each core within 24 h of recovery.

This study presents a description of the employed shipboard preparation and analysis technique, along with some example data. We show land-based datasets that support our decisions to use powder samples and to reduce the original measuring time for onboard analyses. We demonstrate how well the results from shipboard measurements for the various elements compare with the land-based findings. The onboard geochemical data enabled us to establish an element stratigraphy already during the cruise. Correlation of iron, calcium and silicon enrichment trends with an older reference core provided an age model for the newly retrieved cores.

The Spectro Xepos instrument performed without any analytical and technical difficulties which could have been caused by rougher weather conditions or continuous movement and vibration of the research vessel. By now, this XRF technique has been applied during three RV Meteor cruises to approximately 5000 Late Quaternary sediment samples from altogether 23 gravity cores, 25 multicorer cores and two box cores from the eastern South Atlantic off South Africa / Namibia and the eastern Atlantic off NW Africa.

Introduction

X-ray fluorescence (XRF) spectrometry is a common tool for highly accurate and reproducible non-destructive element analyses. In land-based analytical laboratories, it is used routinely for investigation of a wide variety of materials such as minerals, rocks, slags, ceramics, metals, alloys, food, pharmaceuticals and fuels. Advantages include easy sample preparation and instrument operation, which make the technique also convenient for application onboard a research vessel. Thus, XRF analyses of marine sediment cores can provide data on the elemental composition of sediments which complement downcore colour scans or logs of sediment physico-chemical properties.

Previous studies have already described shipboard application of XRF for various purposes on different research vessels, using different instruments. However, analyses were mostly limited to a few samples only. Onboard research vessels, XRF has been applied for assessment of metal contamination in marine sediments. For example, measurements were performed on RV Ecos on 30 wet bulk samples from San Diego Bay using a Spectrace 9000 portable XRF spectrometer. These shipboard analyses allow quick onsite decisions for mapping strategies and detailed

assessments of contaminated areas (Stallard et al. 1995). However, the use of wet sediment samples has the disadvantage that enhanced matrix and particle size effects can reduce the quality of the analyses.

XRF analyses for bulk composition of sediments and rocks have also been carried out for several years on the RV Joides Resolution using a fully automated ARL 8420 wavelength-dispersive spectrograph (Kastens et al. 1987; Detrick et al. 1988). Major and trace element contents were routinely determined on fused disks and pressed pellets respectively (e.g. Kastens et al. 1987; Detrick et al. 1988; Pettigrew et al. 1999; Barker et al. 1999; Dick et al. 1999; Coffin et al. 2000; Christie et al. 2001). For example, Barker et al. (1999) analysed trace elements (Nb, Zr, Y, Sr, Rb, Zn, Cu, Ni, Cr, V and Ba) on pressed pellets of 54 sediment samples during ODP (Ocean Drilling Program) Leg 178. The actual measurements were performed aboard ship. During ODP Leg 183, by contrast, Coffin et al. (2000) analysed 91 rock samples and, during ODP Leg 187, Christie et al. (2001) analysed 44 representative samples of major lithologic units. In both cases, major elements were determined from fused glass disks, trace elements from pressed powder pellets. On RV Sonne, sediment samples have been routinely analysed with the wavelength-dispersive XRF spectrometer Philips PW 1410 (Herzig and Plüger 1988; Plüger et al. 1988). This instrument is permanently installed on board.

Two major problems arise from the preparation of pressed pellets. Sample preparation as such is rather time-consuming, needing roughly 5-10 min for a single sample. In addition, onboard the ship it is difficult to accurately correct sample weight for the effect of analytical additives such as wax. Even more complicated and time-consuming is the shipboard preparation of fused disks.

In view of these limitations, the XRF scanner Cortex (Corescanner Texel) was developed for non-destructive analysis on wet split-core sections. Like other logging facilities, it can be used directly onboard the ship in its own container. Indeed, to date the Cortex is the only core scanner to have been applied onboard the ship. The instrument performs measurements of high resolution (maximum 1 mm), and produces reliable counts for K to Sr (Jansen et al. 1998). Together with other core scanners and, for that matter, other scanning tools such as colour spectrophotometry, however, the Cortex shares the disadvantage of assessing elemental levels only in relative (counts per second) rather than absolute terms.

At the Geosciences Department of Bremen University there are two XRF core scanners, one similar to the Cortex in that it provides element intensities from K through Sr (Röhl and Abrams 2000). The other is a more sophisticated core scanner which measures from Al to Ba (http://www.avaatech.com/index.htm). The two XRF core scanners at Bremen University have been used solely under stationary conditions onland.

An expedition with RV Meteor to the eastern South Atlantic was carried out during January/February 2003, focused on the reconstruction of the Late Quaternary climate history of the southern Benguela system, and the influence of the Agulhas warm water entrainment into the South Atlantic (Schneider and Cruise participants 2003). During cruise M 57-1, investigations of sediment cores from the shelf and continental slope off South Africa were performed with the portable energy-dispersive polarisation X-ray fluorescence (EDPXRF) analyser Spectro Xepos (Spectro Analytical Instruments, Kleve, Germany) for the first time on a large scale. One advantage of this system is that it produces absolute measures of elemental levels.

Most XRF data presented in this study form a key component of a much larger dataset gathered during RV Meteor cruise M 57-1, one aim being to test and improve the new Spectro Xepos shipboard technique, the ultimate goal being to establish palaeoclimate links in the southern Benguela system. Thus, in order for the elemental information to be meaningfully interpreted, it is necessary to evaluate the quality of these measurements performed in a non-stationary laboratory, as well as their consistency with more conventional measurements under stationary conditions onland. Within this context, the aims of the present study are:

1) To present a detailed description of sample preparation and XRF analysis technique for the EDPXRF Spectro Xepos instrument,
2) To determine and compare the accuracy and reproducibility of shipboard and land-based measurements,
3) To compare XRF analyses carried out onland with corresponding inductively coupled plasma atomic emission spectrometry (ICP-AES) measurements on the same material, and
4) To compare shipboard with land-based measurements of absolute levels for some elements.

In addition, we assessed the suitability of the shipboard core data for integration in an age model from a reference core.

Study site

During RV Meteor cruise M 57-1 from Cape Town to Walvis Bay in January/February 2003, five gravity cores were recovered from the eastern South Atlantic off South Africa for onboard XRF geochemical analyses (Table 1; Fig. 1). Four of these coring sites (GeoB 8301, GeoB 8307, GeoB 8310, GeoB 8315) are located in the southern Cape Basin, one (GeoB 8331) further to the north in the Holocene mud belt (Schneider and Cruise participants 2003). Also presented in this study are XRF analyses of three multicorer cores (MUCs) taken during RV Meteor cruises M 57-1 (sites GeoB 8301 and GeoB 8303; Schneider and Cruise participants 2003) and M 58-1 (site GeoB 8501; Schulz and Cruise participants 2003). MUC GeoB 8303 is located in the southern Cape Basin, MUC GeoB 8501-1 in the eastern Atlantic off Mauritania (location not shown in Fig. 1).

Table 1: Cruise and core number, geographic position, water depth, gear type and recovery of all cores referred to in this study, along with available data. *MUC* multicorer, *GC* gravity corer, *GPC* giant piston corer

Cruise	Core no.	Latitude	Longitude	Water depth (m)	Gear type	Recovery (cm)	Available data
M 57-1	GeoB 8301-5	34°46.48′ S	17°41.92′ E	1941	MUC	22	XRF; shipboard
M 57-1	GeoB 8301-6	34°46.00′ S	17°41.54′ E	1952	GC	879	XRF; shipboard
M 57-1	GeoB 8303-5	34°15.67′ S	16°47.09′ E	3447	MUC	21	XRF; shipboard
M 57-1	GeoB 8307-6	33°50.43′ S	16°31.99′ E	2667	GC	843	XRF; shipboard
M 57-1	GeoB 8310-2	32°54.57′ S	16°22.92′ E	1993	GC	833	XRF; shipboard
M 57-1	GeoB 8315-6	32°53.30′ S	15°41.70′ E	2995	GC	851	XRF; shipboard
M 57-1	GeoB 8331-4	29°08.12′ S	16°42.99′ E	97	GC	887	XRF; shipboard
M 58-1	GeoB 8501-1	18°30.26′ N	18°45.51′ W	2995	MUC	32	XRF; shipboard
M 34-2	GeoB 3718-9	24°53.60′ S	13°09.80′ E	1312	GC	1371	ICP-AES [a]
							XRF; land-based
M 23-1	GeoB 2004-3	30°52.10′ S	14°20.50′ E	2572	GC	966	XRF; land-based
NAUSICAA -IMAGES II	MD 962085	29°42′ S	12°56′ E	3001	GPC	3540	colour reflectance [b]
							$\delta^{18}O$ age (planktonic) [c]

[a] Extracted from Heuer (2003)

[b] Extracted from Bertrand and Cruise participants (1997)

[c] Extracted from Chen et al. (2002)

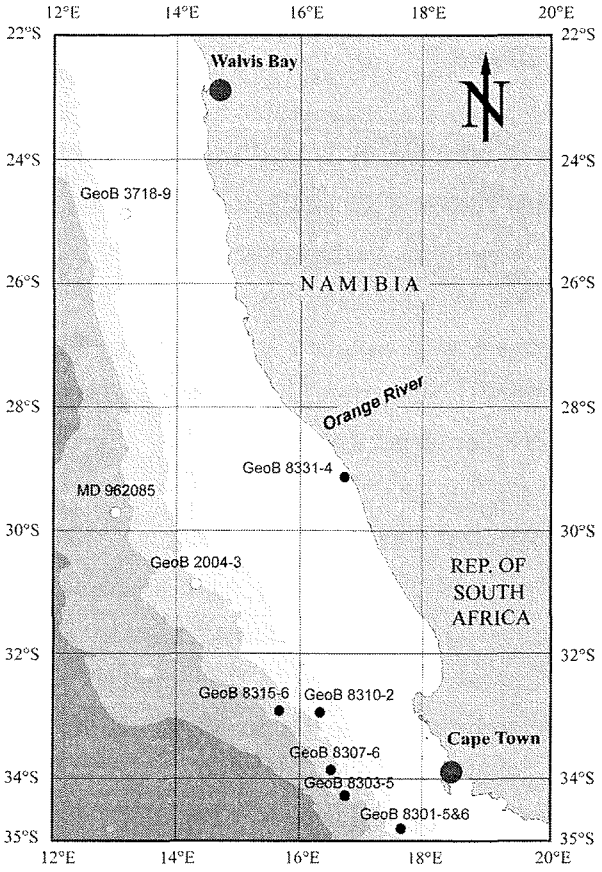

Fig. 1: Bathymetric map of the eastern South Atlantic showing locations of all cores referred to in this study. *Closed circles* indicate selected core positions during RV Meteor cruise M 57-1 (present study); the *open circles* indicate the positions of reference cores GeoB 3718-9 (RV Meteor cruise M 34-2), MD 962085 (RV Marion Dufresne cruise NAUSICAA-IMAGES II) and GeoB 2004-3 (RV Meteor cruise M 23-1). Source: GEBCO

Prior to cruise M 57-1, two archived gravity cores were analysed by means of the Spectro Xepos, these serving as reference cores. Gravity core GeoB 3718-9 was obtained during RV Meteor cruise M 34-2 in January/February 1996 from the continental slope off Namibia, south of Walvis Bay (Schulz and Cruise participants 1996), GeoB 2004-3 during RV Meteor cruise M 23-1 in February 1993 in the northern part of the southern Cape Basin (Spieß and Cruise participants 1993; Fig. 1). Data on a third reference core, the giant piston core MD 962085, were used to fit an age model to core GeoB 2004-3. MD 962085 is located northwestwards of our study area on the lower slope of the eastern South Atlantic, and was taken aboard RV Marion Dufresne during the NAUSICAA-IMAGES II cruise in October/November 1996 (Bertrand and Cruise participants 1997; Table 1; Fig. 1).

Materials and methods

Land-based laboratory work

Prior to cruise M 57-1, an appropriate XRF preparation and analysis technique was developed in the land-based laboratory. Besides analyses with the certified standard reference material MAG-1 (e.g. Govindaraju 1994), the laboratory work involved analysis of the two archived reference cores GeoB 3718-9 and GeoB 2004-3.

A set of 77 ICP-AES analyses of core GeoB 3718-9 from Heuer (2003) was used to control the quality of the land-based Spectro Xepos XRF analyses. Unfortunately, it was not possible to use aliquots of the original ICP-AES samples, because the amount of leftover material was too small. For this reason, GeoB 3718-9 was resampled at the same depths. This material was powdered, homogenised and, in each case, 4 g was weighed accurately (two decimal places) and analysed using the XRF method Turboquant (Schramm and Heckel 1998) which is generally used at a specified measuring time of 300 s per target and sample.

In addition, MAG-1 standard material was used to develop an XRF measuring technique better suited for onboard application. Three main aspects were assessed: (1) the suitability of using powdered material lightly compressed by hand, thereby saving in time and equipment needed for the more traditional usage of pressed pellets; (2) the suitability of estimating sample mass indirectly in terms of volume, thereby avoiding the problems associated with the deployment of a balance under non-stationary conditions aboard ship; and (3) the suitability of reducing measuring time from 300 to 100 s per target and sample, thereby increasing sample throughput.

In the shore-based laboratory, element profiles were established for core GeoB 2004-3 using the reduced 100-s measuring option. In order to use this core for age-fitting purposes during cruise M 57-1, it was dated by correlation with the giant piston core MD 962085 which has an age

model based on Foraminifera oxygen isotope records (Chen et al. 2002). Thus, colour reflectance data (700 nm) for MD 962085 (Bertrand and Cruise participants 1997) were correlated with XRF Ca data for GeoB 2004-3. The main argument for using core GeoB 2004-3 as reference was that it allowed easily fitting age models to other study cores by means of a complete XRF element suite, in addition to the colour reflectance data of the dated reference core MD 962085.

Shipboard sample preparation

After recovery, 1-m sections were cut from each 8-9 m gravity core, capped immediately, and divided lengthways by sawing through the core liner and sediment. Subsamples were obtained from each split-core section by using the U-channel sampling technique (Figs. 2 and 3). A plastic U-shaped channel ("conduit") with a cross section of 1.5×2 cm and 1 m in length was pressed into the interior part of the split-core section, this being the region least affected by the coring operation. This strip of sediment was subsequently separated from the core section by means of a plastic wire. These U-channel samples allowed continuous subsampling at a length resolution of 4 cm. In this way, 200 to 225 discrete samples were taken from each gravity core. In the present case, a U-channel was preferred to sampling with syringes. Thus, although element contents were integrated over 4 cm, no information was lost as may occur when inserting syringes at discrete depths. MUCs were sampled at a resolution of 2 cm (GeoB 8301-5, GeoB 8303-5) or of 1 cm for the top 10 cm, and a resolution of 2 cm below this depth (GeoB 8501-1).

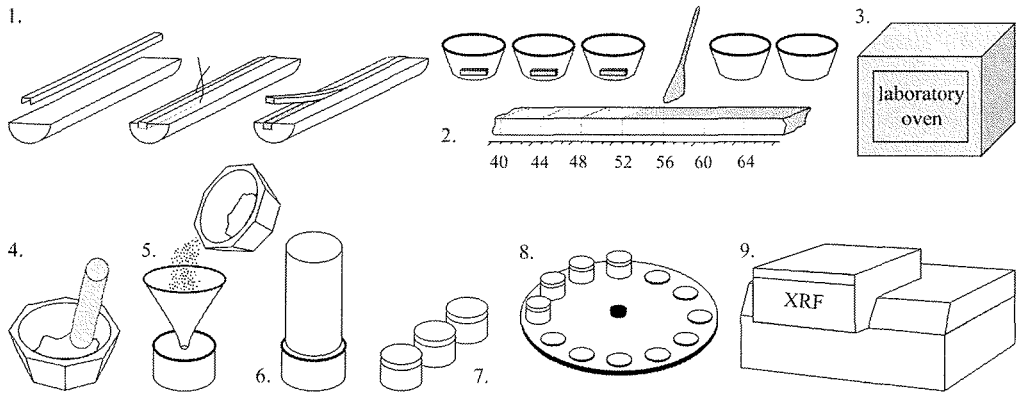

Fig. 2: Schematic illustration of sample preparation for shipboard XRF analyses.
1 U-channel sampling; *2* subsample transfer into crystallising dishes; *3* drying; *4* grinding; *5* transfer of sediment powder into sample cup; *6* compacting the powder; *7* capping the sample cups; *8* arrangement of sample cups on a 12-position rotating tray; *9* XRF analysis

The sediment samples were transferred into crystallising dishes and subsequently dried in a laboratory oven at 200°C for 60 min. This procedure eliminates abundant pore water typical for muddy continental shelf sediments, which otherwise would have a negative impact on the quality of the analyses. After removing the samples from the oven and cooling to room temperature, the material was ground and homogenised manually by means of an agate or ceramic pestle and mortar. The powder was then poured into previously prepared sample cups.

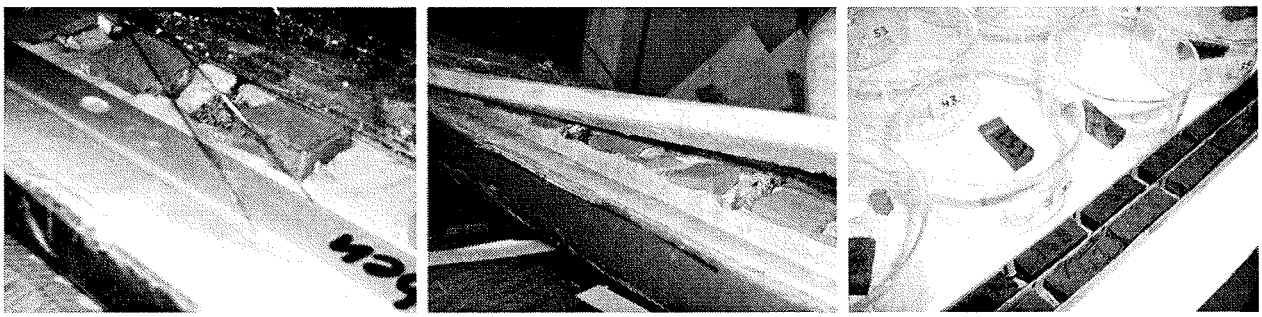

Fig. 3: Photographs showing various steps of XRF sample preparation.
Left: cutting a sediment strip from the split-core section using the U-channel and plastic wire; *centre*: removing the sediment-filled U-channel; *right*: subsampling at a depth resolution of 4 cm

Each sample cup consists of a top and a bottom ring, 4-µm prolene foil serving for the sides and the bottom. Spectro Analytical Instruments suggests a sample amount of 2-4 g dry sediment for XRF analysis. Since it is inconvenient to use highly accurate balances onboard the ship, sample dimensions had been predetermined in the land-based laboratory so that each cup, when filled to the brim with loose material, contained the desired mass for analysis. Note that this assumes a constant density for sediments in the study area. After filling, the material was compressed by means of a pestle so as to obtain a flat and even surface and to eliminate air in interstices. After capping, the cups were arranged on a 12-position rotating tray, which was then inserted into the measuring chamber of the Spectro Xepos analyser.

Shipboard XRF analyses

The compact benchtop EDPXRF analysis system Spectro Xepos used for the analyses is shown in Fig. 4. Its small size (31×60×69 cm) and weight (≈ 45 kg) allow easy use and transport outside a traditional land-based laboratory. Onboard ship, the instrument was immediately set up in standby mode to allow for adjustment. For one, thermic stabilisation is critical for the detector. The XRF was allowed to stabilise 2 h before being used for simultaneous measurements of elements from Mg (atomic number 12) through to U (atomic number 92). Elements important for this study are Si, Ti, Al, Fe, Mn, Mg, Ca, K, Sr, Ba, Rb, Cu, Ni, Zn, P, S, Cl and Br. All XRF datasets presented in this study are available on the Pangaea database http://www.wdc-mare.org/PangaVista?query=@Ref25739.

Spectro Xepos uses a Pd-target end window tube at a maximum power of 50 W and a maximum voltage of 50 kV. The excitation radiation is optimised for three groups of elements, each with a specific target for modification in excitation energy and excitation energy distribution. The principle of this optimised excitation is already well known (Heckel et al. 1992). Targets, associated voltage values, and measured elements are listed in Table 2. Excitation conditions are not influenced by measuring time. The fluorescent radiation is measured with a Si(Li) semiconductor detector (RÖNTEC-Xflash) which is operated at a temperature of -10°C

(optimum temperature: -5 to -15°C). Cooling is accomplished thermoelectrically by integration of a Peltier element into the detector module (Spectro Xepos 2000).

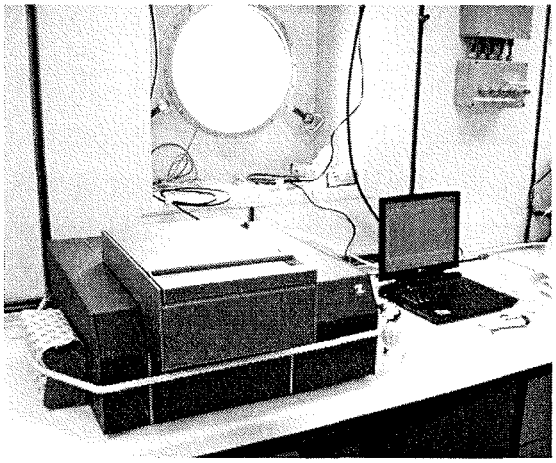

Fig. 4: Shipboard application of the XRF analyser Spectro Xepos

Table 2: Excitation conditions used for the Spectro Xepos

Target	Voltage (kV)	Elements
Mo secondary target	45	Cr-Y, Hf-U
Al_2O_3 polarisation target	49.5	Zr-Ce
HOPG crystal	25	Mg-V

The sample chamber is flushed with helium to avoid loss of energy caused by scattering in air. This improves the sensitivity for light elements such as Mg, Al and Si. A 50-l helium gas bottle (200 bar) is sufficient for approximately 1,000 analyses performed with the 100-s measuring time option.

The instrument was operated by means of the software Spectro X-Lab Pro, version 2.4, using the so-called Turboquant method. This is a fundamental parameters method for fluorescence and scattering, and allows preliminary screening of samples (Schramm and Heckel 1998). The method is generally used at a specified measuring time of 300 s per target and sample.

Readjustment of the multi-channel analyser (MCA) calibration of the XRF instrument was done weekly with a specially prepared glass disk. The calibration curves convert the MCA channel scale to a kiloelectronvolt (keV) scale and thus, shift the peaks to the desired positions. Accuracy and reproducibility of the XRF instrument were assessed by daily analyses of the standard reference material MAG-1 (e.g. Govindaraju 1994). For this purpose, pressed pellets of the standard (4 g MAG-1 standard powder + 0.9 g Hoechst Wax) had been prepared in the land-based laboratory prior to the cruise. The standard pellets had been accurately weighed onland, thereby avoiding the problem of not being able to accurately correct for wax mass during difficult shipboard operations. To exclude errors due to sample preparation, however, reproducibility and accuracy were determined by repeated measurement of one and the same pellet whereas the remaining pressed pellets served as backups.

Results

Accuracy, reproducibility and detection limits (MAG-1 standard reference material)

A comparison of analyses performed on a single pressed pellet of certified standard reference material MAG-1 allowed to assess the analytical quality of the Spectro Xepos instrument for the original 300-s method as well as for the time-reduced 100-s method, both onland and aboard.

Note that this pressed pellet had been prepared from the MAG-1 powder sample which had been analysed earlier with the 300-s measuring time option in the land-based laboratory.

Pressed pellet

Table 3 shows 300-s and 100-s accuracy and reproducibility data for both land-based and shipboard XRF analyses of a single pressed pellet of MAG-1 standard reference material (cf. the standard deviation is an inverse measure of reproducibility). For the 300-s measuring time option under land-based laboratory conditions, reproducibility values are <5% for all listed elements except Ba, Cu, Ni, P and Cl, and ≤1% for Si and Al. Thus, reproducibility is generally good. Accuracy is sometimes excellent (100±8% for Sr, Ba, Rb, Cu, Ni, Zn) but mostly biased towards overestimating element contents, except for Sr and Rb, which tend to be underestimated. Because reproducibility is generally good, this bias is consistent.

Reduction of the measuring time to 100 s in the land-based laboratory leads to a decrease of accuracy and reproducibility, especially for Mn, Mg, Ba, Cu and Rb. Reproducibility values are >5% for Ti, Ba, Cu, Ni, P and Cl, ≤5% for Mn, Mg, Ca, Sr, Rb, Zn, S and Br, and ≤1% for Si, Al, Fe and K. Accuracy remains similar to the 300-s measurements, showing excellent values (100±8%) for Ti, Sr, Ba, Rb, Cu, Ni and Zn but usually overestimating element contents, except for Sr. A comparison of these land-based data justifies our choice of the 100-s measuring time for the shipboard analyses.

Shipboard 300-s measurements of the same pressed pellet of MAG-1 standard reference material even exceed the quality of land-based 300-s measurements in terms of reproducibility. Values are <5% except for Cu and Cl, and ≤1% for Si, Al, Fe, Ca, K, Sr, S and Br. Accuracy decreases slightly by 1-2% for most elements but it is excellent (100±8%) for Sr, Ba, Rb, Cu, Ni and Zn. Again, there is a bias towards overestimating element contents, except for Sr.

Although reproducibility of shipboard 100-s measurements decreases in comparison to both land-based and shipboard 300-s measurements, values are still ≤1% for Si, Al and Fe, and <5% for the other elements, except Ti, Ba, Cu, Ni, P and Cl. Accuracy is excellent (100±8%) for Sr, Ba, Rb, Cu, Ni and Zn, but mostly element contents are overestimated, except for Sr. A comparison of the land-based 300-s and shipboard 100-s measurements of the MAG-1 pressed pellet shows a decrease of both accuracy and reproducibility for Mn and Mg. Standard deviations of Ba and P increase from 6.7 to 14.3, and 5.0 to 7.7% respectively. Overestimation of element contents is highest for P (131-150% relative accuracy) and Mg (130-141% relative accuracy) with all four methods. On the other hand, the accuracy of shipboard 100-s measurements of Ca, K and Sr exceeds that of land-based 300-s measurements. For most other elements, shipboard 100-s data show either better reproducibility but lower accuracy than land-based 300-s data (Si, Al, Fe) or vice versa (Ti, Ba, Cu, Ni, Zn, P).

Table 3: Compilation of land-based and shipboard data, both for the original 300-s and the time-reduced 100-s measuring times, for a pressed pellet of MAG-1 standard reference material. *SD* standard deviation, *n* number of replicate analyses

Element	**Si**	**Ti**	**Al**	**Fe**	**Mn**	**Mg**	**Ca**	**K**	**Sr**	**Ba**	**Rb**	**Cu**	**Ni**	**Zn**	**P**	**S**	**Cl**	**Br**
Certified (mg/kg)	235600 ± 4500	4496 ± 420	86800 ± 1600	47560 ± 4200	759 ± 70	18090 ± 600	9790 ± 710	29470 ± 1410	150 ± 15	480 ± 41	150 ± 6	30 ± 3	53 ± 8	130 ± 6	698 ± 92			
Land-based, 300-s; n=91																		
Measured mean (mg/kg)	285700	4950	10530	53430	887	23510	10810	32450	139.6	508	146.6	31.8	55.2	137.1	1045	3556	17950	226.2
SD (mg/kg)	2800	225	1000	600	31	520	250	620	2.3	34	2.3	2.7	2.9	3.4	52	47	2840	3.7
Relative SD (%)	1.0	4.6	0.9	1.1	3.5	2.2	2.3	1.9	1.7	6.7	1.6	8.4	5.2	2.5	5.0	1.3	15.8	1.6
Relative accuracy (%)	121	110	121	112	117	130	110	110	93	106	98	106	104	105	150			
Detection limit (mg/kg)	8400	675	3000	1800	93	1560	750	1860	6.9	102	6.9	8.1	8.7	10.2	156	141	8520	11.1
Land-based, 100-s; n=99																		
Measured mean (mg/kg)	289004	4814	10582	54056	907	24880	10825	32493	140.3	515	148.0	32.2	52.4	135.5	935	3472	13724	221.9
SD (mg/kg)	2319	266	694	422	37	709	148	309	2.4	60	2.6	3.4	5.3	4.3	64	48	1567	4.1
Relative SD (%)	0.8	5.5	0.7	0.8	4.0	2.9	1.4	1.0	1.7	11.7	1.8	10.6	10.1	3.2	6.9	1.4	11.4	1.8
Relative accuracy (%)	123	107	122	114	120	138	111	110	94	107	99	107	99	104	134			
Detection limit (mg/kg)	6957	798	2082	1266	111	2127	444	927	7.2	180	7.8	10.2	15.9	12.9	192	144	4701	12.3
Shipboard, 300-s; n=97																		
Measured mean (mg/kg)	286600	5124	10580	53960	899	24490	11020	32950	140.5	507	147.7	31.3	55.9	135.6	970	3458	14040	225.1
SD (mg/kg)	1700	119	600	160	23	550	90	270	1.4	24	1.8	2.9	2.5	2.5	26	29	890	2.2
Relative SD (%)	0.6	2.3	0.5	0.3	2.5	2.2	0.8	0.8	1.0	4.8	1.1	9.3	4.4	1.9	2.7	0.8	6.3	1.0
Relative accuracy (%)	122	114	122	113	118	135	113	112	94	106	99	104	106	105	139			
Detection limit (mg/kg)	5100	357	1800	480	69	1650	270	810	4.2	72	5.4	8.7	7.5	7.5	78	87	2670	6.6
Shipboard, 100-s; n=80																		
Measured mean (mg/kg)	288800	4872	10640	53810	893	25580	10780	32370	139.6	491	146.9	29.5	53.3	134.7	915	3387	11830	220.6
SD (mg/kg)	1700	254	700	520	34	650	200	440	2.3	70	3.0	4.2	5.2	4.3	71	53	940	4.1
Relative SD (%)	0.6	5.2	0.7	1.0	3.8	2.5	1.8	1.4	1.6	14.3	2.1	14.2	9.7	3.2	7.7	1.6	8.0	1.9
Relative accuracy (%)	123	108	123	113	118	141	110	110	93	102	98	99	101	104	131			
Detection limit (mg/kg)	5100	762	2100	1560	102	1950	600	1320	6.9	210	9	12.6	15.6	12.9	213	159	2820	12.3

Powder sample

Land-based 300-s measurements of a single powder sample of MAG-1 standard reference material are shown in Table 4. Reproducibility values are <5% for all listed elements except Ba and Cu, and ≤1% for Si, Ti, Al, Fe, Ca, K, Sr, S and Br. Among the major elements, only Mg and Mn show values of 2.0%, P of 2.4%. Accuracy exceeds that of the pressed pellet for the major elements, with excellent values for Si, Ti, Fe, Mn and Ca, and also for the trace element Ni. For the trace elements Sr, Ba, Rb, Cu and Zn, however, accuracy is lower in the powder sample than in the pressed pellet. Except for P, Mg and Si, there is a bias to underestimate element contents. This bias is most significant for Sr, Ba and Rb which are underestimated by 15-19%. P shows the lowest accuracy, being overestimated by 30%. A comparison of land-based 300-s measurements of both the MAG-1 pressed pellet and the powder sample justifies our choice to use powder samples aboard.

Table 4: Compilation of land-based data for the original 300-s measuring time for a powder sample of MAG-1 standard reference material. *SD* standard deviation, *n* number of replicate analyses

Element	**Si**	**Ti**	**Al**	**Fe**	**Mn**	**Mg**	**Ca**	**K**	**Sr**
Certified (mg/kg)	235600 ± 4500	4496 ± 420	86800 ± 1600	47560 ± 4200	759 ± 70	18090 ± 600	9790 ± 710	29470 ± 1410	150 ± 15
Land-based, 300-s; n=21									
Measured mean (mg/kg)	236262	4236	82296	45425	747	19564	9320	27510	122.0
SD (mg/kg)	953	43	411	120	15	390	92	194	1
Relative SD (%)	0.4	1.0	0.5	0.3	2.0	2.0	1.0	0.7	0.9
Relative accuracy (%)	100	94	95	96	98	108	95	93	81
Detection limit (mg/kg)	2859	129	1233	360	45	1170	276	582	3

Element	**Ba**	**Rb**	**Cu**	**Ni**	**Zn**	**P**	**S**	**Cl**	**Br**
Certified (mg/kg)	480 ± 41	150 ± 6	30 ± 3	53 ± 8	130 ± 6	698 ± 92			
Land-based, 300-s; n=21									
Measured mean (mg/kg)	391	127.7	26.8	45.5	117.1	908	3275	19839	196.1
SD (mg/kg)	34	1.4	2.0	1.7	2.2	22	34	292	1.9
Relative SD (%)	8.7	1.1	7.5	3.7	1.9	2.4	1.0	1.5	1.0
Relative accuracy (%)	81	85	89	86	90	130			
Detection limit (mg/kg)	102	4.2	6	5.1	6.6	66	102	876	5.7

The detection limit is defined as the element content corresponding to a signal three times the standard deviation. For measurements of both the powdered and pelleted MAG-1 standard reference material with the four methods, detection limits are well below (factor >10) certified levels for Si, Al, Fe, Mg, Ca, K, Sr, Rb, Zn, S and Br. Only for those elements with detection limits closer to certified levels, especially Ba, Ni and P, did instrument performance improve substantially with increasing measuring time.

Comparison of land-based XRF and ICP-AES analyses

This is a comparison of two distinctly different methods, the XRF method being applied to the original solid phase samples, whereas the sediment samples used for ICP-AES analysis were fully digested. Results from linear regression analysis and statistical parameters are presented in Table 5 and Figs. 5 and 6. Element contents from ICP-AES analyses were set at 100%, and the relative accuracy represents the deviation of the XRF data from this reference level. Minimum and maximum values in relative accuracy represent the scattering of the data but note that, in the present case, this scatter can be attributed partly to resampling for XRF analyses and thus, to the inherent inhomogeneity of marine sediments. Outlier data are probably caused by the presence of, amongst others, larger shells or mineral grains. Outlier data for Al, Fe, Mg and K derive from sample 7, for Ti from samples 7, 15 and 63, and for Ni, Cu and Zn from samples 7, 8 and 9.

Coefficients of determination are highest (≥0.7) for Ca, Sr, K, Al, Fe, Ni and S, and lowest (<0.7) for Ti, Mn, Mg, Cu and Zn. Ba shows a seemingly good correlation but this results largely from the wide range of Ba content (320-6,015 mg/kg) in core GeoB 3718-9. Thus, a reduced Ba dataset (Fig. 6), comprising only those data points with lower element contents (<1,000 mg/kg), shows a much poorer correlation. The mean relative accuracy of the XRF values is ±100% for Ti, Mn, Mg, Ca, Cu and Zn but much lower (68%) for Ba.

Table 5: Comparison of ICP-AES and land-based XRF analyses (powder samples; accurate sample weight; 300-s measuring time) of gravity core GeoB 3718-9

Element	ICP-AES; element content (mg/kg) [a]	XRF; relative accuracy (%)		
	Range	Mean	Min – max (outlier data in brackets [b])	R^2
Ti	870 – 2498	101	76 (53) – 136 (174)	0.40
Al	15500 – 52500	81	69 – 100 (104)	0.74
Fe	9670 – 33290	92	78 – 117 (119)	0.74
Mn	71 – 191	105	84 – 144	0.33
Mg	6410 – 12800	97	85 – 123 (126)	0.48
Ca	59430 – 274330	103	77 – 131 (196)	0.87
K	5260 – 15810	92	80 – 115 (116)	0.71
Sr	279 – 1146	88	64 – 117 (140)	0.86
Ba	320 – 6015	68	47 – 111 (125)	0.98
Cu	48 – 106	100	78 – 118 (130)	0.66
Ni	54 – 123	88	75 – 99 (115)	0.73
Zn	53 – 141	101	77 – 123 (134)	0.46
S	4940 – 23413	84	72 – 103	0.89

[a] ICP-AES analyses of core GeoB 3718-9 extracted from Heuer (2003)

[b] Outlier data have been encircled in Figs. 5 and 6

Comparison of shipboard and land-based XRF analyses

To assess the performance of the Spectro Xepos instrument aboard ship, 40 powder samples from three MUCs (GeoB 8301-5, GeoB 8303-5, GeoB 8501-1) were analysed with the 300-s and the time-reduced 100-s methods, both aboard and subsequently onland. For the post-cruise analyses, the samples were accurately weighed in order to estimate whether the quality of shipboard measurements had been impaired by the volume-based weighing procedure.

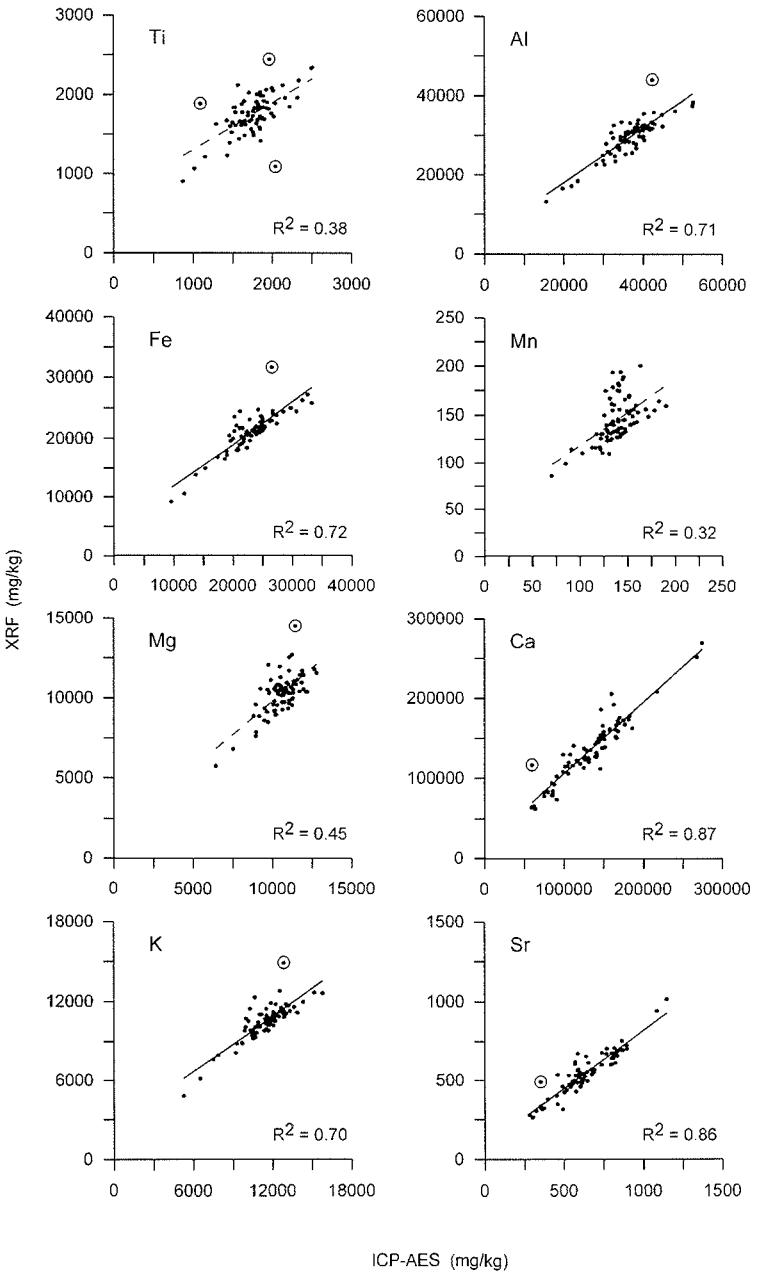

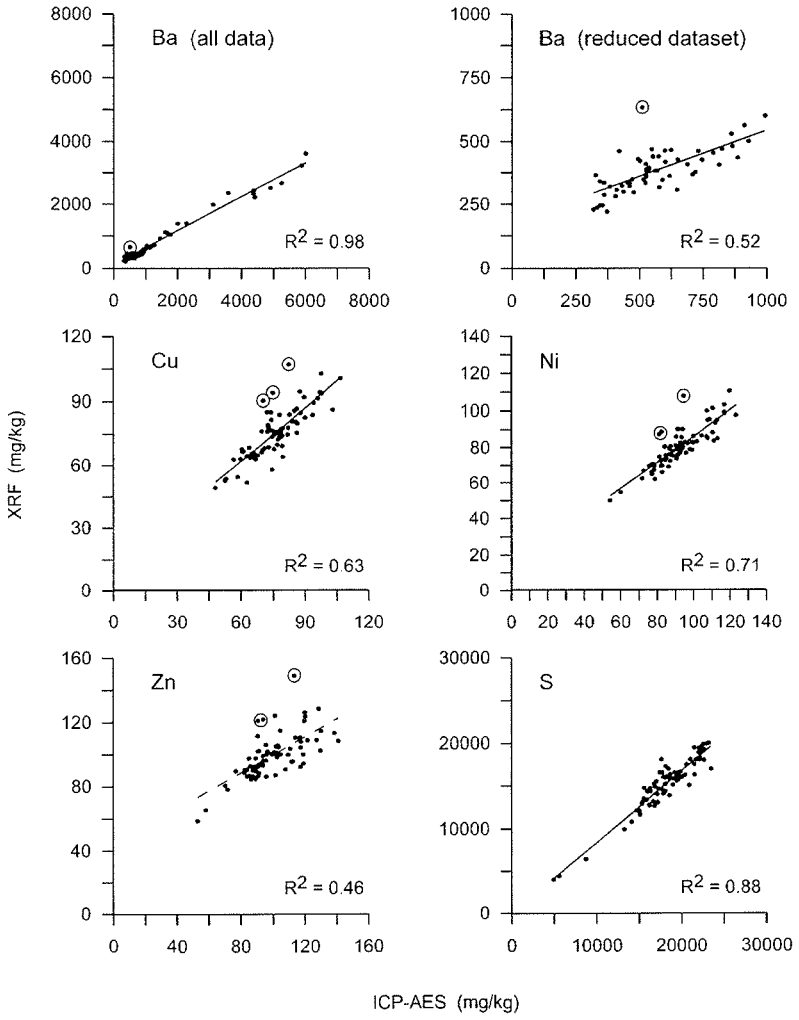

Figs. 5 & 6: Results from linear regression analysis for the elements Ti, Al, Fe, Mn, Mg, Ca, K and Sr (**Fig. 5**, *left*) and Ba, Cu, Ni, Zn and S (**Fig. 6**, *above*), with ICP-AES data as independent and XRF data as dependent variables (core GeoB 3718-9). Part of the *scatter* has been caused by resampling for XRF analyses, rather than using the original ICP-AES samples, and thus results from the inherent inhomogeneity of marine sediments. Outlier data caused by extreme inhomogeneity are *encircled*

For both the shipboard and land-based datasets, the relationships between the 100-s and 300-s methods show regression lines all running through the origin. Correlations are excellent ($R^2 \geq 0.99$) for Si, Al, Fe, Mn, Ca, K, Sr, S, Cl and Br, good for Ti, Mg, Rb and Zn ($R^2 = 0.9$ to 0.99), whereas Cu, Ni, P and especially Ba show a higher scatter of data ($R^2 < 0.9$; Figs. 7-9).

If shipboard and land-based measurements were to correspond perfectly, then a sample measured both aboard (triangles in Figs. 7, 8, 9) and onland (crosses in Figs. 7, 8, 9) would plot essentially as a single data point. A good correspondence exists between shipboard 100-s and land-based 300-s measurements, with an average deviation of ≤5% for Si, Al, Fe, Ca, K, Sr and Br. For Rb, Zn, S and Cl, the average deviation is ≤10%, whereas it is >10% for Ti, Mn, Mg, Ba, Cu, Ni and P. The seemingly low scatter in the Mn plot in Fig. 7 results largely from the wide range of Mn content from approximately 0.1 to 4.0 g/kg. The onboard procedure of estimating sample weight relatively crudely in terms of sample volume generally has only a minor effect on data accuracy.

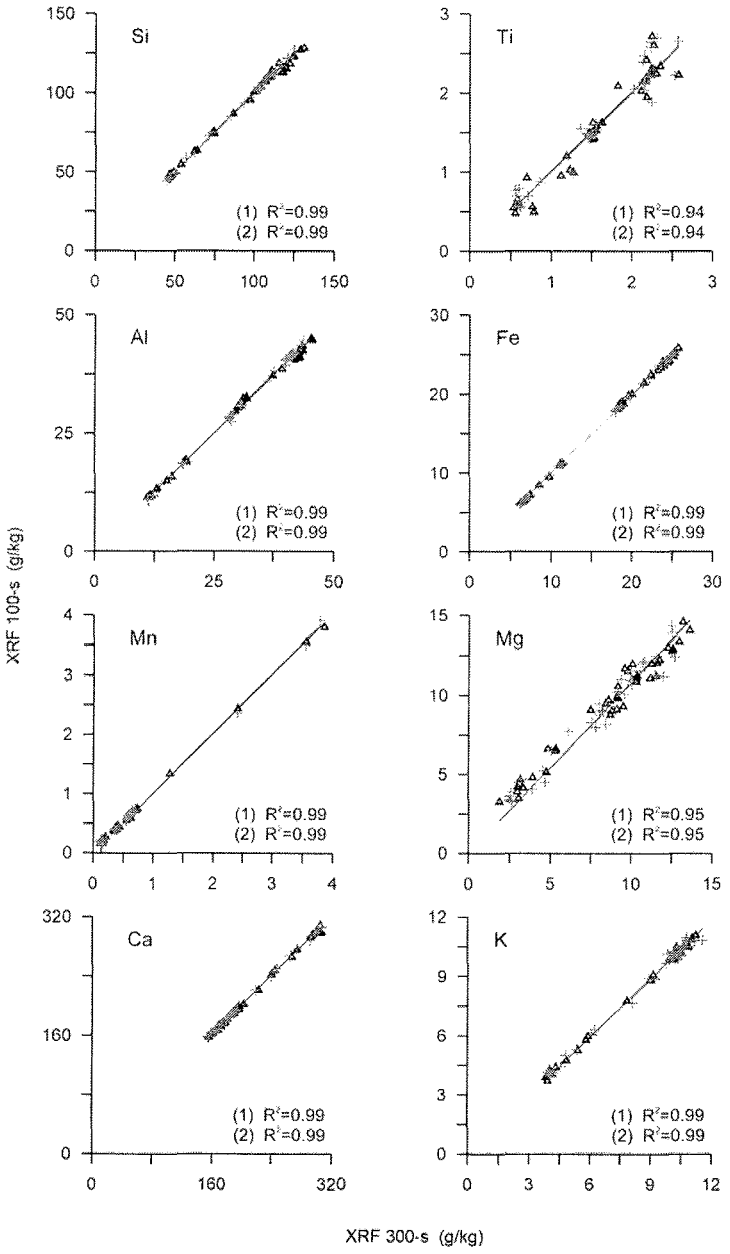

Fig. 7: Results from linear regression analysis of shipboard (*1*) and land-based (*2*) XRF measurements on three MUCs (cores GeoB 8301-5, GeoB 8303-5, GeoB 8501-1) for the elements Si, Ti, Al, Fe, Mn, Mg, Ca and K, with 300-s data as independent and 100-s data as dependent variables. *Triangles* denote shipboard, *crosses* denote land-based analyses. In each of these plots there are two *regression lines*, one for shipboard, one for land-based analyses

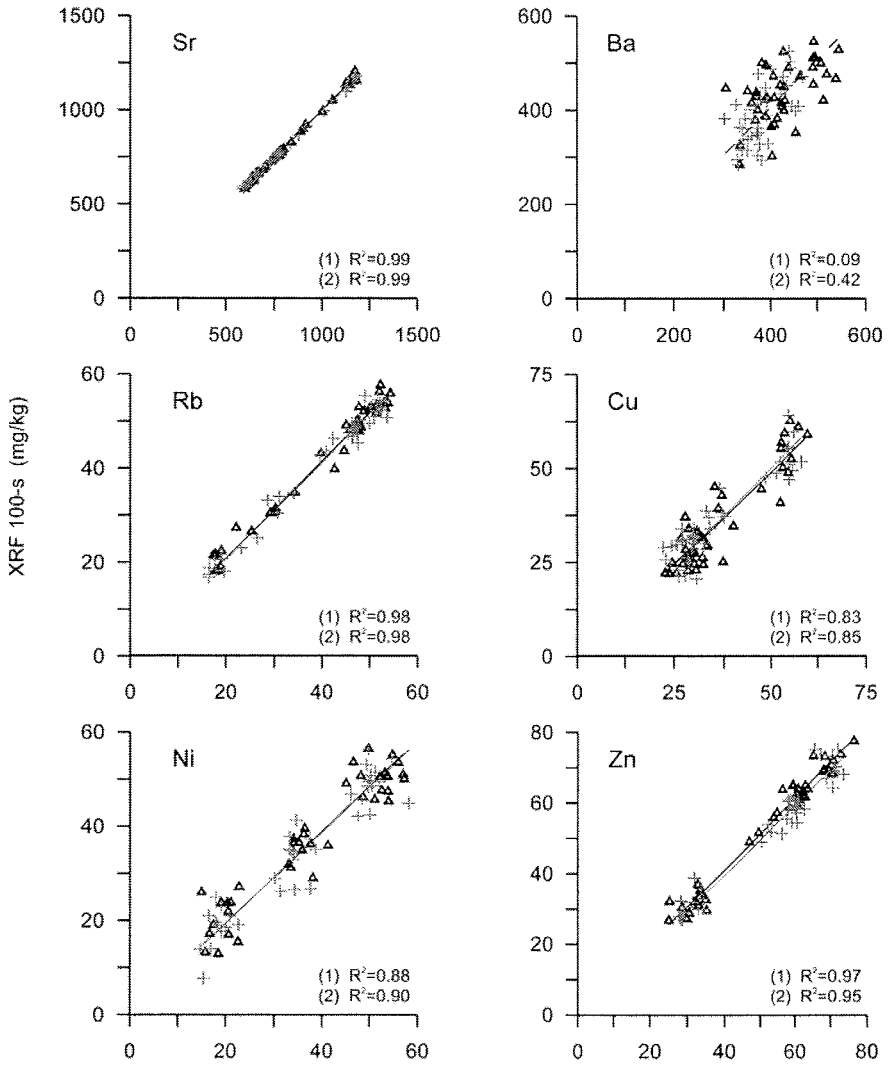

Fig. 8: Results from linear regression analysis of shipboard (*1*) and land-based (*2*) XRF measurements on three MUCs (cores GeoB 8301-5, GeoB 8303-5, GeoB 8501-1) for the elements Sr, Ba, Rb, Cu, Ni and Zn, with 300-s data as independent and 100-s data as dependent variables. *Triangles* denote shipboard, *crosses* denote land-based analyses. In each of these plots there are two *regression lines*, one for shipboard, one for land-based analyses

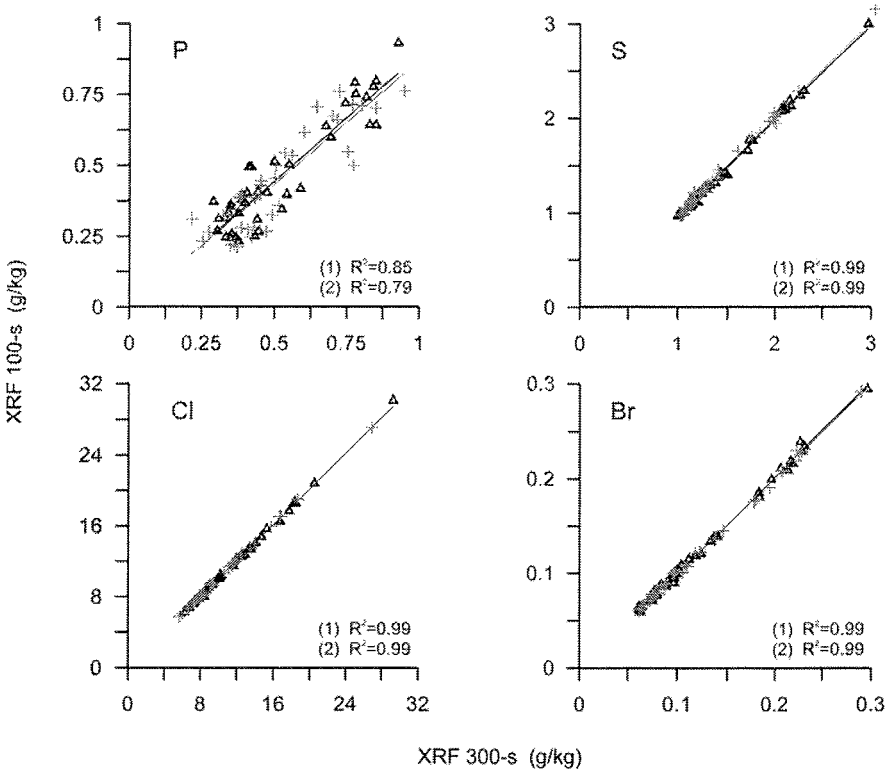

Fig. 9: Results from linear regression analysis of shipboard (*1*) and land-based (*2*) XRF measurements on three MUCs (cores GeoB 8301-5, GeoB 8303-5, GeoB 8501-1) for the elements P, S, Cl and Br, with 300-s data as independent and 100-s data as dependent variables. *Triangles* denote shipboard, *crosses* denote land-based analyses. In each of these plots there are two *regression lines*, one for shipboard, one for land-based analyses

Instrument performance at sea

After 2 h of stabilisation in the standby mode, necessary to adjust instrument parameters, the Spectro Xepos showed no irregularities in functioning which could have been caused by transport. At a measuring time of 100 s per target and sample, a complete analysis of one sample with all three targets takes 5 min, and a 12-position rotating tray is analysed within 80 min, rather than 200 min at the original measuring time of 300 s. Geochemical information on several elements (18 in the present case) is available immediately after analysis.

Spectro Xepos is generally capable of detecting all elements from Mg through U from powdered material in cups. For many elements (e.g. V, Cr, Co, As, Y, Zr, Mo, Ag, Cd, Sn, Pb, U) in the samples analysed, however, the detection limits of the instrument were above or close to naturally occurring levels at the study site. This is a core-specific result and not due to shipboard effects. The "missing" elements would not have been reliably detected onland either.

Occasionally, single shipboard XRF analyses deviated from the general trend in the cores, for instance, for the elements Si, Ca, Al, Fe, K, Mg and S. Subsequent re-analyses of these samples often confirmed that the initial values were not erroneous. Presumably, the deviation from the general trend was caused by the inherent inhomogeneity of the sediments at the study site. However, 0.5% of the measurements performed during the three cruises M 57-1 (Schneider and Cruise participants 2003), M 58-1 (Schulz and Cruise participants 2003) and M 58-2a & b (Bleil and Cruise participants 2004) was found to be erroneous, the value being 0.6% for cruise M 57-1 on its own. It is as yet not known whether this could have been due at least partly to unfavourable weather conditions. Dates of XRF analyses performed during cruise M 57-1 and prevailing weather conditions are listed in Table 6. The instrument certainly remained operational during heavy weather conditions, even at wind speed 8 to 9 B (19-22.5 m/s) and swells of 3 to 4 m.

Table 6: Dates of XRF analyses during RV Meteor cruise M 57-1, dominating wind speed and swell during day of analysis, number of samples and erroneous measurements

Core no.	Date of XRF analysis	Wind speed (B)	Wind speed (m/s)	Swell (m)	Number of samples	Erroneous measurements
GeoB 8301-5	21.01.2003	1-3	1.0-4.5	3	11	0
GeoB 8301-6	22.01.2003	3-6	4.5-12.5	2-2.5	219	1
	23.01.2003	7-9	15.5-22.5	3		
GeoB 8303-5	22.01.2003	3-6	4.5-12.5	2-2.5	12	0
	24.01.2003	6-8	12.5-19.0	2.5-3		
GeoB 8307-6	26.01.2003	4-5	6.5-9.5	1.5-2	211	2
	27.01.2003	5-6	9.5-12.5	2		
GeoB 8310-2	28.01.2003	6	12.5	1.5-2.5	208	0
	29.01.2003	5-7	9.5-15.5	2.5		
GeoB 8315-6	31.01.2003	5	9.5	2.5-3	212	1
	01.02.2003	3-5	4.5-9.5	1.5-2		
GeoB 8331-4	02.02.2003	5	9.5	2.5-3	220	3
	03.02.2003	4-5	6.5-9.5	1.5		
	04.02.2003	3-5	4.5-9.5	1-1.5		

The shipboard data show typical XRF trends, commonly observed in continental margin sediments. Example spectra are presented in Figs. 10 and 11 for the Mo-target and HOPG-crystal excitation for two samples collected at 9- and 193-cm core length in GeoB 8301-6. Note that both figures show an expanded energy scale. There is an excellent differentiation in the measured intensities of common elements such as Fe, Br and Sr (Fig. 10), and also Al, Si, S, Cl, K and Ca (Fig. 11). In particular, note the good sensitivity for the Al and Si peaks, a potential problem when using benchtop XRF equipment.

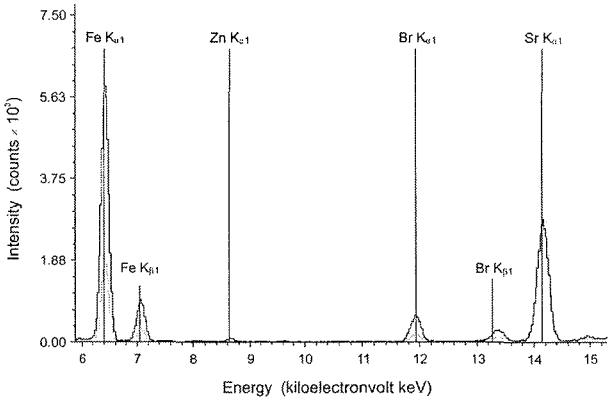

Fig. 10: View of the ≈6-15 keV region in spectra of two different samples from GeoB 8301-6 (9-cm core length, *bold line*; 193-cm core length, *shaded line*), using the Mo-target excitation (0-25 keV)

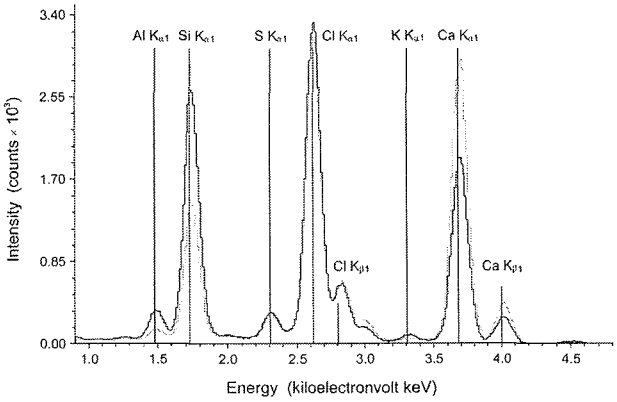

Fig. 11: View of the ≈1-4.5 keV region in spectra of two different samples from GeoB 8301-6 (9-cm core length, *bold line*; 193-cm core length, *shaded line*), using the HOPG-crystal excitation (0-12.5 keV)

Downcore data

Shipboard downcore elemental variations are illustrated on the basis of selected datasets for four cores collected in the southern Cape Basin during RV Meteor cruise M 57-1 (Schneider and Cruise participants 2003), combined with the age data for one reference core collected earlier during RV Meteor cruise M 23-1 (Spieß and Cruise participants 1993) and analysed onland. Fig. 12 a-c shows good correlation of the Fe, Si and Ca profiles between the dated reference core GeoB 2004-3 and the gravity cores GeoB 8315-6, GeoB 8307-6, GeoB 8310-2 and GeoB 8301-6. Core GeoB 2004-3 allows age-depth correlation back to 300 ka. Cores GeoB 8310-2 and GeoB 8301-6 are younger than 300 ka, whereas cores GeoB 8315-6 and GeoB 8307-6 exceed this age. An age of approximately 190 ka is the oldest identified in all five gravity cores in the present study.

A more complete dataset for core GeoB 8301-6 (Fig. 13) indicates that the elements showing lowest relative standard deviations are Si, Al, Fe, Ca, K, Sr, Rb, Zn, S, Cl and Br, evident in the rather smooth appearance of specific peaks in the graph (cf. relatively low standard deviations in Tables 3, 4). More "noisy" are the profiles for Ti, Mg, Cu, and especially Mn, Ba, Ni and P, reflecting the higher standard deviations (cf. Tables 3, 4).

a **Iron content (g/kg)**

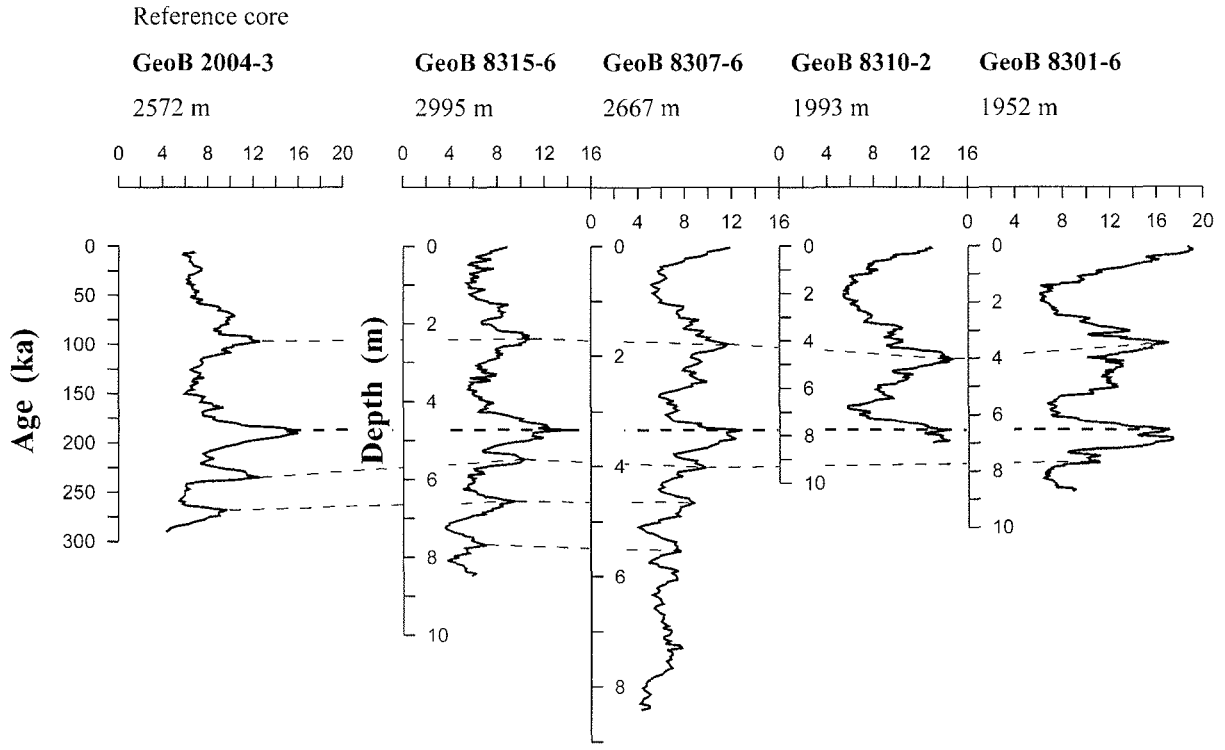

Sedimentation rates up to 190 ka

GeoB 2004-3	GeoB 8315-6	GeoB 8307-6	GeoB 8310-2	GeoB 8301-6
3.6 cm/10^3 year	2.4 cm/10^3 year	1.7 cm/10^3 year	4.2 cm/10^3 year	3.4 cm/10^3 year

b **Silicon content (g/kg)**

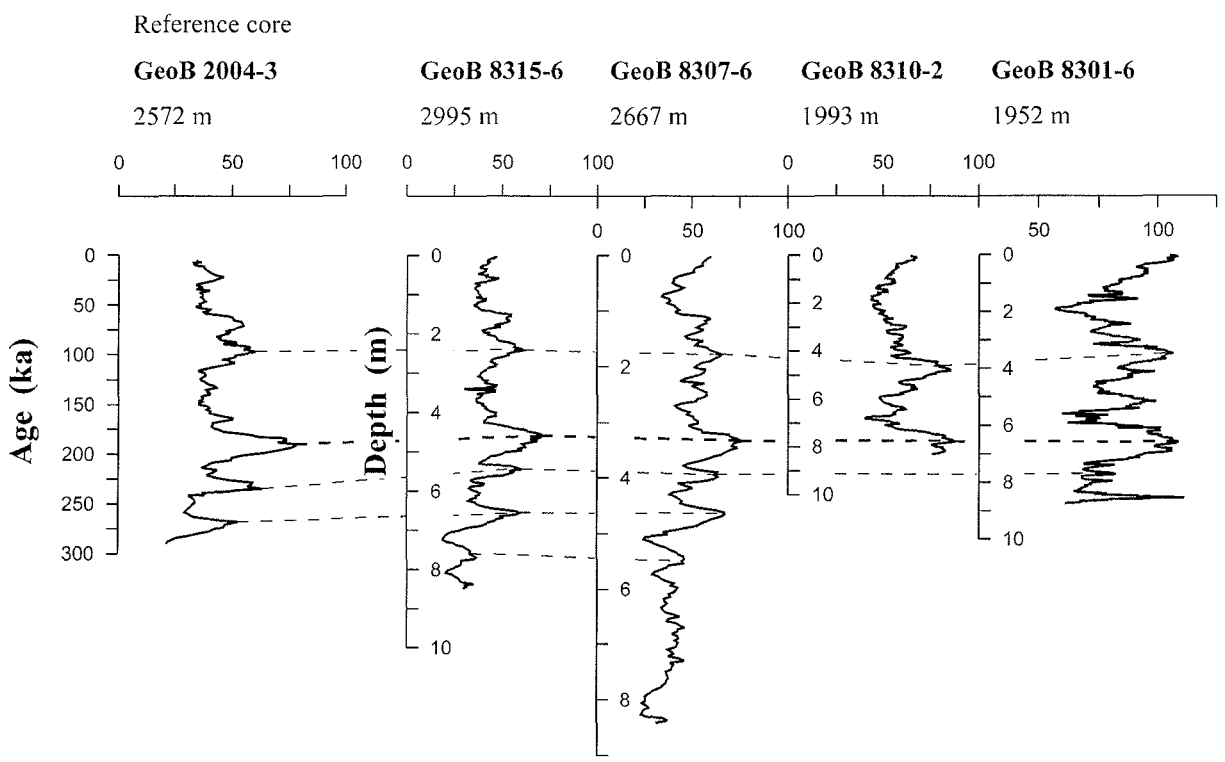

(to be continued)

Figure 12 (continued)

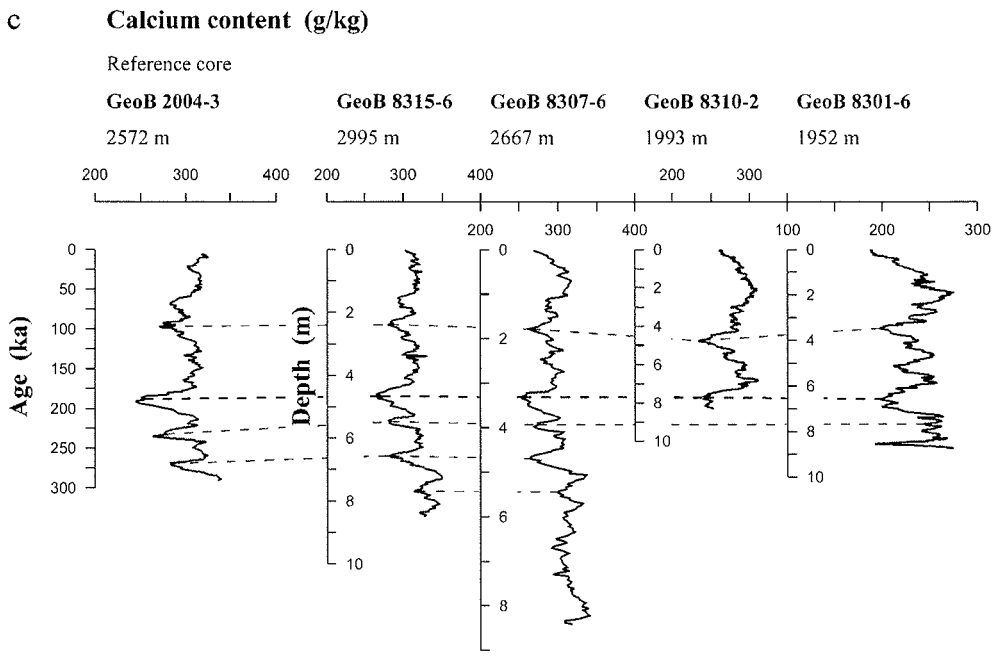

Fig. 12 a-c: Correlation of **a** Fe, **b** Si and **c** Ca profiles between the four study cores analysed onboard with the 100-s method and the reference core GeoB 2004-3 analysed onland with the 100-s method. Peaks which are well correlated are indicated by *dashed lines*. The *bold dashed line* marks the oldest age (190 ka) identified in all five cores in the present study. Depth-integrated sedimentation rates in **a** were estimated up to 190 ka

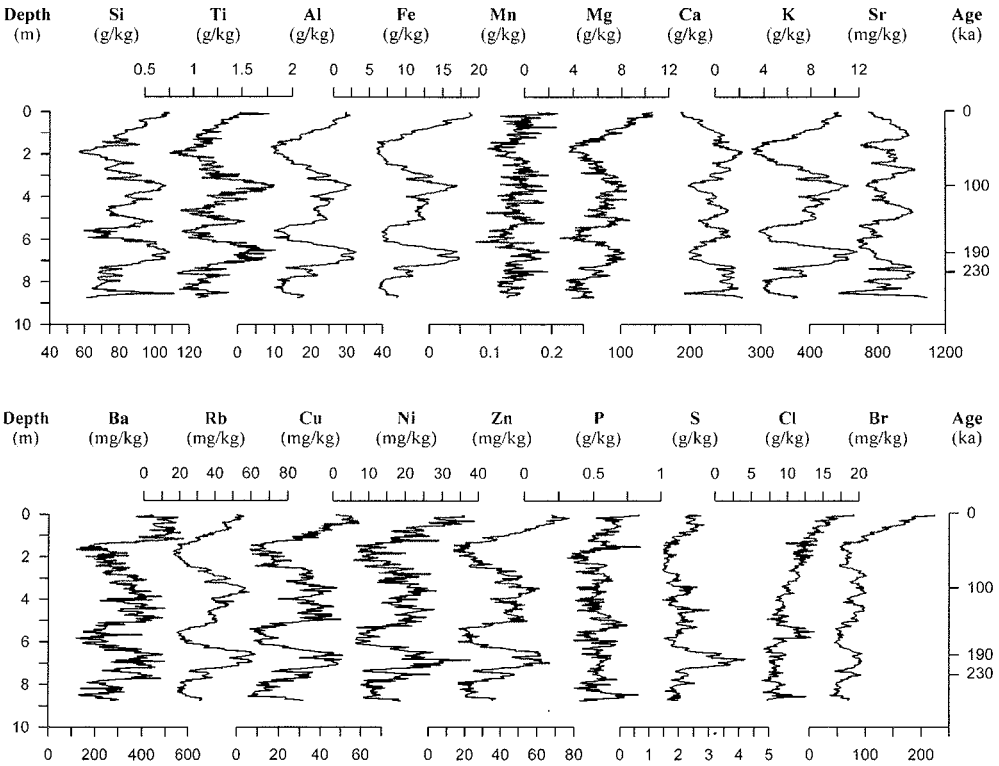

Fig. 13: Downcore variations in 18 elements detected by shipboard 100-s measurements of gravity core GeoB 8301-6. Age model based on correlation with reference cores MD 962085 (Bertrand and Cruise participants 1997; Chen et al. 2002) and GeoB 2004-3

Discussion and conclusions

Shipboard measurements carried out by means of Spectro Xepos were integrated downcore at a resolution of 4 cm, using dry material which had been ground and compressed conveniently by hand. Together with instrument-specific timesaving steps, this enabled us to prepare and analyse more than 200 samples for various elements within 24 h only. By now, the XRF technique has been applied during three RV Meteor cruises to approximately 5000 Late Quaternary sediment samples from altogether 23 gravity cores, 25 multicorer cores and two box cores from the eastern South Atlantic off South Africa / Namibia and the eastern Atlantic off NW Africa.

The findings of the present study convincingly demonstrate a generally excellent agreement between land-based and shipboard datasets. Reproducibility of XRF analyses is good for elements which commonly occur at high levels in marine sediments, such as Si, Al, Fe, Ca, K and Sr. Elements occurring at lower levels, such as Ba and Cu, however, show standard deviations exceeding 5% for both shipboard and land-based analyses. Thus, Spectro Xepos XRF analysis of marine sediments evidently yields the best results for major elements. The quality of the XRF data is only marginally affected by the problem of not being able to determine highly accurate sample weights aboard ship, as long as the amount of sample material is sufficient to fill at least half the sample cup.

Analyses of a pressed pellet of the MAG-1 standard show good accuracy for the minor elements, but major element contents are generally biased towards overestimation. This bias can not be explained by the duration of the measurement (300-s or 100-s measuring time) or by the running of the instrument under stationary or non-stationary conditions. Analyses of a MAG-1 powder sample are in the range of or close to certified values for major elements whereas trace elements tend to be underestimated. Land-based laboratory work with corresponding powder samples and pressed pellets, both of other standard reference materials (Asso, Nod-P1, PACS-1) and sediments from core GeoB 3718-9, showed element contents in pressed pellets to be almost always higher than those in the powder samples (Wien et al., unpublished data). Especially for analysis of major elements, therefore, powder samples are to be preferred whereas analytical quality for minor elements increases by the usage of pressed pellets. Our focus of interest being the major elements as well as a much faster and easier sample preparation is the main argument for using powder samples for shipboard XRF analyses. It should be borne in mind that the absolute values for element contents are based on an internal calibration provided by the Turboquant method. The resulting bias towards over- or underestimating element contents can be easily reduced by subsequent external calibration with element-specific factors.

One reason for the better quality (higher reproducibility) of shipboard 300-s vs. land-based 300-s measurements of the MAG-1 pressed pellet may be linked to the essentially continuous operation

of the Spectro Xepos during the cruise aboard the RV Meteor. Shipboard analyses were performed every day and, if necessary, even overnight during the 3-week M 57-1 cruise (Schneider and Cruise participants 2003). The land-based analyses, on the other side, comprise a time span of 8 months during which the instrument was not operated that often. The high data quality resulting from a tight work schedule is also indicated by the comparison of shipboard 300-s measurements of the MAG-1 pressed pellet with the land-based 300-s measurements of the MAG-1 powder sample. The MAG-1 powder sample was analysed 21 times during a time span of only 8 days, before being processed into the pressed pellet. Reproducibility values are similar for both datasets.

The time-reduced 100-s measuring method is highly suitable for shipboard work because the duration of analysis of 100 samples is reduced from approximately 28 to 11 h. Thus, the method represents a substantial financial saving in terms of manpower and ship costs. Evidently, the high-quality data obtained by onboard 100-s measurements can be used meaningfully for comparisons of elemental profiles between cores. Since data from 300-s and 100-s measurements correspond so well, we have now adopted the 100-s measuring time and the use of powder samples for routine work in our land-based laboratory at Bremen University. Only for more difficult analyses of Ba do we improve analytical quality by using the original 300-s measuring time option. Moreover, for long-term documentation of instrument accuracy and reproducibility, both during shipboard operations and in the land-based laboratory, it is more convenient to use standard reference material in form of pressed pellets rather than powder.

Onboard application of the Spectro Xepos instrument was not limited by stormy weather conditions. During RV Meteor cruise M 57-1, wind speeds exceeded 6 B (12.5 m/s) during 7 days, and swells were ≥2 m during 14 days and ≥3 m during 6 days. Erroneous values may have been caused by stronger than usual movement of the ship at the time of analysis. However, we did not observe an obvious link between outlier data and stormier weather conditions and, besides, outlier data have been observed to a similar extent in the land-based analyses as well.

There are several aspects which argue in favour of the Spectro Xepos analyser aboard a research vessel. The XRF technique can provide fast and reliable data on the elemental composition of sediment cores. It is possible, for instance, to gain immediate information on the distribution of terrigenous versus marine material in continental shelf or margin sediments. These data can be qualitatively and quantitatively linked with terrigenous input, water mass chemistry, atmospheric circulation or ocean currents, and thus are highly important in studies of palaeoclimate, palaeoenvironment and palaeoceanography. For example, onboard XRF measurements were performed during Meteor cruise M 58-1 for the first time on highly disrupted sediment cores retrieved from the continental slope off NW Africa (Schulz and Cruise participants 2003). These sediments are strongly influenced by transport processes such as slides, debris flows and

turbidity currents, one core from an intra-channel site comprising approximately 45% turbidite material. Downcore elemental profiles provided valuable stratigraphic information and thus, reliable age models for emplacement times of debris flows and turbidites, as has already been confirmed by subsequent radiocarbon dating (Wien et al., unpublished data). Thus, XRF data help tremendously to support scientific discussion on processes governing changes in sediment composition, related either to climate or to local sedimentation processes, or both, and this already during the cruise. Since geochemical data are available within 24 h after recovering a sediment core, it is possible for scientists to react quickly to new results by intensifying investigations in the study area before the end of the cruise. Thus, the geochemical data obtained by XRF analysis can guide onsite decisions for mapping and more detailed sampling and, moreover, form a key element of post-cruise studies and perspectives.

The most important advantage of the Spectro Xepos analyser over other well-established logging or scanning tools (e.g. multi-sensor core logger, colour spectrophotometry, XRF core scanner) is its capability to measure absolute element contents in sediments. These data allow interpretation both of absolute element values in a core and their downcore variations and thus, can be directly correlated with environmental processes on a quantitative basis. By contrast, various XRF core scanners provide data on element intensities which basically only mirror downcore variations. In order to use these data on a quantitative basis, they have to be calibrated for each region or suite of cores with reference material analysed with other techniques such as ICP-AES, ICP-MS or AAS.

Elemental composition of the sediment is not affected by alteration due to atmospheric oxygen as, for example, is sediment colour, nor is information lost due to post-depositional reduction diagenesis, as is often observed for magnetic parameters. Moreover, sediment colour and physical properties are composite signals, with sediment colour, for example, depending on a variety of parameters such as mineral composition, species assemblage, organic matter content, bulk density, and also roughness of the scanned sediment surface. Although element content is not entirely unaffected either, interferences are less manifold and transport paths and processes are better known.

Another key advantage of the Spectro Xepos is its small size which allows operation even if shipboard laboratory facilities are limited. Even on smaller vessels, onboard measurements performed immediately after core recovery avoid potential elemental changes, for instance, carbonate dissolution or translocation of Mn, which may be caused during transport and subsequent long-term storage in a core tank.

In the present study, we have shown that shipboard Spectro Xepos XRF analyses can approach the quality of measurements performed under stationary conditions onland. Our future goal is

directed towards a considerable simplification of the sample preparation technique for onboard XRF analysis.

Acknowledgements

Karsten Enneking, Silvana Hessler, Luzie Schnieders and Rainer Zahn are gratefully acknowledged for helping with the laboratory work on the RV Meteor. We owe thanks to the captains and all crew members of the RV Meteor expeditions M 57-1, M 58-1 and M 58-2a & b, and to Ralph Schneider who as chief scientist took care of organisation and the selection of sites during RV Meteor cruise M 57-1. We are grateful to Rik Tjallingi and Christoph Vogt for helpful suggestions throughout this paper, which also benefited greatly from valuable comments by two reviewers. Funded by the Deutsche Forschungsgemeinschaft as part of the DFG-Research Center 'Ocean Margins' of the University of Bremen No. RCOM0206.

2.2 Close correlation between Sr/Ca ratios in bulk sediments from the southern Cape Basin and the SPECMAP record

KATHARINA WIEN, MARTIN KÖLLING AND HORST D. SCHULZ

Department of Earth Sciences (FB 5), University of Bremen, P.O. Box 330440, 28359 Bremen, Germany

Abstract

High-resolution records of Ca and Sr were obtained from shipboard XRF analyses of bulk sediments in five gravity cores from the southern Cape Basin, South Atlantic Ocean. Sr/Ca ratios display regular glacial/interglacial variations of 14-40% and reveal a close correlation with the SPECMAP record, minimum Sr/Ca ratios appearing during glacial ($\delta^{18}O$) maxima, distinct increases during periods of deglaciation, and highest ratios in interstadials. Shifts in carbonate-producing phyto- and/or zooplankton assemblages over glacial/interglacial cycles are suggested to be the main cause for the observed variations in Sr/Ca patterns. Quick assessment of the relationship between Sr/Ca ratios and the SPECMAP record made it possible to easily transfer an age model to the newly collected cores already during the cruise.

Introduction

The oxygen isotope composition ($\delta^{18}O$) of ocean water is determined by variations in the global ice volume, local temperature and salinity (Emiliani 1955; Shackleton and Opdyke 1973). Stacked foraminiferal $\delta^{18}O$ records from low- and mid-latitudinal open ocean sites reveal strong coherency with orbital variations in precession (19 and 23 ka), obliquity (41 ka) and eccentricity (100 ka), and thus monitor oceanic responses to major changes in the global climate (Imbrie et al. 1984; Pisias et al. 1984; Martinson et al. 1987). These $\delta^{18}O$ records have been compiled into the SPECMAP (Mapping Spectral Variability in Global Climate Project) datasets (Imbrie et al. 1984; Martinson et al. 1987), which are widely used to correlate the oxygen isotope profiles of marine sediment cores worldwide and to assign ages to these cores.

In addition to being reflected in Foraminifera $\delta^{18}O$ records, glacial/interglacial sea-level cycles also influence the Sr budget of the ocean (Stoll and Schrag 1996). The amplitude of Sr/Ca variation in modern surface ocean water is less than 2% (de Villiers et al. 1994; de Villiers 1999). By contrast, Sr/Ca variation over Quaternary glacial/interglacial cycles has been reported to be in the range of 1-3% (Stoll and Schrag 1998), and is attributed mainly to the recrystallisation of shelf aragonite into calcite, resulting in increased Sr/Ca ratios during glacial maxima (Schlanger 1988; Stoll and Schrag 1998). Variable incorporation of Sr by carbonate-producing marine organisms is, however, controlled by diverse factors other than only seawater Sr levels. For instance, Sr incorporation by foraminifers and coccolithophores (gold-brown algae) has been suggested to vary on a species-to-species basis (e.g. Elderfield et al. 2000), or with changes in growth and calcification rates (e.g. Stoll and Schrag 2000) respectively. Thus, marine carbonate production, composition and amount of terrigenous components, and recrystallisation and dissolution of carbonate are all important in this context, making it difficult to unambiguously trace any single key cause of Sr/Ca variations in bulk sediments. Nevertheless, Sr/Ca patterns can give valuable insight into biogenic/hydrographic conditions in the geological past.

The southern Cape Basin, South Atlantic Ocean, lends itself well to investigating such aspects. The unique character of this basin results from its location at the southern extremity of the Benguela upwelling system, which is influenced by the intersection of several important water masses and current systems and, therefore, highly variable hydrographic conditions (e.g. Lutjeharms 1996; Shannon and Nelson 1996; Gordon 2003). The complexity of the Benguela system, which interacts at its southern and northern boundaries with the warm water regimes of the Agulhas Current and the Angola Current respectively (e.g. Shannon and Nelson 1996), renders it highly susceptible to shifts in species ranges. Previous studies in this region indicate sometimes subtle responses of various nano- and microfossil groups to changes in productivity, water temperature and water circulation (e.g. Giraudeau 1993; Giraudeau and Rogers 1994; Schmiedl and Mackensen 1997; Gingele and Schmiedl 1999; Abrantes 2000). Since 1981, the interdisciplinary Benguela Ecology Programme (BEP) has been concerned with the shelf and adjacent offshore waters off southern Africa (e.g. Lutjeharms et al. 1995; Boyd and Nelson 1998; Gammelsrød et al. 1998; Nelson et al. 1998; Skogen 1999; Steinke and Ward 2003; Demarcq et al. 2003), and the impacts of physicochemical variability on the shelf environment and its living resources (e.g. Crawford 1998; Mitchell-Innes et al. 1999; Griffiths 2003; Skogen et al. 2003).

RV Meteor cruise M 57-1 to the eastern South Atlantic Ocean was dedicated to the reconstruction of the Late Quaternary climate history of the southern Benguela system, and the influence of Agulhas warm water entrainment from the Indian Ocean into the South Atlantic Ocean (Schneider and Cruise Participants 2003). The primary objective of the present study was to assess any correspondence of Sr/Ca ratios in bulk sediments in the southern Cape Basin with the SPECMAP record (Imbrie et al. 1984, 1989; McIntyre et al. 1989). By correlating these data with a dated reference core, we also aimed to assign an age model to newly collected gravity cores, and this already during the cruise. Within this context, we performed shipboard XRF analyses on bulk sediments from the cores, using the new portable Spectro Xepos analyser (cf. Wien et al. 2005, this issue).

Materials and methods

During RV Meteor cruise M 57-1 in January/February 2003, altogether 19 gravity cores were recovered from the southern (and central) Cape Basin in the southern Benguela upwelling system (Schneider and Cruise Participants 2003). Onboard descriptions of cores from the southern Cape Basin provide evidence of the occurrence of foraminifer-bearing nanofossil ooze in several cases (cores GeoB 8303-6, GeoB 8307-6 and GeoB 8308-1) and, in one core (GeoB 8306-2), the sediment is described as foraminifer- and coccolith-bearing mud (Schneider and Cruise Participants 2003).

The present study is based on data from four of these cores (Table 1; Fig. 1). Core GeoB 8301-6 is composed largely of mud and sand, core GeoB 8307-6 of foraminifer-bearing nanofossil ooze, core GeoB 8310-2 of mud and foraminifer-bearing sandy mud, and core GeoB 8315-6 of foraminifer-bearing mud.

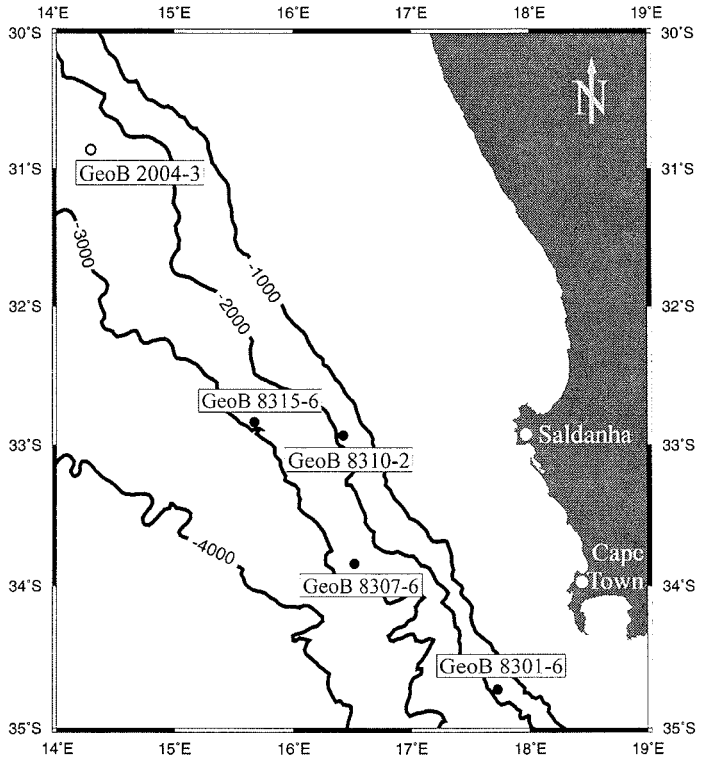

Fig. 1: Locations of the gravity cores in the southern Cape Basin. *Closed circles* selected core positions during RV Meteor cruise M 57-1 (present study), *open circle* position of reference core GeoB 2004-3 (RV Meteor cruise M 23-1)

Table 1: Core number, geographic position, water depth and recovery of the gravity cores in the southern Cape Basin

Core no.	Latitude	Longitude	Water depth (m)	Recovery (m)
GeoB 8301-6	34°46.00′S	17°41.54′E	1,952	879
GeoB 8307-6	33°50.43′S	16°31.99′E	2,667	843
GeoB 8310-2	32°54.57′S	16°22.92′E	1,993	833
GeoB 8315-6	32°53.30′S	15°41.70′E	2,995	851
GeoB 2004-3	30°52.10′S	14°20.50′E	2,572	950

The gravity cores were sampled at regular depth intervals of 4 cm, and the aliquots dried at 200°C in a laboratory oven and ground manually. For the shipboard elemental analyses, approximately 4 g of this material was poured into sample cups, firmly pressed to remove air from the interstices, and analysed using the compact benchtop energy-dispersive polarisation X-ray fluorescence (EDPXRF) analysis system Spectro Xepos (Wien et al. 2005, this issue). In all, 18 elements were measured (Si, Ti, Al, Fe, Mn, Mg, Ca, K, Sr, Ba, Rb, Cu, Ni, Zn, P, S, Cl and Br), only the Sr and Ca data being reported in the present study. Sr/Ca ratios were calculated as

Sr (mg)/Ca (g). All XRF datasets presented here are available on the Pangaea database homepage http://www.wdc-mare.org/PangaVista?query=@Ref25740.

Gravity core GeoB 2004-3, collected in the northern part of the southern Cape Basin in February 1993 during RV Meteor cruise M 23-1 (Spieß and Cruise Participants 1993), had been analysed earlier in the laboratory at Bremen University, using the same analytical method as that aboard ship. In order to use this core as reference during the cruise, it was correlated with the giant piston core MD 962085 collected on the lower slope off Namibia during RV Marion Dufresne cruise NAUSICAA-IMAGES II in October/November 1996 (Bertrand and Cruise Participants 1997). This piston core has been dated based on Foraminifera $\delta^{18}O$ records (Chen et al. 2002). The age model was fitted by comparing colour reflectance data (700 nm) of MD 962085 (Bertrand and Cruise Participants 1997) with XRF Ca data of GeoB 2004-3. Any correlations between the cores were assessed on the basis of linear interpolation between tie points, using the software AnalySeries, version 1.1 (Paillard et al. 1996).

Results

For the combined dataset comprising the five cores GeoB 8301-6, GeoB 8307-6, GeoB 8310-2, GeoB 8315-6 and GeoB 2004-3, average Sr/Ca ratios vary between 3.633 and 3.886 (Table 2). Core-specific variations in Sr/Ca range from 14 to 40%.

The data also suggest a latitudinal gradient in Sr/Ca variations within the southern Cape Basin. Thus, the largest ranges in Sr/Ca ratios were documented in the SE of the study area, the smallest in the NW (cf. Fig. 1; Table 2). Additionally, these variations seem to decrease with increasing water depth (range 1,952-2,995 m for the five cores; Table 1).

Table 2: Bulk sediment Sr/Ca data of all analysed gravity cores in the southern Cape Basin

Core no.	GeoB 8301-6	GeoB 8307-6	GeoB 8310-2	GeoB 8315-6	GeoB 2004-3
Average Sr/Ca (mg/g)	3.633	3.716	3.688	3.751	3.886
Minimum Sr/Ca (mg/g)	2.770	3.078	3.143	3.363	3.599
Maximum Sr/Ca (mg/g)	4.227	4.350	4.128	4.084	4.148
Range (%)	40	34	27	19	14

The Sr/Ca profiles show a close correlation between all analysed cores (Fig. 2). A comparison of these profiles with the SPECMAP record (Imbrie et al. 1984, 1989; McIntyre et al. 1989) reveals good correspondence between the datasets. Thus, the Sr/Ca ratios of all cores correlate inversely with the $\delta^{18}O$ values, this being most visible in core GeoB 8307-6 which goes furthest back in stratigraphy, postdating to approximately 450 ka. Minimum Sr/Ca ratios appear during glacial ($\delta^{18}O$) maxima – for example, a Sr/Ca ratio of 3.2 during oxygen isotope stage (OIS) 2. By contrast, periods of deglaciation are characterised by distinct increases in Sr/Ca ratios, followed

by interstadials which show the highest Sr/Ca values (e.g. Sr/Ca ratios of 3.9 during OISs 1, 5 and 7). In core GeoB 8307-6 at ~50, 270-330, ~480 and ~650 cm, low Sr/Ca ratios correspond to maximum values in the stacked $\delta^{18}O$ record of the SPECMAP profile at 19, 140-150, 250 and 340 ka respectively.

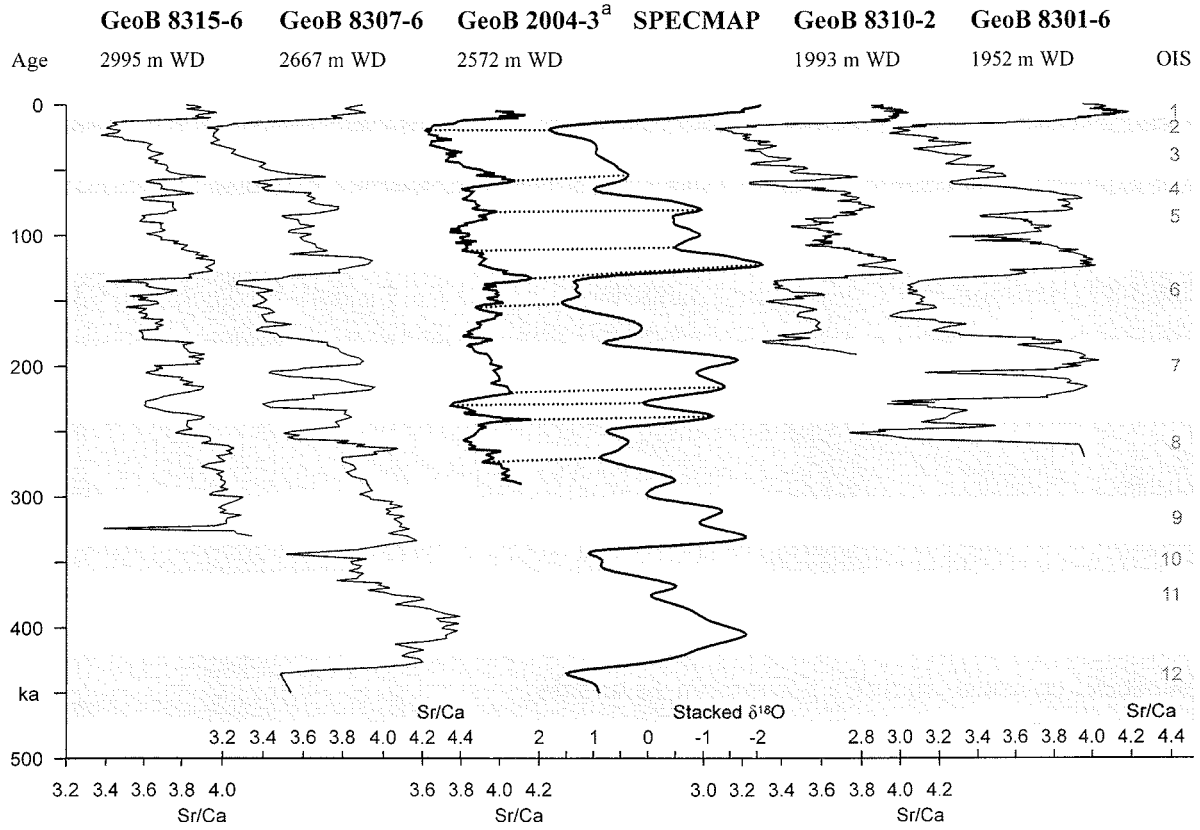

Fig. 2: Correspondence of Sr/Ca ratios (mg/g) in bulk sediments with the SPECMAP record. **a** Core GeoB 2004-3 was recovered during RV Meteor cruise M 23-1 (Spieß and Cruise Participants 1993); the age model is by correlation with core MD 962085 (Chen et al. 2002). The profile for reference core GeoB 2004-3 shows the correspondence of the age model with the SPECMAP record. *Dotted lines* indicate well-correlated peaks. *WD* Water depth, *OIS* oxygen isotope stage

Average sedimentation rates were hindcast to 190 ka, this being the oldest age identified in all five cores combined (Table 3). The values vary between 1.9 and 4.3 cm/10^3 year at the water depths investigated in the present study (cf. Fig. 1, Table 1), and decrease both downslope from the NE to the SW and alongslope from the NW to the SE at the study site. Sedimentation is slower at the deeper sites on the lower slope (1.9-2.7 cm/10^3 year; GeoB 8307-6 and GeoB 8315-6, water depths 2,667 and 2,995 m respectively) than at the shallower sites (3.6-4.3 cm/10^3 year; GeoB 8301-6, GeoB 8310-2 and GeoB 2004-3, water depths 1,952, 1,993 and 2,572 m respectively). A south-eastward decrease of sedimentation rates is obvious when comparing cores from similar water depths but different latitudes alongslope. At water depths of 2,500-3,000 m, values decrease south-eastwards from 3.6 (GeoB 2004-3) through 2.7 (GeoB 8315-6) to

1.9 cm/10^3 year (GeoB 8307-6), and at water depths of 1,950-2,000 m from 4.3 (GeoB 8310-2) to 3.6 cm/10^3 year (GeoB 8301-6).

Table 3: Sedimentation rates for all gravity cores, estimated back to 190 ka

Core no.	Sedimentation rate (cm/10^3 year)
GeoB 8301-6	3.6
GeoB 8307-6	1.9
GeoB 8310-2	4.3
GeoB 8315-6	2.7
GeoB 2004-3	3.6

Discussion and conclusions

The findings of the present study convincingly demonstrate inverse relationships between bulk sediment Sr/Ca ratios and $\delta^{18}O$ values of the SPECMAP record documented in all study cores from the southern Cape Basin. As pointed out above, the main causes of Sr/Ca variations over glacial/interglacial cycles are (1) fluctuations in the input and burial of biogenic carbonate particles of different Sr/Ca ratios, due either to shifts in species assemblages or to changes in growth and calcification rates; (2) selective dissolution of carbonate. Thus, Sr/Ca ratios ultimately preserved in bulk sediments represent a composite signature integrating all these effects.

Variations in species assemblages of biogenic carbonate producers

The location of the southern Cape Basin in an oceanographically complex area (e.g. Shannon and Nelson 1996; Gordon 2003) is associated with biotic responses to surface hydrological variations which reflect global glacial/interglacial cycles (Flores et al. 1999; Rau et al. 2002; Peeters et al. 2004) and additional pulses due to local (Agulhas Current) and regional (Subtropical Convergence and associated subantarctic water masses) ocean dynamics (Rau et al. 2002). Bulk carbonate in the modern ocean is sequestered mainly in coccoliths, foraminifers and, at shallower sites, aragonitic pteropods (e.g. Schiebel 2002). According to onboard descriptions, the dominant carbonate producers in the study cores are coccoliths and foraminifers (Schneider and Cruise Participants 2003).

Former studies on cores recovered from the continental margin off Cape Town, South Africa, report fluctuations in bulk coccolith abundances over glacial/interglacial cycles, with higher values during interglacial OISs 1, 5 and 7, and lower values during glacial OISs 2-4 and 6 (Flores et al. 1999; Boeckel 2003). Among the planktonic Foraminifera, especially the tropical-subtropical Agulhas fauna shows a distinct glacial/interglacial periodicity, higher abundances having been recorded during interglacial periods (Peeters et al. 2004). These fluctuations are in

general agreement with the patterns in Sr/Ca variations documented in the bulk sediments of our cores from the southern Cape Basin.

Variations in growth and calcification rates of biogenic carbonate producers

For many carbonate producers, Sr/Ca variations of shells and skeletons considerably exceed the 1-3% global range proposed for ocean water over the last 100,000s of years (Stoll and Schrag 1998). This results partially from changes in the growth and calcification rates of the different species. Generally, Sr/Ca ratios of coccolith carbonate significantly exceed those for most Foraminifera (Stoll et al. 1999; Stoll and Schrag 2000), nearly by factor 2 (Stoll et al. 2002). Moreover, in various time-series records Foraminifera show less Sr/Ca variability than do coccoliths (e.g. Martin et al. 1999; Stoll et al. 1999; Elderfield et al. 2000; Stoll and Schrag 2000; Shen et al. 2001).

For our study cores, there is some independent evidence that the Sr/Ca signal is affected by fluctuations in coccolith assemblages. Stoll and Schrag (2000) report Sr/Ca variations of nearly 20% over the last 250 ka in the downcore fine "coccolith" fraction from the equatorial Pacific, with minimum Sr/Ca values corresponding to glacial ($\delta^{18}O$) maxima in the composite benthic $\delta^{18}O$ curve of Martinson et al. (1987). These data agree with our findings, in terms of both the range (15-40%) as well as the general trend of Sr/Ca variations (cf. Sr/Ca minima during glacial maxima) in bulk sediments from the southern Cape Basin.

Carbonate dissolution

Species-dependent dissolution of carbonate particles in the water column and on the seafloor (Berger 1970; Berger et al. 1982; Berger and Wefer 1996) may also bias the Sr/Ca ratios of sediments, as does selective dissolution due to different within-species reactivites (e.g. Lohmann 1995; Brown and Elderfield 1996; Stoll et al. 1999). Hence, dissolution may cause sediments to become enriched with resistant species at the expense of more susceptible ones (Berger 1970). Carbonate dissolution is controlled mainly by the positions of the aragonite and calcite lysoclines, both of which varied over glacial/interglacial cycles (e.g. Berger 1977). However, since all our study sites are located in relatively shallow water at ca. 2,000-3,000 m water depth, preservation of coccolith and foraminifer calcite is assumed to be generally good in this case (see also Flores et al. 1999; Boeckel 2003). Pteropods, on the other hand, are known to be only rarely preserved in deep-sea sediments, and may only sporadically be present in deglaciation preservation spikes. In our study area in the southern Cape Basin, it is only during the intense carbonate dissolution event in the early OIS 6 (Bertrand et al. 2002) that the deeper sites GeoB 2004, GeoB 8307 and GeoB 8315 may possibly have been positioned at or below the calcite lysocline and, therefore, have been affected by enhanced carbonate dissolution.

Compared to the highly productive Benguela upwelling system off Namibia, upwelling in the southern Cape Basin is subdued and the region is subjected to incursions from the South Atlantic Current and eddies from the Agulhas retroflection. Moreover, nutrient concentrations decrease southwards in these thermocline waters (Berger et al. 2002). This is consistent with the results of the present study which show that sedimentation rates decrease from the NW to the SE in the study area. By contrast, Sr/Ca variations are highest in the south-eastern part of the southern Cape Basin, and decrease both north-westwards and with increasing water depth. This may reflect a changing influence especially of warm water entrainment from the Indian Ocean at the Agulhas retroflection, coupled with shifts in species assemblages over glacial/interglacial cycles caused by extensions of species distributions beyond present-day warmer regions in the Indian Ocean off south-eastern Africa.

In conclusion, the diversity of factors controlling Sr/Ca variations in bulk sediments in the southern Cape Basin is too complex to be fully deciphered by the data available to date. Further studies need to focus on the complete assemblage of calcareous organisms in this region, and to unravel individual Sr/Ca signals. The most obvious use of the preserved Sr/Ca signal is for correlating and age dating of cores from this region.

Acknowledgements

Karsten Enneking, Silvana Hessler, Luzie Schnieders and Rainer Zahn are gratefully acknowledged for helping with the laboratory work during RV Meteor cruise M 57-1. We thank the captain and crew members of this expedition, and Ralph Schneider who, as chief scientist of this leg, took care of organisation and the selection of sites. This research has benefited greatly from discussions with Syee Weldeab and from many helpful suggestions by W.H. Berger. Funded by the Deutsche Forschungsgemeinschaft as part of the DFG-Research Center 'Ocean Margins' of the University of Bremen project no. RCOM0207.

2.3 Age models for pelagites and turbidites from the Cap Timiris Canyon off Mauritania

KATHARINA WIEN, CHRISTINE HOLZ, MARTIN KÖLLING AND HORST D. SCHULZ

Department of Earth Sciences (FB 5), University of Bremen, P.O. Box 330440, 28359 Bremen, Germany

Abstract

This study of sediments from the Cap Timiris Canyon demonstrates that geochemical data can provide reliable age-depth correlation even of highly turbiditic cores and attempts to improve our understanding of how turbidite emplacement is linked to climatic-related sea-level changes. The canyon incises the continental margin off NW Africa and is an active conduit for turbidity currents. In sediment cores from levee and intrachannel sites turbidites make up 6-42 % of sediment columns. Age models were fitted to all studied cores by correlating downcore element data to dated reference cores, once turbidite beds had been removed from the dataset. These age models enabled us to determine turbidite emplacement times. The Cap Timiris Canyon has been active at least over the last 245 kyr, with turbidite deposition seemingly linked to stage boundaries and glacial stages. The highly turbiditic core from the intrachannel site postdates to ≈ 15 kyr and comprises Holocene and late Pleistocene sediments. Turbidite deposition at this site was associated especially with the rapid sea-level rise at the Pleistocene/Holocene transition. During the Holocene, turbidity current activity decreased but did not cease.

Keywords: submarine canyons; turbidites; sea-level

Introduction

Submarine canyon systems are common on ocean margins and are conduits for channelised mass transport mainly in form of turbidity currents. The resulting depositional pattern is characterised by pelagic sediments interbedded with turbidites (e.g. Bouma, 1962; 2000; Stow and Shanmugam, 1980; Bouma et al., 1985). Various types of turbidite deposition during the Pleistocene and Holocene can be observed along the NW African continental margin (e.g. Simm et al., 1991; Weaver et al., 1992; Masson, 1994; Wynn et al., 2000a; 2000b; 2002), along the NE Atlantic margin (e.g. Davies et al., 1997; Weaver et al., 2000), in the Mediterranean Sea (e.g. Rothwell et al., 1998; 2000; Reeder et al., 2000), or in large turbidite systems such as the Amazon Fan (e.g. Lopez, 2001), the Bengal Fan (e.g. Weber et al., 1997; 2003) and the Zaire Fan (e.g. Babonneau et al., 2002; Droz et al., 2003).

Age dating of these sediments is necessary to obtain information on depositional frequency and emplacement times of the turbidites. However, conventional methods such as oxygen isotope ($\delta^{18}O$) analyses, radiocarbon dating or biostratigraphy are time-consuming and expensive, and indirect dating methods such as geochemical correlation are desirable as tools to fit age models. Pearce and Jarvis (1995), for example, used metre-thick turbidites from the Madeira Abyssal Plain off Morocco as geochemical marker beds and correlated them over distances of > 500 km. The intervening centimetre-thick pelagites were assigned to their corresponding oxygen isotope stages (OISs) based on biostratigraphy.

The main purpose of this paper is to show that geochemical correlation of pelagic sequences can be applied to sediment cores which contain from 6-42 % turbidite layers, and that it is possible to fit age models to these cores by correlation. Cores from the Cap Timiris Canyon in the Atlantic Ocean off Mauritania (Krastel et al., 2004) are suitable to introduce this new method. The canyon was discovered during RV Meteor cruise M 58-1 in April/May 2003 and investigated by combined employment of seismo-acoustic, sedimentological and geochemical techniques (Schulz and Cruise Participants, 2003). In this study we primarily present geochemical data from four sites in the Cap Timiris Canyon, three of which are located on levee structures and one from the interior part of the channel, where sediment was accumulating.

In our approach we created age models for the pelagic sequences in all cores based on their downcore element variations. These were correlated to well-dated variations of the carbonate content in two dated reference records obtained from literature. The age models provide information on frequency and emplacement times of turbidites and hence contribute to our understanding of, and quantify, the processes of turbidity-current generation. Main objectives of this paper are

1) to introduce a method for core-to-core correlation using geochemical data on turbidite-containing cores, and
2) to determine turbidite emplacement times in the cores and assess emplacement to sea-level stand and climatic conditions.

Study site

The Cap Timiris Canyon is an example of an active canyon system off the Mauritanian coast which incises the NW African shelf and continental slope (Krastel et al., 2004). The canyon head abuts the topography-deduced Tamanrasset River System which, although not discharging under present-day climatic conditions, ranks among the largest river systems worldwide. The mouth of this potential river system is located off Cap Timiris whereas its flow pathways, as postulated by Vörösmarty et al. (2000), are now covered by extensive Saharan sand dunes. For the western Sahara Desert in Mauritania, Lancaster et al. (2002) describe three main periods of dune generation from 25-15 kyr, 13-10 kyr and after 5 kyr. The dunes may relate to the Pleistocene/Holocene history of the Tamanrasset River System in that they covered its flow pathways (as is the case today) and accumulated considerable amounts of sand in dry river beds (wadis). This material may have been transported episodically into the ocean, and thereby into the Cap Timiris Canyon, during flash floods.

Channelised gravity-driven mass transport processes deliver sediment from the shelf and upper continental slope to the deep-sea abyssal plain. Today sediment feeding into the canyon mainly derives from eolian dust from the sub-Sahara and Sahel region (Tetzlaff and Wolter, 1980;

Pye, 1987; Wefer and Fischer, 1993) and from intensive biomass production due to upwelling, especially in the proximal parts of the canyon (e.g. Fütterer, 1983; Bertrand et al., 1996; Martinez et al., 1999). Upwelling activity is considered to generally have been most intense during glacial conditions (Diester-Haas and Chamley, 1982). Terrigenous input likewise increased during glacial periods, mainly due to enhanced availability of source material and strength of transporting winds (Matthewson et al., 1995; deMenocal et al., 2000).

Materials

In this study, geochemical analyses were performed onboard during RV Meteor cruise M 58-1 in April/May 2003 (Schulz and Cruise Participants, 2003) on four gravity cores and their corresponding multicorer cores (MUCs) from the Cap Timiris Canyon (Fig. 1 and Table 1). Three of these coring sites are on levee structures (GeoB 8502, GeoB 8506, GeoB 8507) and one at an intrachannel location (GeoB 8509). GeoB 8502 is a pelagic site in the lower reaches of the canyon whereas sites GeoB 8506, GeoB 8507 and GeoB 8509 are under the marginal influence of the organic carbon-rich Cape Blanc depocenter (Bertrand et al., 1996; Martinez et al., 1999). The highly turbiditic core GeoB 8509-2 was recovered from the interior of the Cap Timiris Canyon directly opposite site GeoB 8507, where the channel widens into a NE-SW elongated basin of about 4 km width and 160 m depth relative to the levees. Incised into this basin is a 200-300 m wide gully or thalweg which marks the most active part of the channel (Schulz and Cruise Participants, 2003). It is likely that on exiting the narrow channelised pathway and entering this basin, turbidity currents will lose flow energy, leading to deposition of part of their sediment load. The coarser fraction will settle out of suspension and will be deposited without major erosion of the substrate. This area with sediment accumulation was sampled to ensure intercalation of turbiditic material with pelagic sediments. A detailed bathymetric map of the Cap Timiris Canyon is published in Krastel et al. (2004).

Gravity core GeoB 7919-5, obtained off Cape Blanc during RV Meteor cruise M 53-1c in April/May 2002 (Meggers and Cruise Participants, 2003), was analysed geochemically prior to our cruise in order to provide a master record for use onboard. Its downcore Ca profile was correlated with detailed total carbonate data of core CD 53-30, retrieved from the Cape Verde Terrace, and well-dated back to $\approx$ 290 kyr based on Foraminifera $\delta^{18}O$ records (Matthewson et al., 1995). Core from Ocean Drilling Program (ODP) Site 658C, recovered off Cape Blanc during Leg 108 (Ruddiman et al., 1988), also served as a high resolution reference by supplying a radiocarbon age back to $\approx$ 25 kyr and detailed biogenic carbonate data (deMenocal et al., 2000; Fig. 1 and Table 1).

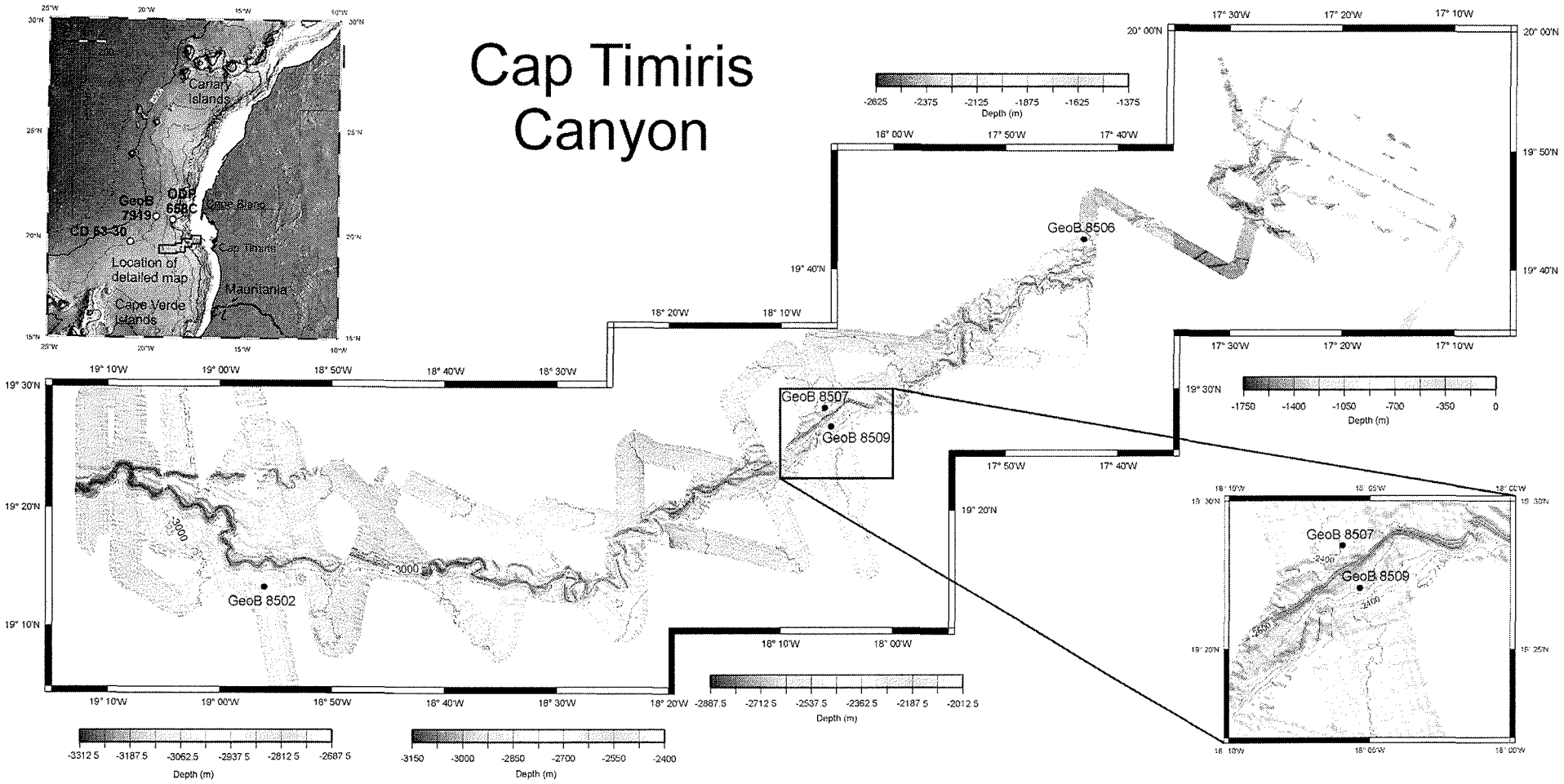

Fig. 1: Overview of the study area. *Upper left*: general map of the Atlantic Ocean offshore NW Africa with locations of the reference cores (*open circles*) GeoB 7919-5 (Meggers et al., 2003), CD 53-30 (Matthewson et al., 1995) and ODP 658C (Ruddiman et al., 1988). *Main map*: locations of selected coring positions (*closed circles*) in the Cap Timiris Canyon during RV Meteor cruise M 58-1 (this study). *Lower right*: close-up view of the intra-channel site GeoB 8509 and the adjacent site GeoB 8507 on the northern levee. Slightly modified from Krastel et al. (2004)

Table 1: Key parameters of cores discussed in this study including core number, geographic position, water depth, location in the canyon system, gear type, recovery and available data. *MUC* = multicorer, *GC* = gravity corer

Core no.	Latitude (°N)	Longitude (°W)	Water depth (m)	Location in canyon system	Gear type	Recovery (cm)	Available data
Cores from the Cap Timiris Canyon							
GeoB 8502-4	19°13.21	18°56.05	2952	levee	MUC	24	XRF; shipboard
GeoB 8502-2	19°13.27	18°56.04	2956	levee	GC	1478	XRF; shipboard
GeoB 8506-1	19°42.56	17°42.94	1828	levee	MUC	30	XRF; shipboard
GeoB 8506-2	19°42.57	17°42.95	1827	levee	GC	1008	XRF; shipboard
GeoB 8507-1	19°28.49	18°05.97	2414	levee	MUC	34	XRF; shipboard
GeoB 8507-3	19°28.50	18°05.97	2411	levee	GC	1000	XRF; shipboard
GeoB 8509-3	19°27.01	18°05.34	2584	intrachannel	MUC	20	XRF; shipboard
GeoB 8509-2	19°27.03	18°05.34	2585	intrachannel	GC	904	XRF; shipboard
Reference cores							
GeoB 7919-5	20°56.41	19°23.38	3420	-	GC	1458	XRF; land-based
CD 53-30	19°42.78	20°42.81	3565	-			total carbonate, oxygen isotope data [a]
ODP 658C	20°45	18°35	2263	-			biogenic carbonate, radiocarbon data [b]

[a] Extracted from Matthewson et al. (1995)

[b] Extracted from deMenocal et al. (2000)

Methods

Land-based and onboard geochemical analyses

Downcore element profiles were determined for the reference core GeoB 7919-5 prior to the cruise at Bremen University on syringe samples in 5 cm intervals. The four gravity cores and their corresponding MUCs from the Cap Timiris Canyon were analysed onboard ship. MUCs were sampled at a resolution of 1 cm for the upper 10 cm and a resolution of 2 cm below this depth. Continuous strips of sediment were collected from the gravity cores in plastic U-channels with a cross-section of 1.5×2 cm and the complete U-channel was sectioned in 4 cm increments. All samples were oven-dried at 200°C for 60 min and ground manually. Reliable contents for eighteen elements (Si, Ti, Al, Fe, Mn, Mg, Ca, K, Sr, Ba, Rb, Cu, Ni, Zn, P, S, Cl and Br) were determined by energy-dispersive polarisation X-ray fluorescence (EDPXRF) spectrometry using a Spectro Xepos instrument. Analytical quality was assessed by daily analyses of a pressed pellet of MAG-1 standard reference material (4 g MAG-1 standard powder + 0.9 g Hoechst Wax; e.g. Govindaraju, 1994). The XRF analytical method employed is described in detail elsewhere (Wien et al., 2005). All geochemical data presented in this study are available on the Pangaea database (www.wdc-mare.org/PangaVista?query=@Ref26537).

Distinction between turbidites and pelagites

Sediments collected from the Cap Timiris Canyon mainly consist of bioturbated pelagic mud and turbidite layers. Yet a visual distinction between the homogenous upper part of a turbidite and the overlying pelagite is often complicated, especially when there is a gradational transition due to bioturbation instead of a distinct discontinuity at the boundary. A multi-proxy approach was used to determine the limits of the turbidites as exactly as possible. Uncertain bed boundaries were fixed by combined visual investigation of the split core together with corresponding X-ray radiographs, and additional information obtained from grain size (Holz, 2005) and geochemical analyses. Several intercalated turbidites could be clearly distinguished from pelagites by their Si/Al or Si/Fe ratios (Fig. 2a-d). Possible occurrence of depositional lamination is commonly obscured by intense bioturbation especially if turbidites are thin (Weaver et al., 1992). Lamination is a certain indicator for turbidite deposits whereas uniformly distributed foraminifera within a sediment interval are an indicator of pelagic sediments.

Prior to geochemical correlation of the sediment cores it was necessary to remove from the dataset all analyses made on turbiditic material. Turbidite boundaries from visual sedimentological investigations (core description; X-ray radiographs) were read off with 0.5 cm accuracy whereas geochemical analyses were done in 4 cm increments. All XRF samples were taken continuously and therefore, sample breaks did not necessarily correspond exactly with observed boundaries between turbidite and pelagite beds. Whenever XRF was performed on a sample containing both sediment types (turbidite/pelagite), it remained within the dataset only if the amount of turbidite material comprised less than half the sample (< 2 cm). The resulting error had no direct influence on the correlation as it only affects the analyses immediately above and below the individual turbidite layers and not the pelagic sequences in between. Only sediments which had been unambiguously identified as turbidites were removed from the dataset whereas material which had neither clear pelagic nor turbiditic signature remained. Consequently, the reported amount of turbidite material is the minimum present.

Core-to-core correlation

The cores from the Cap Timiris Canyon were tied into a stratigraphic framework by correlating their downcore Ca content profiles with carbonate data from the reference cores CD 53-30 (Matthewson et al., 1995) and ODP 658C (deMenocal et al., 2000). Core GeoB 7919-5 was also included as its geochemical data allowed fit of age models for all analysed elements. Since this core was examined pre-cruise using XRF, its whole element suite supplemented carbonate data of the two reference cores. Prior to correlation, MUCs were tied to the tops of their corresponding gravity cores as the core tops of the latter were disturbed by the coring process. The overlapping section was determined on the absolute values of the major elements. The geochemical analyses of the top few centimetres of the gravity core were substituted by the

equivalent higher resolution analyses of the MUC. The MUC tops are defined to have an age of 0 kyr, representing the present sediment surface.

Correlation and fitting of ages to the pelagic intervals of all cores were made by linear interpolation between tie points using the software "AnalySeries", version 1.1 (Paillard et al., 1996). Each turbidite was numbered according to its position within the sedimentary sequence, with T 1 at the top (most recent) and T X at the base. In the following text turbidites will be referred to according to the notation T X-GeoB 85XX. Composite beds where two or more turbidites are deposited directly on top of each other without interbedded pelagites (e.g. T 3-GeoB 8506 in Fig. 2c; T 12-GeoB 8509 in Fig. 2d) are labelled using one number only as it was not possible to decide whether such multiple turbidites were deposited consecutively in the course of one event or during several subsequent events. Therefore, the labels neither reflect the actual number of turbidite events nor the actual number of turbidite layers. The geochemical age model for core GeoB 8509-2 was constrained using nine accelerator mass spectrometer (AMS) radiocarbon dates of monospecific samples of the planktonic foraminifer *Globigerinoides ruber* (Holz, 2005).

Before applying the correlation technique it was necessary to make some assumptions and to assess possible sources of errors. It was assumed that in the study area pelagites and turbidites were and are still accumulating, and that turbidites caused little or nil erosion. Possible sources of error include uncertainties in precisely defining turbidite-pelagite boundaries, and unidentified turbidites (especially thin mud turbidites). Because of these uncertainties care must be taken with correlation of turbiditic cores.

Results

Geochemical analyses

Turbidite position and selected geochemical data for each core from the Cap Timiris Canyon were plotted to assess downcore variations (Fig. 2a-d). There is a clear contrast between the pelagite and turbidite distribution on the levees and at the intrachannel site. The three levee cores GeoB 8502-2, GeoB 8507-3 and GeoB 8506-2 contain relatively little turbidite sediment (≈ 6-8 % of the sediment column). Core GeoB 8509-2 taken from the interior of the canyon comprises approximately 42 % turbidite material (Table 4). The downcore Ca and Al profiles represent compositional variations in the time-series record and, in addition, indicate a frequent element enrichment or depletion in turbidite layers compared to the over- and underlying pelagites. The element ratios Si/Fe and Si/Al in contrast represent the amount of siliciclastic material in the turbidites with respect to the pelagic sediments. Note that turbidite layers are often, though not necessarily, characterised by element contents or element ratios which deviate from the general

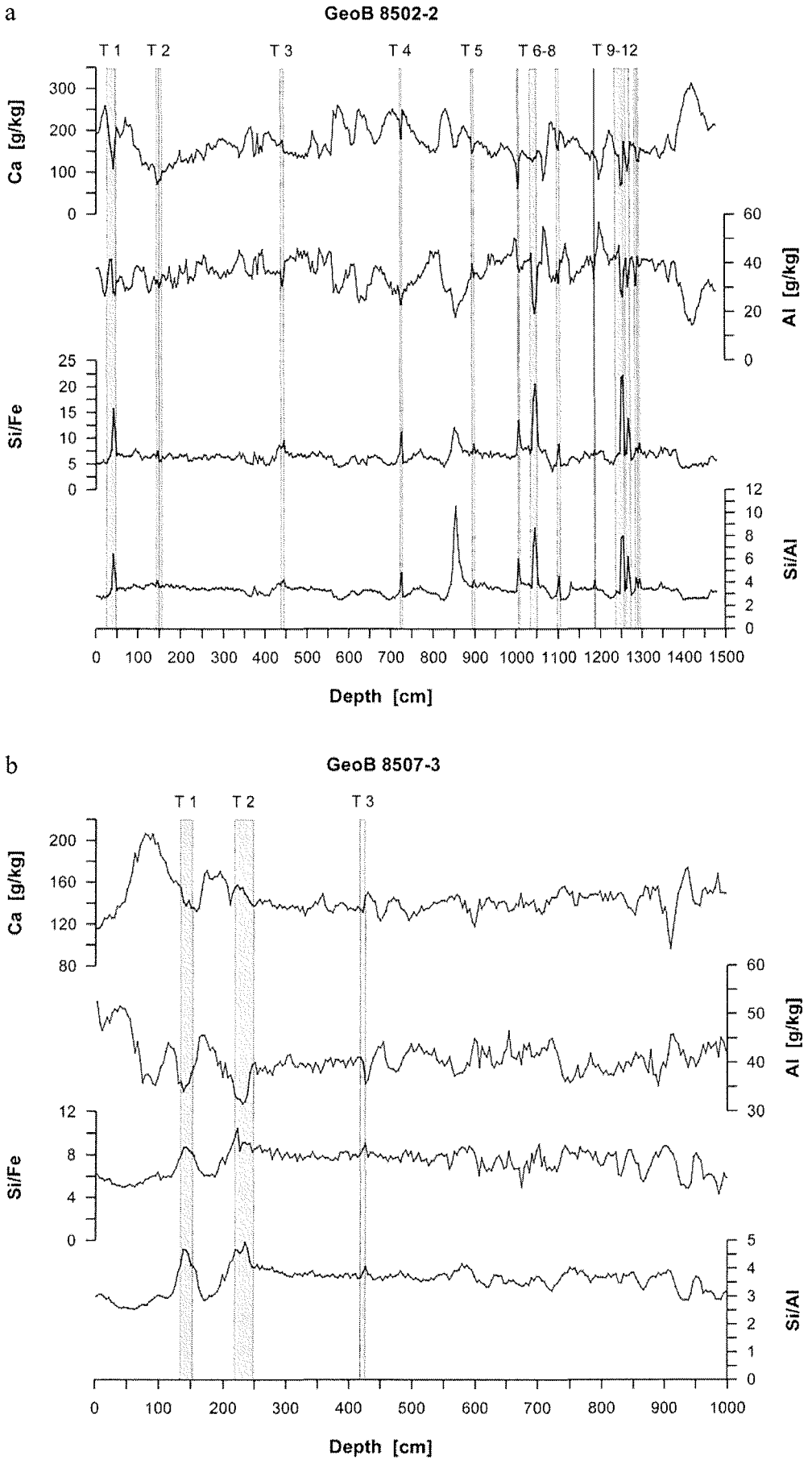

(to be continued)

Figure 2 (continued)

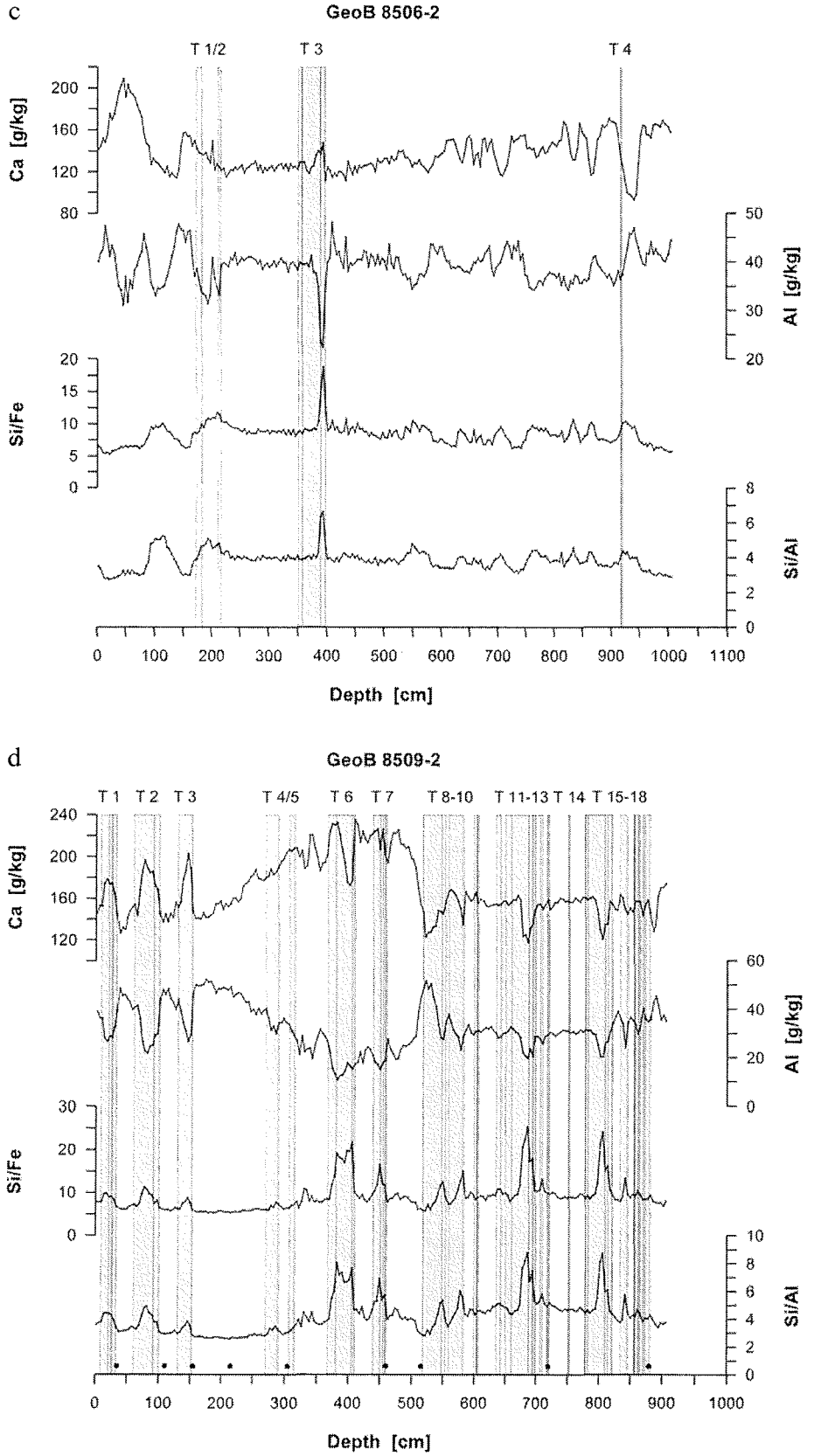

Fig. 2a-d: Ca, Al, Si/Fe and Si/Al downcore profiles in gravity cores from the Cap Timiris Canyon. *Grey bars* mark the positions of the turbidites. Turbidites have been coded by numbers with T 1 being the most recent. *Closed circles* in Fig. 2d indicate the depths selected for AMS ^{14}C analyses in core GeoB 8509-2 (see Holz, 2005)

trend. This is best seen in turbidites T 1-3-GeoB 8509 and T 1, 7, 10, 11-GeoB 8502. Occasionally, Si/Fe and Si/Al ratios pretend the presence of turbidites but this may result from sand-filled burrows which can be distinguished from turbidites by core description and X-ray radiographs (e.g. Si/Al and Si/Fe peaks at 850-870 cm depth in GeoB 8502-2, at ≈ 110 cm depth in GeoB 8506-2).

Age models for the pelagites

An age model was initially fitted from the $\delta^{18}O$ dated reference core CD 53-30 (Matthewson et al., 1995) via GeoB 7919-5 to GeoB 8502-2 by correlation of total carbonate and downcore Ca variation (Fig. 3). All three cores extend from the present to nearly 290 kyr. The geochemical data suggest a hiatus is present in the lower part of GeoB 8502-2 (indicated by a question mark in Fig. 3). This hiatus comprises nearly the entire OIS 7 and occurs at the same stratigraphic position where a hiatus of approximately 37 kyr is recorded in core CD 53-30. The latter is probably due to an erosive event which deposited a thin turbidite layer (Matthewson et al., 1995). However, no mass gravity deposit is seen in core GeoB 8502-2.

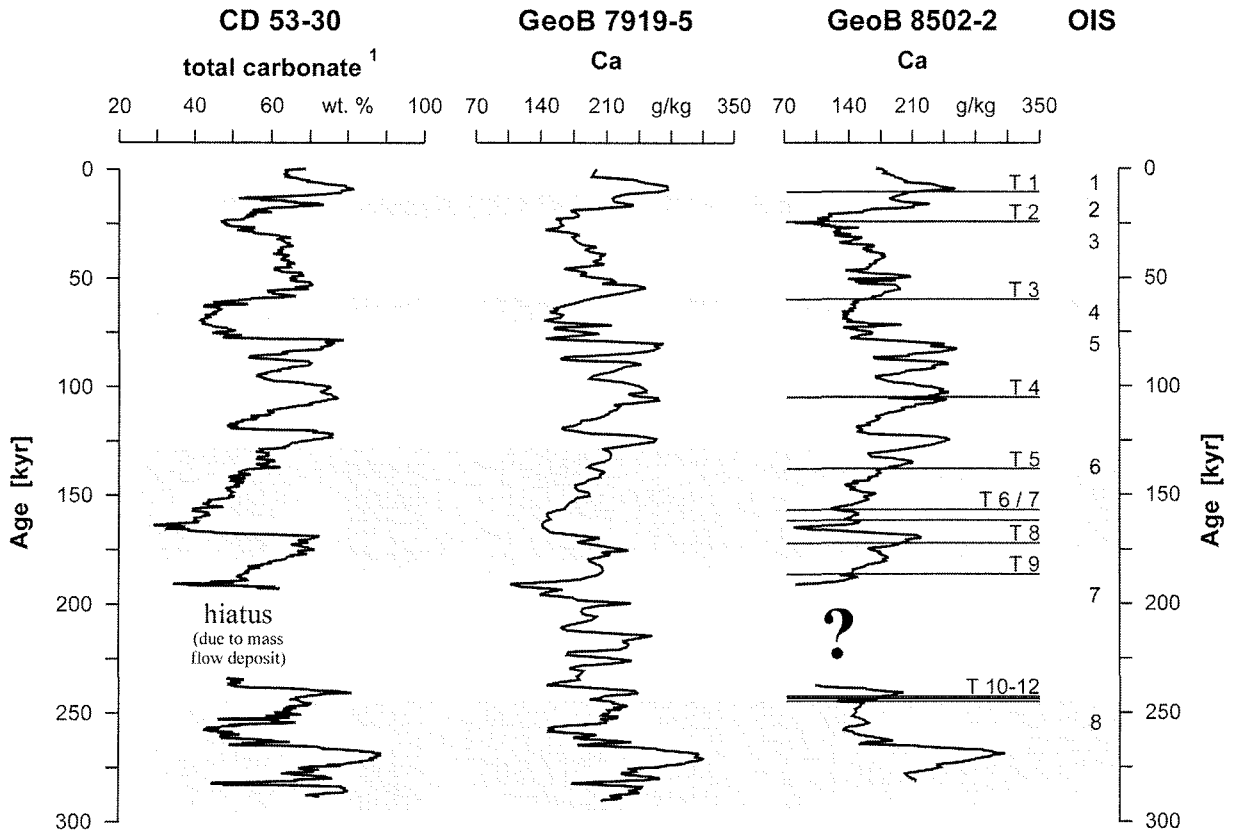

[1] Extracted from Matthewson et al. (1995)

Fig. 3: Correlation of the cores CD 53-30 (Matthewson et al., 1995), GeoB 7919-5 and GeoB 8502-2 based on total carbonate and Ca data. T 1 to T 10 mark the downcore positions of turbidites present in core GeoB 8502-2. The question mark indicates the interval where part of the sediment in this core is presumed to be missing. A hiatus at the same stratigraphic position in reference core CD 53-30 is due to erosion by a mass gravity flow

The Ca record of the pelagites from the intrachannel core GeoB 8509-2 was correlated with ODP Core 658C, taking advantage of its detailed biogenic carbonate record for the last 25 kyr (deMenocal et al., 2000; Fig. 4). Note that only the last 14.8 kyr of ODP 658C carbonate data are shown in Fig. 4 as there is a hiatus between 14.8 and 17.4 kyr. According to the correlation, GeoB 8509-2 dates back to ≈ 15 kyr. This age model agrees with the radiocarbon data (Holz, 2005) for the last 5 kyr, however, discrepancies of up to 1.9 kyr between the radiocarbon data and the fitted age model are seen in the lower part of the core. Four radiocarbon ages are younger than would be predicted by the correlation and one is older (Table 2).

The cores GeoB 8506-2 and GeoB 8507-3 were adjusted using their Ca and Al data (Figs. 5 and 6), and fitted with age models by correlation with GeoB 8502-2. This correlation is reliable for the upper two distinct Ca peaks in cores GeoB 8506-2 and GeoB 8507-3 which date back to ≈ 20 kyr. Below these peaks, correlation up to ≈ 55 kyr was more difficult as the Ca content profiles lack significant peaks. Lastly, Ca profiles from all cores from the Cap Timiris Canyon were plotted as shown in Fig. 6.

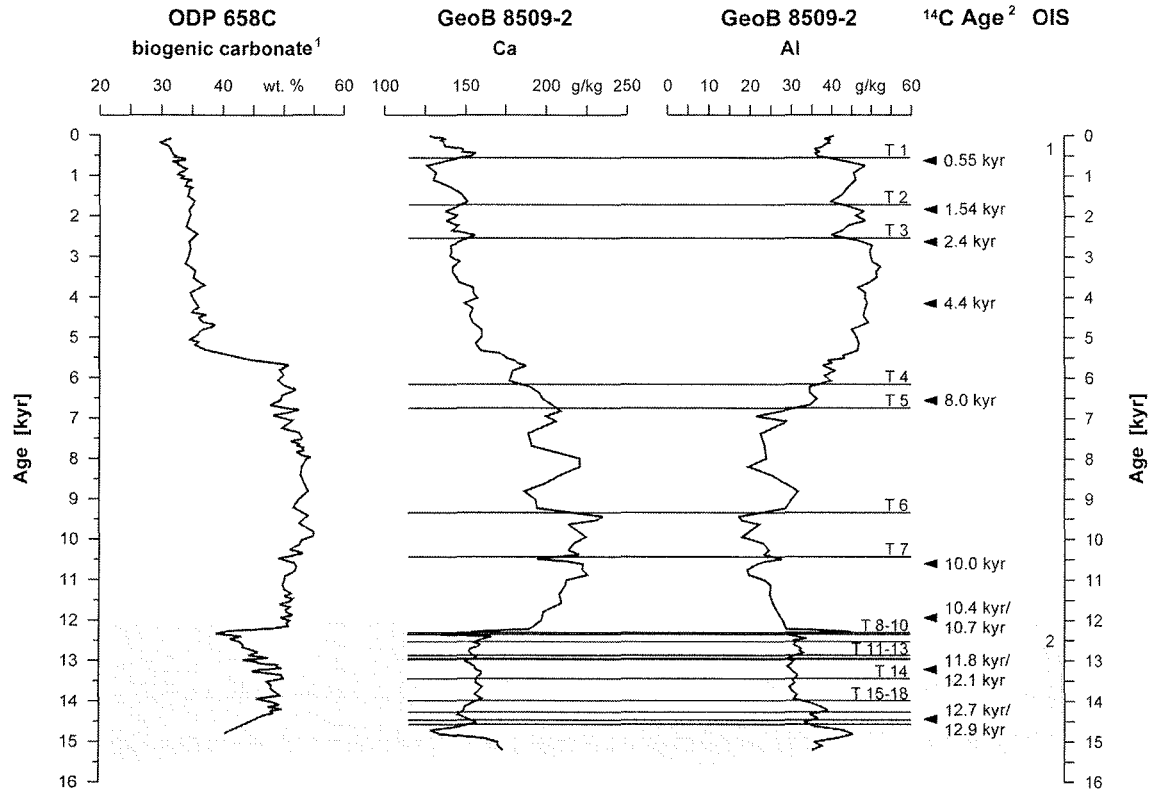

[1] Extracted from deMenocal et al. (2000)

[2] Extracted from Holz (2005)

Fig. 4: Correlation of GeoB 8509-2 Ca data with biogenic carbonate data for the upper 3.3 m (the last 14.8 kyr) of the reference core from ODP Site 658C (deMenocal et al., 2000). Also shown is the Al record of GeoB 8509-2 which mirrors the Ca content profile. The positions of the AMS ^{14}C analyses in core GeoB 8509-2 are indicated by *arrows*. Theses ages agree for the last 5 kyr, however, discrepancies can be observed at older time. AMS ^{14}C data from Holz (2005)

Table 2: Discrepancies between radiocarbon data and fitted age model at five depths in core GeoB 8509-2

Depth (cm)	Radiocarbon age (kyr)	Geochemical age model (kyr)	Discrepancy (kyr)
305	8.0	6.7	1.3
460	10.0	10.4	0.4
515	10.4 / 10.7	12.2	1.8 / 1.5
720	11.8 / 12.1	13.0	1.2 / 0.9
881	12.7 / 12.9	14.3	1.6 / 1.4

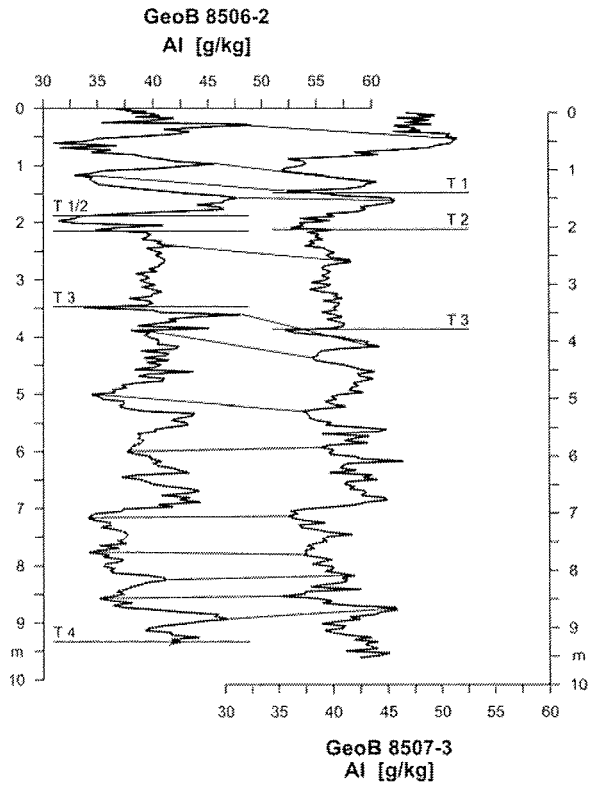

Fig. 5: Correlation of downcore Al data on the cores GeoB 8506-2 and GeoB 8507-3

Turbidite emplacement times

As can be seen in Figs. 3 and 6, turbidity currents delivered sediments predominantly at stage boundaries and during glacial periods. Turbidites at the levee sites GeoB 8502, GeoB 8507 and GeoB 8506 were emplaced at transitions from glacial to interglacial/interstadial, and at transitions from interglacial/interstadial to glacial. Eight turbidites are at mid-stage positions during glacial OISs 6 and 2. Only T 4-GeoB 8502 and T 4-GeoB 8506 were deposited during interglacial OIS 5 and interstadial OIS 3 respectively.

A clear contrast can be seen at intrachannel site GeoB 8509 where most turbidites (T 18-8-GeoB 8509) are linked to late glacial OIS 2 and the stage boundary 1/2 whereas the remainder (T 7-1-GeoB 8509) was deposited during Holocene time (OIS 1). The three most recent turbidites at this site were emplaced ≈ 0.5, 1.7 and 2.5 kyr ago. Owing to the very different ages and thus, sedimentation rates of the four study cores, it was rarely possible to link intrachannel turbidites and overspill turbidites on the levees across the Cap Timiris Canyon. Only four examples where two or three deposits may be related to the same turbidite event were recognised at ≈ 10 kyr, at ≈ 14 kyr, at 17-18 kyr and at 24-25 kyr (Fig. 6 and Table 3).

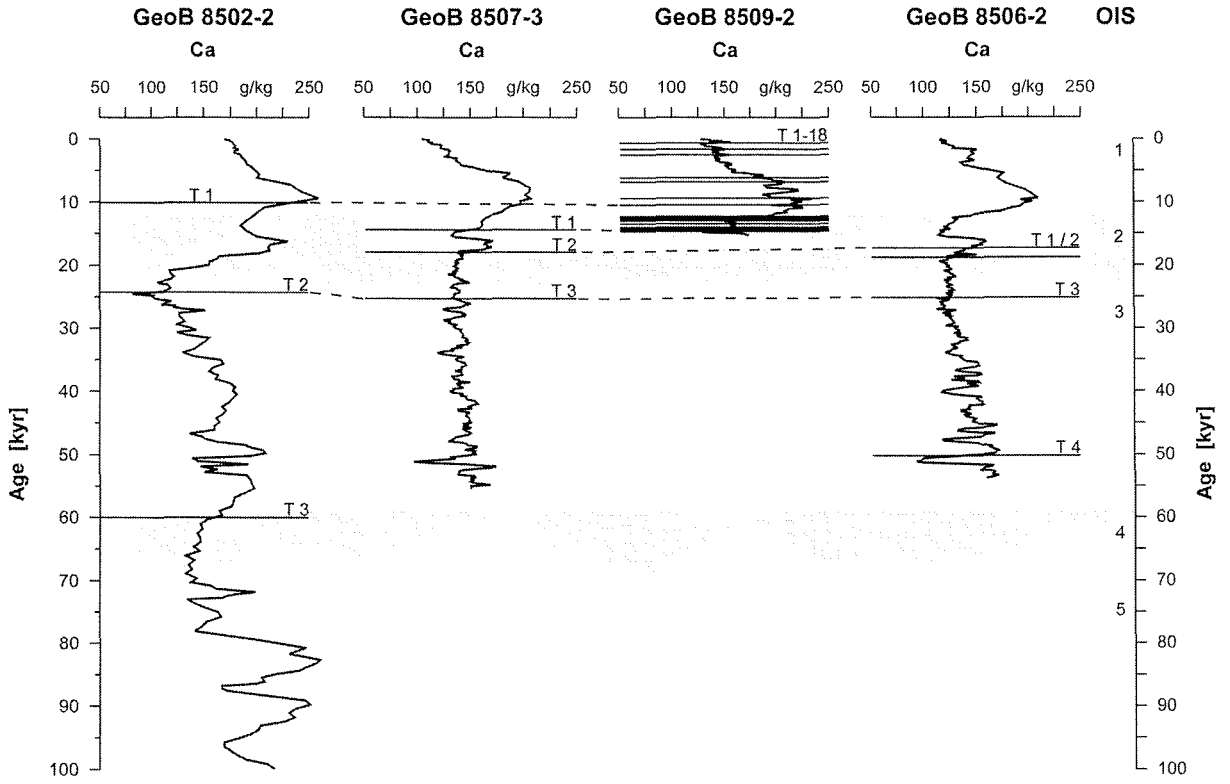

Fig. 6: Age models for the four cores GeoB 8502-2, GeoB 8507-3, GeoB 8509-2 and GeoB 8506-2 from the Cap Timiris Canyon based on correlation of their downcore Ca content profiles. *Dotted lines* indicate well-correlated turbidite layers. The entire length of core GeoB 8502-2 is not shown but for illustration purposes only the interval back to an age of 100 kyr

Pelagic and turbidite sedimentation rates

Average sedimentation rates were determined from these age models for the pelagic and intercalated turbidite beds of all study cores (Table 4). Note that in this study all sedimentation rates have been calculated over the entire core lengths and not back to a certain age, owing to the very different time-resolutions of the cores. For the three levee sites, pelagic sedimentation rates vary significantly, being lowest (≈ 7.0 cm/kyr) at the deepest site GeoB 8502 and increasing significantly upslope nearly three-fold to 17-18 cm/kyr at sites GeoB 8507 and GeoB 8506. The most prominent shift, however, occurs at the intrachannel site GeoB 8509 (≈ 35 cm/kyr) where pelagic sedimentation rates are doubled compared to the directly adjacent levee site GeoB 8507.

Turbidite sedimentation rates are low (between ≈ 0.7 and 1.2 cm/kyr) at the levee locations, but show much higher average values of ≈ 25 cm/kyr at the intrachannel site. Owing to the temporally very different turbidite abundances at the latter location, sedimentation rates were calculated separately for the Holocene (0-12 kyr) and the late Pleistocene (12-15.2 kyr). The values indicate that the pre-Holocene turbidites at the intrachannel site had accumulated at an average rate of approximately 64 cm/kyr with an average recurrence interval of ≈ 300 years. In

contrast, average sedimentation rates for Holocene turbidites are much lower (≈ 15 cm/kyr) with a recurrence interval of ≈ 1.7 kyr in average (Fig. 4).

Table 3: Core number, location in the canyon system, turbidite notation, turbidite depth and turbidite emplacement time in all study cores from the Cap Timiris Canyon as determined from the geochemical age models

Core no.	Location in canyon system	Turbidite no.	Turbidite depth (cm)	Turbidite emplacement time (kyr)
GeoB 8502-2	levee	T 1	25 – 46	10.1
		T 2	142 – 155	24
		T 3	437.5 – 445	60
		T 4	722 – 727	105
		T 5	892 – 898	138
		T 6	1005 – 1009	157
		T 7	1034 – 1050	162
		T 8	1096.5 – 1103	172
		T 9	1184.5 – 1186.5	188
		T 10	1234.5 – 1254.5	243
		T 11	1259 – 1271	243
		T 12	1282 – 1293	245
GeoB 8506-2	levee	T 1	172 – 182	17.3
		T 2	211 – 216	18.9
		T 3	350 – 397	25
		T 4	918 – 919	50
GeoB 8507-3	levee	T 1	133 – 151	14.4
		T 2	217 – 247	17.9
GeoB 8509-2	intrachannel	T 1	8 – 32	0.5
		T 2	60 – 100	1.7
		T 3	129 – 152.5	2.5
		T 4	269 – 289	6.1
		T 5	306 – 314	6.7
		T 6	366 – 409	9.3
		T 7	438 – 459	10.4
		T 8	517 – 553	12.3
		T 9	557.5 – 581.5	12.3
		T 10	598 – 605	12.5
		T 11	634 – 642	12.9
		T 12	649 – 710	12.9
		T 13	717 – 719.5	13.0
		T 14	750 – 752	13.4
		T 15	777 – 780.5	14.0
			782 – 820	
		T 16	833 – 844.5	14.3
		T 17	855 – 856.5	14.5
			857.5 – 861.5	
			862.5 – 865	
		T 18	868.5 – 871.5	14.6
			873.5 – 880	

Core GeoB 8509-2 from the interior part of the Cap Timiris Canyon shows a change in sediment geochemistry between ≈ 5.2 and ≈ 3.0 m depth which corresponds to the age between ≈ 12.3 and ≈ 6.5 kyr. This change is clearly visible in the Ca and Al content profiles (Figs. 2d and 4) where Ca shows a shift to higher and Al a depletion to lower values between 5.2 and 3.0 m.

Table 4: Core number, location in the canyon system, percent of sediment column made up of turbidites, maximum ages and average pelagic and turbiditic sedimentation rates. Sedimentation rates were calculated from the maximum age at the base of each core instead of a corresponding age for all cores. Average pelagic sedimentation rates for core CD 53-30 are from Matthewson et al. (1995); for core ODP 658C from deMenocal et al. (2000)

Core no.	Location in canyon system	Percent of sediment column made up of turbidites (%)	Maximum age at base of core (kyr)	Average pelagic sedimentation rates (cm/kyr)	Average turbidite sedimentation rates (cm/kyr)
CD 53-30	-	-	≈ 290	2.4; variation between 1.5-5.6	-
GeoB 7919-5	-	-	≈ 290	4.6	-
ODP 658C	-	-	≈ 25	18	-
GeoB 8502-2	levee	8	≈ 190 [a] (?280 [b])	7.0 [a]	0.7 [a]
GeoB 8507-3	levee	6	≈ 55	17	0.9
GeoB 8506-2	levee	6	≈ 55	18	1.2
GeoB 8509-2	intrachannel	42	≈ 15	35 (28 [c]; 63 [d])	25 (15 [c]; 64 [d])

[a] At ≈ 12 m core length

[b] At ≈ 14.8 m core length

[c] From 0-12 kyr

[d] From 12-15.2 kyr

Discussion

Turbidite emplacement in the Cap Timiris Canyon

Indirect dating has allowed ages of emplacement to be assigned to each turbidite unit and thus allows estimation of the frequency of turbidite emplacement in the Cap Timiris Canyon. Turbidites in the lower part of core GeoB 8502-2 suggest that the Cap Timiris Canyon was active for at least the last 245 kyr. On this time scale, the data, especially on the three levee cores, suggest turbidite activity was controlled by sea-level fluctuations over the last glacial-interglacial cycles. Turbidity currents seem to have been preferentially triggered at stage boundaries at changes from one climatic regime to another, accompanied both by sea-level changes (cf. Weaver and Kuijpers, 1983; Weaver and Rothwell, 1987; Simm et al., 1991; Rothwell et al., 1992; Weaver et al., 1992; Lopez, 2001; Wynn et al., 2002) and perhaps changes in the ocean current system during sea-level low-stands (cf. Shanmugam and Moiola, 1982; 1984; Stow et al., 1984; Posamentier and Vail, 1988; Lopez, 2001).

The most detailed record of turbidity current activity at the transition from the last glacial to the Holocene is preserved in the intrachannel core GeoB 8509-2. The Ca record of this core corresponds to the carbonate record of the reference core from ODP Site 658C where shifts in sediment composition indicate the onset and termination of the African Humid Period (14.8 and 5.5 kyr) and the termination of the Younger Dryas cool period (12.3 kyr; deMenocal

et al., 2000). Turbidites at site GeoB 8509 clearly accumulated during the end of the last glacial period and occur with an average emplacement frequency of 1 event every 300 years from the beginning of the African Humid Period until the end of the Younger Dryas cool period. These events occured during the deglaciation and the rapid sea-level rise at the Pleistocene/Holocene transition. Turbidity current activity in the Cap Timiris Canyon decreases, but does not cease, during the Holocene and therefore, provides an example for continued mass transport at a time of high sea-level, as has also been noted in other turbidite settings (e.g. Weber et al., 1997; 2003; Babonneau et al., 2002; Wynn et al., 2002; Droz et al., 2003).

The correlation of core GeoB 8509-2 with ODP Site 658C highlights a discrepancy between the geochemical age model and the radiocarbon ages especially in the lower half of the core. The higher radiocarbon age of 7.95 kyr (geochemical age model: 6.7 kyr) may possibly be explained by supply of older material from the upper slope through a turbidite event. This explanation, however, can not be applied to the radiocarbon ages which are younger than predicted by the correlation. However, for the purpose of correlation the ODP 658C carbonate data were the most appropriate choice because this site is located close to the Cap Timiris Canyon at a similar water depth as GeoB 8509. The high resolution carbonate profile of this reference core for the last 25 kyr allowed the best fit of an age model to our study core GeoB 8509-2.

Turbidity current activity in the Cap Timiris Canyon often coincides with other reported mass transport events along the NW African continental margin and in the Mediterranean Sea (Table 5). Deposition of turbidite T 2-GeoB 8502 at 24 kyr, for example, corresponds to the emplacement of the Balearic Basin Megaturbidite in the western Mediterranean Sea around 22 kyr at the height of the last glacial maximum (Rothwell et al., 2000). At this time, sea-level approached its lowest stand during the last 130 kyr, approximately -120 m relative to the present (Shackleton, 1987). Turbidite T 3-GeoB 8502 (60 kyr) occurs at approximately the same time as the Saharan Debris Flow (60 kyr; Gee et al., 1999) and turbidites *d* on the Madeira Abyssal Plain (Rothwell et al., 1992; Weaver et al., 1992), *AB5* in the Agadir Basin (Wynn et al., 2002) and *Se* on the Seine Abyssal Plain (Davies et al., 1997) which were emplaced 59 kyr ago at the stage boundary 3/4. Deposition of turbidite T 8-GeoB 8502 at 172 kyr is almost synchronous with a $\approx$ 170 kyr old slide that onlaps a distal part of the canyon (Krastel et al., 2004). However, apparent synchronous emplacement of turbidites in the Cap Timiris Canyon with mass flow deposits from different source areas suggests temporal episodes of instability and deposition of separate events closely spaced in time. Mass flow deposits from other regions do not correlate with the turbidites in the Cap Timiris Canyon.

Sea-level control on turbidite emplacement

Sea-level changes seem to be important driving forces for the advective sediment flux through a canyon. Our data support findings in this regard, and even though they do not furnish information on the underlying physical mechanisms, which are to date still poorly understood, we may speculate about these mechanisms. Relative sea-level changes control the accommodation space available for sediments (e.g. Posamentier et al., 1988; Posamentier and Vail, 1988; Vail et al., 1991), and within this context, several factors may possibly govern the stability of the accumulated sediment masses on a passive continental margin. Sea-level fall, for one, causes enhanced sediment transport to the shelf edge, thereby inducing depositional oversteepening of the slope. Once the sea-level falls below the shelf break a loss of buoyancy in the upper slope sediments may promote slope instability. Sea-level changes also influence the hydrostatic pressure on a sediment column. Excess pore water pressure in the near-surface sediments may, for example, result from low permeability of overlying sediments and/or high sedimentation rates (e.g. Einsele et al., 1996). In addition, sea-level changes may induce changes in the circulation pattern and hydrological properties of the bottom (e.g. contour) currents which can undercut the foot of the slope and erode, mould, transport and redistribute sediments (cf. Simm et al., 1991; Einsele, 1996; Weaver et al., 2000; Imbo et al., 2003). The magnitude of sea-level change has further been suggested to broadly correlate with the volume of turbidites on the Madeira Abyssal Plain (Weaver and Rothwell, 1987).

Sedimentation rates in the Cap Timiris Canyon

The large range of average pelagic sedimentation rates recorded at the four core sites in the Cap Timiris Canyon reflects their different depositional environments and different response to factors such as terrigenous input, regional productivity, or dynamic settings within the canyon system. All sites receive high eolian input due to their positions below the African dust plume (Tetzlaff and Wolter, 1980; Pye, 1987; Wefer and Fischer, 1993). However, site GeoB 8502 is located in a deeper, more distal part of the canyon well outside the high-productivity upwelling region off Cape Blanc. Consequently, sediments here show less high pelagic sedimentation rates of $\approx$ 7.0 cm/kyr which are similar to values of $\approx$ 4.6 cm/kyr in core GeoB 7919-5 and $\approx$ 1.5-5.6 cm/kyr in core CD 53-30 (Matthewson et al., 1995).

Higher sedimentation rates are seen at the levee sites GeoB 8506 and GeoB 8507. Both sites are positioned in the more proximal part of the canyon and receive higher aeolian input from the African dust plume. Additionally, they are under the marginal influence of the upper slope Cape Blanc depocenter which today extends northwards from approximately 20° to 22°N between 1000 and 2000 m water depth (Fütterer, 1983; Bertrand et al., 1996; Martinez et al., 1999). For ODP Site 658C, which is located $\approx$ 1° further to the north off Cape Blanc at a water depth of 2263 m, an average sedimentation rate of $\approx$ 18 cm/kyr is reported by deMenocal et al. (2000).

Table 5: Compilation of mass gravity flows that coincide with turbidites in the Cap Timiris Canyon. Synchronous units may have been triggered at the same sea-level/climatic conditions but they are not correlative with the turbidites in the Cap Timiris Canyon. *AB* = Agadir Basin, *MAP* = Madeira Abyssal Plain, *SAP* = Seine Abyssal Plain, *LGM* = Last Glacial Maximum

Turbidite no. in GeoB 8502-2	**Emplacement time (kyr)**	**Turbidite no. in GeoB 8506-2**	**Emplacement time (kyr)**	**Turbidite no. in GeoB 8507-3**	**Emplacement time (kyr)**	**Turbidite no. in GeoB 8509-2**	**Emplacement time (kyr)**	**Emplacement synchronous with ...**	**Climate/sea-level changes**
						T 1	0.5	Turbidite *a*, MAP (< 1 kyr) [a, b] Turbidite *AB1*, AB (< 1 kyr) [c]	
						T 2	1.7		
						T 3	2.5		
						T 4	6.1		
						T 5	6.7		
						T 6	9.3		
T 1	10.1					T 7	10.4		
						T 8	12.3	Turbidite *b*, MAP (12 kyr) [d, b]	stage boundary 1/2 (12 kyr);
						T 9	12.3	Turbidite *AB2*, AB (12 kyr) [c]	Termination I;
						T 10	12.5	Turbidite Sc, SAP (12 kyr) [h]	rapid sea-level rise at
						T 11	12.9	Mauritanian Slide Complex (≈ 11-14 kyr) (own	Pleistocene/Holocene transition
						T 12	12.9	unpublished data)	
						T 13	13.0		
						T 14	13.4		
						T 15	14.0		
				T 1	14.4	T 16	14.3	Canary Debris Flow (15 kyr) [e]	
						T 17	14.5		
						T 18	14.6		

(to be continued)

Table 5 (continued)

		T 1 T 2	17.3 18.9	T 2	17.9				lowest sea-level (-120 m) during Weichselian glaciation [f]
T 2	24	T 3	25					Balearic Basin Megaturbidite (≈ 22 kyr) [g] Turbidite *AB3*, AB (24 kyr) [c] Turbidite *Sd*, SAP (24 kyr) [h] Herodotus Basin Megaturbidite (≈ 27 kyr) [i, g]	stage boundary 2/3 (24 kyr); rapid sea-level lowering to its lowest stand (-120 m) during Weichselian glaciation [f]
		T 4	50						
T 3	60							Turbidite *d*, MAP (59 kyr) [d, a] Turbidite *AB5*, AB (59 kyr) [c] Turbidite *Se*, SAP (59 kyr) [h] Saharan Debris Flow (60 kyr) [j]	stage boundary 3/4 (59 kyr)
T 4	138							Turbidite *AB13*, AB (130-190 kyr) [c] Turbidite *Si*, SAP (130 kyr) [h]	rapid sea-level lowering to its lowest stand (-150 m) during Saalian glaciation [k]
T 5 T 6 T 7	157 162 172							Cape Blanc Debris Flow (155 kyr) (own unpublished data) major sediment slide onlapping the levees of the distal Cap Timiris Canyon (170 kyr) [l]	
T 8	243							Turbidite *i*, MAP (245 kyr) [d, a] Turbidite *Sr*, *Ss*, SAP (244 kyr) [h]	stage boundary 7/8 (245 kyr); Termination III
T 9 T 10	243 245								

From [a] Weaver et al. (1992); [b] Weaver and Thomson (1993); [c] Wynn et al. (2002); [d] Rothwell et al. (1992); [e] Masson (1996); [f] Shackleton (1987); [g] Rothwell et al. (2000); [h] Davies et al. (1997); [i] Reeder et al. (2000); [j] Gee et al. (1999); [k] Chappell and Shackleton (1986); [l] Krastel et al. (2004)

This value agrees with our findings for sites GeoB 8506 and GeoB 8507. According to our age model, average pelagic sedimentation rates appear to be doubled at site GeoB 8509 with respect to the directly adjacent levee structure (site GeoB 8507). These high sedimentation rates at site GeoB 8509 provide a detailed temporal resolution for determining turbidite emplacement times.

High productivity off Cape Blanc and the African dust plume principally account for the increased average pelagic sedimentation rates at the levee sites in the canyon system. High sedimentation may also be attributed to turbidite overspill which results from separation from a turbidite flow during downslope transport. The sandy bedload is restricted to the canyon pathway whereas the fine grained suspended fraction may be unconfined and can overspill onto the adjacent levee structures (Masson, 1994; Wynn et al., 2002). This laterally dispersed mud on the levees cannot always be identified conclusively as individual turbidites (Dott 1983; Einsele et al., 1996). It may dilute pelagites without actually forming distinct layers and thus is reflected in enhanced pelagic sedimentation rates. This dilution effect may also be the reason for the remarkably low amount of identifiable turbidite material at levee site GeoB 8507 (≈ 6 %) in contrast to the directly adjacent highly turbiditic site GeoB 8509 (≈ 42 %).

Erosiveness of turbidites

Significant intra-element correlations are seen between total carbonate and the Ca data of cores CD 53-30 (Matthewson et al., 1995), GeoB 7919-5 and the turbidite-bearing levee core GeoB 8502-2. Despite interbedded turbidites, the latter core does not show significant omission of pelagic material except for one sediment sequence in the lower part. We suggest this hiatus results from the same erosive event which deposited the thin turbidite layer in core CD 53-30 (Matthewson et al., 1995). Most likely this event was triggered at the time of sea-level lowering at the stage boundary 6/7 around 190 kyr (cf. Fig. 3).

It is unlikely that even larger-volume turbidity currents travelling channelised in the Cap Timiris Canyon eroded more than a few centimetres into the underlying substrate at the distal levee site GeoB 8502. The good correspondence with the reference cores supports virtually non- or minor-erosive turbidity currents at the low gradient slope off NW Africa (e.g. Weaver and Kuijpers, 1983; Masson, 1994; Weaver, 1994). This seems also to be true for the two other levee-cores GeoB 8506-2 and GeoB 8507-3 further upslope.

Even at intrachannel site GeoB 8509 sedimentation has been accumulative at least over the last 15 kyr. Groups of turbidite layers are frequently amalgamated to form thicker composite beds such as T 1, 6, 12, 15-GeoB 8509 (cf. Fig. 2d). This suggests that either one series of overlying turbidite layers was fed from several tributaries during the same event or in several, consecutive phases. Alternatively, originally subjacent pelagites may have been eroded and entrained into the turbidite flow during the next event (Weaver, 1994).

The young canyon fill at intrachannel site GeoB 8509 raises the question of how long this accumulative state can be maintained. Eventually, persistant high sedimentation rates in this part of the canyon will mean that it will become filled with sediments. Some large-scale turbidite events should be sufficient to clear the pathway, however. Although during the Holocene only small volume turbidites were emplaced, larger-volume turbidites were deposited during other times and apparently were erosive enough to remove the previous canyon fill and thus maintain the pathway (for instance such as those that deposited the distinctive layers on the levees especially during glacial OISs or at stage boundaries). We suggest highly erosive turbidite events at the stage boundary 2/3 (cf. T 2-GeoB 8502, T 3-GeoB 8507 and T 3-GeoB 8506 in Fig. 6) and within glacial OIS 2 around 17-18 kyr (cf. T 1-GeoB 8506 and T 2-GeoB 8507 in Fig. 6).

Conclusions

Application of core-to-core correlation to disturbed sedimentary sequences can be a reliable method of specifying ages for mass transport processes and can add to our knowledge of turbidity current processes and their relationship to sea-level/climatic changes. Element data together with appropriately developed age models can be used to

1) estimate the emplacement times of turbidites,
2) estimate the frequency of turbidite emplacement with respect to climatic and sea-level changes, and
3) provide information to quantify mass transport within canyon systems.

The age models for pelagites and turbidites presented in this study provide data which are necessary to create a mass balance for gravity-driven downslope transport in the Cap Timiris Canyon. Although, of course, seismo-acoustic and sedimentological data are essential to determine the areal and spatial distribution of turbidite deposits and to understand and quantify the processes of turbidity current production.

Acknowledgements

We are indebted to Karsten Enneking, Simone Pannike, Luzie Schnieders and all other cruise participants for assisting with the laboratory work during the RV Meteor cruise M 58-1. We likewise owe thanks to the Captain and crew members. The quality of the manuscript was improved by helpful suggestions of two anonymous reviewers. This research was supported by a grant from the DFG Research Centre Ocean Margins at Bremen University.

2.4 Age models for the Cape Blanc Debris Flow and the Mauritania Slide Complex in the Atlantic Ocean off NW Africa

KATHARINA WIEN, MARTIN KÖLLING AND HORST D. SCHULZ

Department of Earth Sciences (FB 5), University of Bremen, P.O. Box 330440, 28359 Bremen, Germany

Abstract

Age models for the emplacement time of mass flow deposits from the Cape Blanc Debris Flow, the Mauritania Slide Complex and a levee of the Mauritania Canyon were obtained by offshore XRF element stratigraphy on five gravity cores, allowing the assessment of slope instability in this part of the NW African continental margin with respect to climate-related sea-level variations during the Quaternary. The Cape Blanc Debris Flow emplaced during the Saalian glaciation approximately 155 kyr ago whereas deposition of the Mauritania Slide Complex is linked to the rapid sea-level rise at the Pleistocene/Holocene boundary. Turbidites on a levee of the Mauritania Canyon close to the Mauritania Slide Complex occurred at stage boundaries. These findings agree with other studies which show that the NW African continental margin has been unstable over the last Quaternary cycles, and that downslope sediment transport is frequently coupled to periods of climatic changes at stage boundaries.

Keywords: mass transport; element stratigraphy; age model; sea-level

1 Introduction

Continental slope instabilities and resulting mass gravity flows mainly in form of slumps, slides, debris flows and turbidity currents play an important role along ocean margins. Slide and debris flow processes can affect volumes of tens to hundreds of cubic kilometres of marine sediments and transfer them several hundreds of kilometres across slopes with angles that are often < 1° (e.g. Embley, 1976, 1980; Jacobi, 1976; Mulder and Cochonat, 1996; Nichols, 1999; Einsele, 2000; Weaver et al., 2000). A great variety of Quaternary slides and debris flows can be found along the NW African continental margin (Jacobi, 1976; Embley, 1980; Kidd et al., 1987) where they cover a volume of approximately 130 000 km^3 (Gee et al., 2001). Among them are some large-scale deposits such as the Saharan Debris Flow (Embley, 1976; Masson et al., 1993; Gee et al., 2001) and the Canary Debris Flow (Masson et al., 1997, 1998). Large mass flow deposits have also been found between 17° and 18°N in the region of the Cape Verde Islands (Jacobi, 1976; Kidd et al., 1987).

Rare and random occurrence of downslope transport processes, however, complicate their prediction and direct measurement. Age models for pelagic sediments embedding mass gravity deposits are therefore important to estimate when and how frequent such processes occurred in the geological past, and to link them to their possible trigger mechanisms. There are several reasons why continental margin sediments are rendered prone to failure, including oversteepening of the slope by sedimentation processes, underconsolidation of sediments due to high sedimentation rates, undercutting of the slope, gas build-up or gas hydrate decomposition, ice-sheet cover in glacial areas and seismicity (e.g. Embley, 1982; Bugge et al., 1988; Einsele et al., 1996; Mulder and Cochonat, 1996; Nichols, 1999; Imbo et al., 2003; Mienert et al., 2003).

The RV Meteor cruise M 58-1 was conducted to investigate gravity-driven sediment transport processes along the NW African continental margin (Schulz et al., 2003). This paper primarily presents data on five gravity cores from the Cape Blanc Debris Flow and the Mauritania Slide Complex. Geochemical analyses especially of the pelagic units in these cores were performed by X-ray fluorescence (XRF) spectrometry. Our strategy was to indirectly determine the ages of the mass flow events based on a correlation of elemental data on the pelagites above the mass flow deposits with carbonate and elemental data on dated reference cores. We present age models for both mass flow deposits with suggestions for the controls on failure. Geochemical data on the gravity cores from the Mauritania Slide Complex give rise to speculations whether its deposition was a single or a multi-phase event.

2 Regional setting

Both mass flow deposits formed on the NW African continental margin (cf. Seibold and Hinz, 1974; Jacobi, 1976; Kidd et al., 1987) where the slope angle generally ranges between 0.5° and 2° (Weaver et al., 2000). The Cape Blanc Debris Flow is located at a pelagic site on the lower slope off Cape Blanc. The Mauritania Slide Complex on the lower slope off Cape Verde ranks among the largest mass gravity deposits known along the NW African continental margin and extends to a width of more than 120 km. To the southwest it borders on the channel-levee system of the Mauritania Canyon (Schulz et al., 2003).

Recent sedimentation in this area is influenced by the African dust plume which transports high quantities of terrigenous material from the sub-Sahara and Sahel regions into the Atlantic Ocean (Tetzlaff and Wolter, 1980; Pye, 1987; Wefer and Fischer, 1993), whereas permanent fluvial input can be excluded at present (Weaver et al., 2000; Mienert et al., 2003). Several upwelling cells (Sarnthein et al., 1982) cause high accumulation rates along the upper slope and shelf edge (Weaver et al., 2000), one depocenter for organic carbon occuring for example between 20° and 22°N further upslope between 1000 and 2000 m water depth (Bertrand et al., 1996; Martinez et al., 1999). At the present, productivity on the NW African continental margin is highest between 16° and 25°N (Schemainda et al., 1975). On a longer time-scale, productivity is reported to have been high especially during glacial periods (Diester-Haass and Chamley, 1982). Terrigenous input increased during glacial periods as well, mainly due to enhanced availability of source material and strength of transporting winds (cf. Matthewson et al., 1995; deMenocal et al., 2000).

3 Materials

Cape Blanc Debris Flow and Mauritania Slide Complex were both mapped and sampled during research cruise M 58-1 with RV Meteor in May/June 2003 (Schulz et al., 2003). For this research, altogether five gravity cores and, if available, their corresponding multicorer cores

were selected for onboard geochemical analyses (table 1 and figure 1). Core GeoB 8504-3 was recovered from the Cape Blanc Debris Flow where the mass gravity deposit was recorded below approximately 8 m of pelagic sediments.

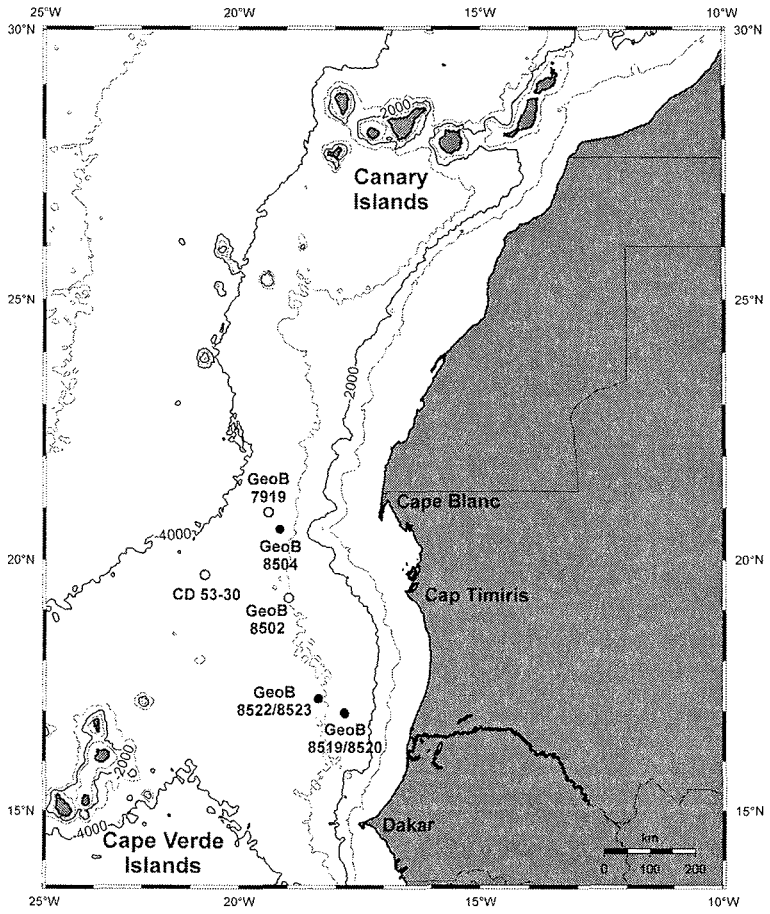

Fig. 1: Locations of coring sites offshore NW Africa. Closed circles indicate selected core positions during RV Meteor cruise M 58-1 (present study), open circles indicate positions of the reference cores CD 53-30 (Matthewson et al., 1995), GeoB 7919-5 (RV Meteor cruise M 53-1c) and GeoB 8502-2 (RV Meteor cruise M 58-1)

The Mauritania Slide Complex further southward was sampled near its edge in order to obtain both the overlying and underlying pelagic horizons bracketing the slide. The present study of the Mauritania Slide Complex is based on data from four gravity cores obtained from two different parts of the deposit. Two sites (GeoB 8519, GeoB 8520) are located in an area where a small tongue protrudes from the main slide body and forms the southern part of the slide complex (cf. Krastel et al., subm.). The uppermost unit of this tongue onlaps the base of a levee of the Mauritania Canyon and pinches out against it. This levee structure appears to have prevented spillover of the slide into the channel to the southwest. Core GeoB 8519-3 was recovered directly from the top of the levee structure just outside the slide and thus, was supposed to serve as a master record by supplying an age model for the pelagites in the direct vicinity of the slide complex. Intercalated into the pelagic unit at site GeoB 8519, however, are four turbidite layers

which are presumably related to transport processes in the Mauritania Canyon. Site GeoB 8520 is directly adjacent to GeoB 8519 at the edge of the slide where its thickness approximates 7 m.

Table 1: Key characteristics of all sediment cores presented in this study including core number, geographic position, water depth, gear type, recovery and available data. MUC = multicorer, GC = gravity corer

Core no.	Latitude (° N)	Longitude (° W)	Water depth (m)	Gear type	Recovery (cm)	Available data
Cores from the Cape Blanc Debris Flow						
GeoB 8504-1	20°35.09	19°10.03	3246	MUC	26	XRF; offshore
GeoB 8504-3	20°35.12	19°10.02	3209	GC	980	XRF; shipboard
Cores from the Mauritania Slide Complex						
GeoB 8519-3	16°58.07	17°49.54	2676	GC	708	XRF; offshore
GeoB 8520-3	16°58.58	17°49.58	2689	MUC	30	XRF; offshore
GeoB 8520-1	16°58.58	17°49.57	2687	GC	1128	XRF; offshore
GeoB 8522-3	17°15.09	18°22.14	3097	MUC	28	XRF; offshore
GeoB 8522-1	17°15.11	18°22.15	3098	GC	561	XRF; offshore
GeoB 8523-1	17°14.74	18°22.12	3092	GC	612	XRF; offshore
Reference cores						
CD 53-30	19°42.78	20°42.81	3565			total carbonate, oxygen isotope data [a]
GeoB 7919-5	20°56.41	19°23.38	3420	GC	1458	XRF; onshore [b]
GeoB 8502-2	19°13.27	18°56.04	2956	GC	1478	XRF; offshore [b]

[a] Extracted from Matthewson et al. (1995)

[b] Extracted from Wien et al. (accpt.)

Two other sites (GeoB 8522, GeoB 8523) in the Mauritania Slide Complex are closely spaced to each other approximately 65 km northwestward from sites GeoB 8519 and GeoB 8520, in an area where the ≈ 1.5-3 m thick slide is closely associated with an overlying turbidite layer of ≈ 40-80 cm in thickness. The boundary between slide and turbidite is formed by a sharp erosional unconformity. Intercalated into the pelagites underlying the slide at these two northwestern sites are several small-scale turbidites. The turbidites in all study cores were numbered consecutively downcore, beginning with T 1-GeoB 85XX at the top. Note that turbidites with the same number (e.g. T 1-GeoB 8519 and T 1-GeoB 8523) are not necessarily correlative as the numbering may suggest. The three cores which penetrated the Mauritania Slide Complex (GeoB 8520-1, GeoB 8522-1, GeoB 8523-1) found the mass gravity deposits (i.e. slide or slide + overlying turbidite) buried beneath an approximately 50 cm thick layer of pelagic sediments.

The archived gravity core GeoB 7919-5, obtained off Cape Blanc during RV Meteor cruise M 53-1c in April/May 2002 (Meggers et al., 2003), was analysed geochemically pre-cruise in order to serve as reference aboard (cf. Wien et al., accpt.). Gravity core GeoB 8502-2 was recovered during RV Meteor cruise M 58-1 from a levee of the Cap Timiris Canyon (Schulz et al., 2003) and also serves as reference. The downcore Ca variations of both cores were

correlated to detailed total carbonate data of the core CD 53-30 which was retrieved from the Cape Verde Terrace and is well-dated back to ≈ 290 kyr based on Foraminifera $\delta^{18}O$ records (Matthewson et al., 1995).

4 Methods

We aimed to indirectly date the emplacement of all mass flow deposits in our study cores based on the correlation of downcore geochemical data on the pelagic units with total carbonate and elemental data on dated reference cores.

4.1 Distinction between pelagic and mass flow deposits

In order to accurately fit age models to our study cores it was prerequisite to clearly distinguish between pelagic sediments and mass flow deposits. The different facies, i.e. pelagic, debrite, slide and turbidite facies, were initially distinguished onboard ship based on visual core description (Schulz et al., 2003) and controlled later on land by X-ray radiographs (cf. Henrich et al., subm.). A clear identification of the depths of all facies boundaries was possible, except for the transition of the youngest turbidite units T 1-GeoB 8522 and T 1-GeoB 8523 into the topmost pelagic facies. As the upper fine-grained muddy parts of these turbidite units gradually turn into the pelagic facies, we were only able to indicate a depth range instead of a distinct boundary.

4.2 Onshore and offshore geochemical analyses

Downcore elemental variations were determined for the reference core GeoB 7919-5 prior to the research cruise in the laboratory at Bremen University, and for core GeoB 8502-2 from the Cap Timiris Canyon (cf. Wien et al., accpt.) and the five gravity cores and three multicorer cores from the Cape Blanc Debris Flow and Mauritania Slide Complex aboard RV Meteor. Multicorer cores were sampled at a resolution of 1 cm for the upper 10 cm and a resolution of 2 cm below this depth. Core GeoB 7919-5 was sampled with syringes in 5 cm intervals. From all other gravity cores, sections of 1 m length were sampled using plastic U-channels with a cross-section of 1.5 × 2 cm (cf. Wien et al., 2005). The elemental analysis focussed on both, the pelagic sediment sequences and the turbidites while only parts of the debris flow and slide deposits were analysed.

All samples were dried at 200°C for 60 min and ground manually. Reliable contents of the elements Si, Ti, Al, Fe, Mn, Mg, Ca, K, Sr, Ba, Rb, Cu, Ni, Zn, P, S, Cl and Br were measured on a Spectro Xepos XRF spectrometer. Analytical quality was assessed by daily analyses of a pressed pellet of MAG-1 standard reference material (e.g. Govindaraju, 1994; 4 g MAG-1 standard powder + 0.9 g Hoechst Wax). The XRF geochemical analyses were performed

following the method described in Wien et al. (2005). All elemental data presented in this study are stored in the Pangaea database (http://www.wdc-mare.org/PangaVista?query=@Ref).

The mass flow deposits in the three gravity cores GeoB 8520-1, GeoB 8523-1 and GeoB 8522-1 from the Mauritania Slide Complex are capped by just ≈ 50 cm of pelagic material and consequently, the 4 cm resolution analyses only allowed a relatively rough correlation of their downcore elemental patterns to the reference cores CD 53-30, GeoB 7919-5 and GeoB 8502-2. In order for the geochemical data to be correlated more accurately, post-cruise re-analyses at a higher resolution (1 cm and 2 cm) were performed on the upper sections of all gravity cores from the Mauritania Slide Complex, including the entire capping pelagic units, the turbidite deposits and the top parts of the slide (table 2). For the pelagic units overlying the Mauritania Slide Complex, each 4-cm subsample is equivalent to ≈ 0.9-1.2 kyr, each 1-cm subsample is equivalent to ≈ 0.2-0.3 kyr, depending on the sedimentation rate.

Table 2: Resolution for post-cruise XRF re-analyses performed on the topmost units in the four gravity cores from the Mauritania Slide Complex

Core no.	Core length	Resolution of XRF re-analyses
GeoB 8519-3	0-100 cm	1 cm
GeoB 8520-1	0-60 cm	1 cm
GeoB 8522-1	0-60 cm	1 cm
	60-100 cm	2 cm
GeoB 8523-1	0-60 cm	1 cm
	60-130 cm	2 cm

4.3 Core-to-core correlation

When available, multicorer cores were virtually arranged as core tops of their corresponding gravity cores. For this purpose, the overlapping section (i.e. top centimetres of the gravity core and bottom centimetres of the multicorer core) was determined based on the absolute values of the major elements. The multicorer core tops represent the present sediment surface and are therefore defined to have an age of 0 kyr.

An age model was initially fitted to the cores GeoB 7919-5 and GeoB 8502-2 by correlating their downcore Ca data (cf. Wien et al., accpt.) to total carbonate data on the dated core CD 53-30 (Matthewson et al., 1995). The complete XRF element suites of both GeoB cores were available for correlation and supplemented total carbonate data on CD 53-30. The pelagic units of all study cores from the Cape Blanc Debris Flow and the Mauritania Slide Complex were then referenced to a stratigraphic framework by correlating their downcore elemental profiles with these three reference cores. Altogether eighteen elements aided the fit of age models with the elements Ca, Si, Al, Fe and K being most important. Correlation and age fitting were performed by linear interpolation between tie points with the software "AnalySeries", version 1.1 (Paillard et al., 1996).

5 Results

5.1 Age model for the Cape Blanc Debris Flow

We were able to establish a detailed correlation of the pelagites overlying the Cap Blanc Debris Flow in core GeoB 8504-3, and the reference cores CD 53-30 and GeoB 7919-5 (figure 2). The downcore profiles of total carbonate and Ca content in these three cores match well and indicate debris flow emplacement at approximately 155 kyr within glacial oxygen isotope stage (OIS) 6.

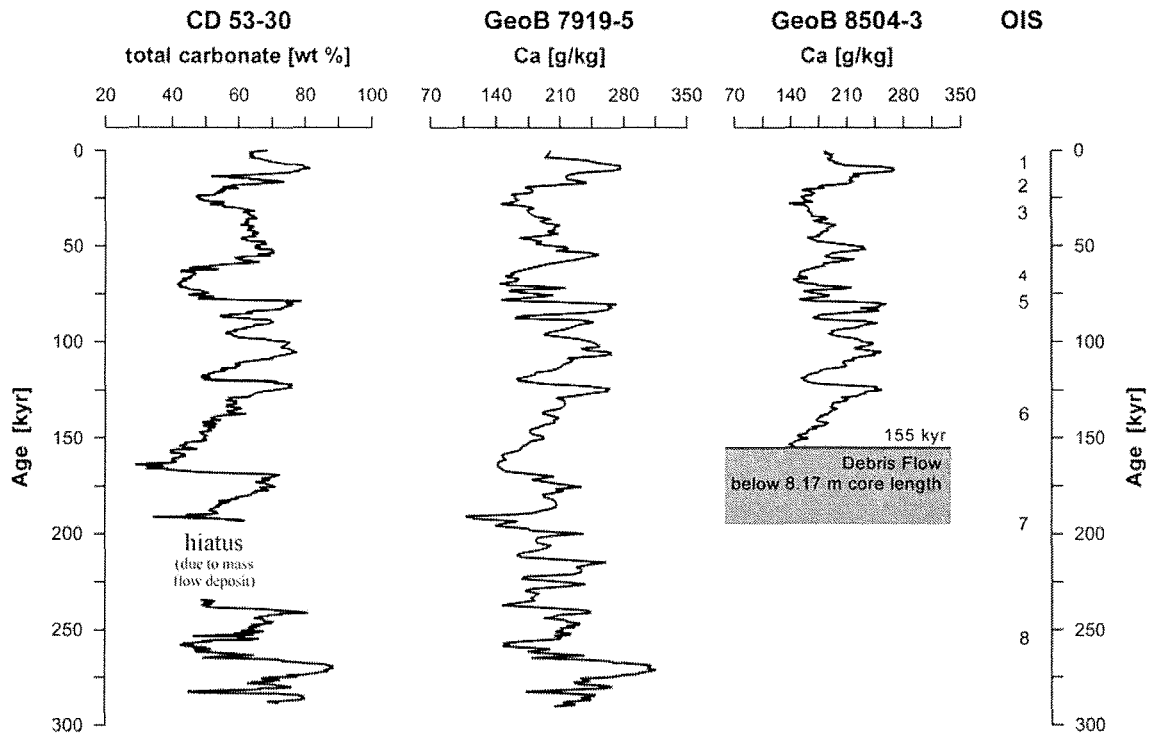

Fig. 2: Correlation of the cores CD 53-30 (Matthewson et al., 1995), GeoB 7919-5 (cf. Wien et al., accpt.) and GeoB 8504-3 based on total carbonate and Ca data. According to this correlation, deposition of the Cape Blanc Debris Flow occurred at ≈ 155 kyr within glacial oxygen isotope stage (OIS) 6

5.2 Age models for the Mauritania Slide Complex

The more detailed study of the Mauritania Slide Complex unravels a depositional history more difficult to interpret (figures 3 and 4). The pelagic master record at site GeoB 8519 postdates to approximately 165 kyr (cf. figure 4). Owing to the position of this site on a levee of the Mauritania Canyon, the pelagites are interrupted by four turbidite layers which occur at stage boundaries 5/6 (128 kyr; T 4, 3-GeoB 8519) and 4/5 (71 kyr; T 2, 1-GeoB 8519; table 3). Turbidite T 2-GeoB 8519 eroded into the underlying pelagic section, thereby causing a hiatus of ≈ 17 kyr covering the upper unit of OIS 5. The topmost pelagic unit comprising OISs 1 to 4 is complete and allows detailed correlation with the pelagites capping the mass flow deposits at sites GeoB 8520, GeoB 8522 and GeoB 8523 (i.e. slide at site GeoB 8520; slide and overlying turbidite at sites GeoB 8522 and GeoB 8523).

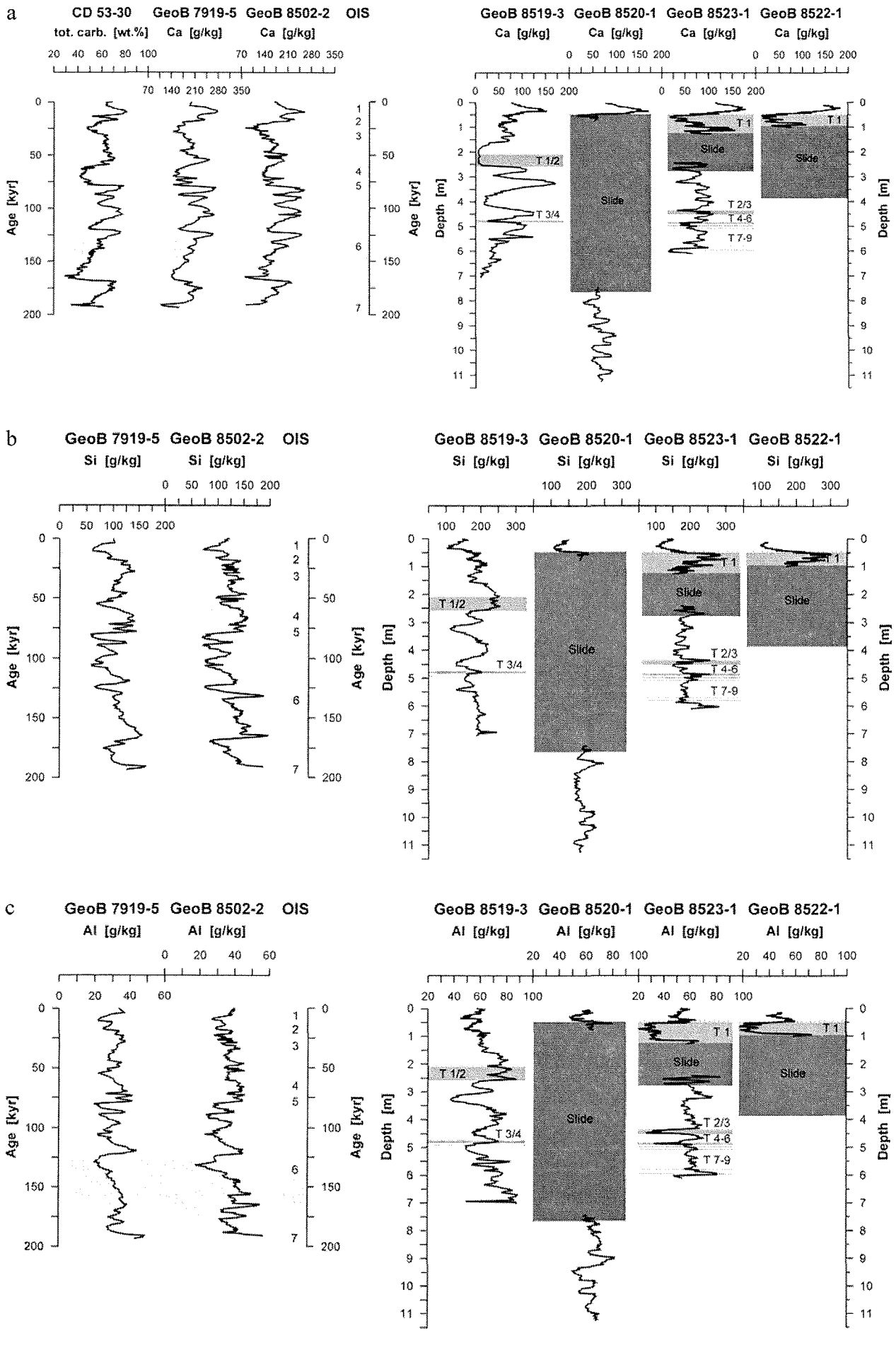
a
CD 53-30
GeoB 7919-5
GeoB 8502-2
OIS
tot. carb. [wt.%]
Ca [g/kg]
Ca [g/kg]
Age [kyr]
GeoB 8519-3
GeoB 8520-1
GeoB 8523-1
GeoB 8522-1
Ca [g/kg]
Depth [m]
T 1/2
T 3/4
Slide
T 1
T 2/3
T 4-6
T 7-9
b
GeoB 7919-5
GeoB 8502-2
OIS
Si [g/kg]
GeoB 8519-3
GeoB 8520-1
GeoB 8523-1
GeoB 8522-1
c
GeoB 7919-5
GeoB 8502-2
OIS
Al [g/kg]
GeoB 8519-3
GeoB 8520-1
GeoB 8523-1
GeoB 8522-1

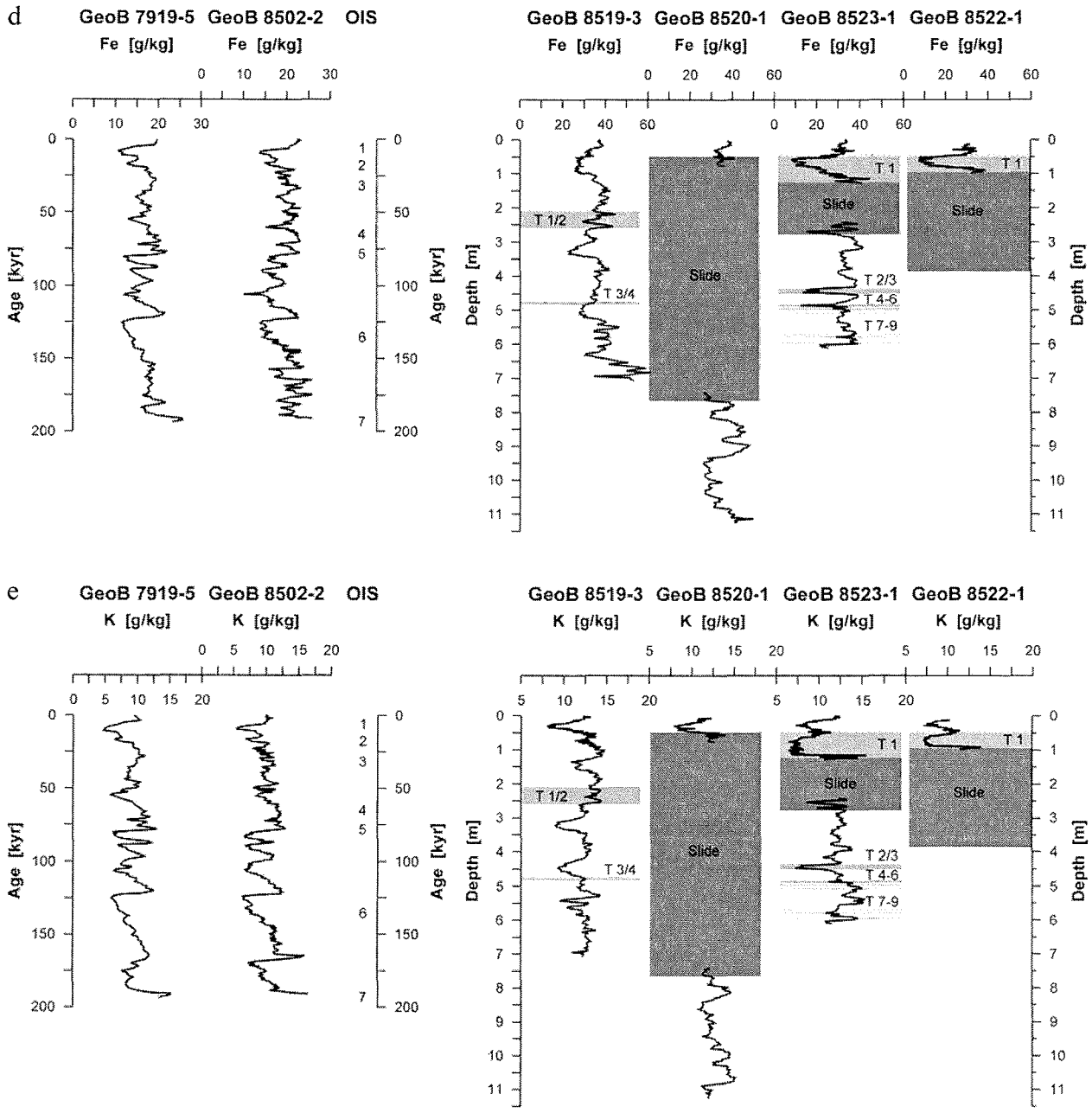

Fig. 3a-e: Selected geochemical data on the reference cores CD 53-30 (Matthewson et al., 1995; only **a**), GeoB 7919-5 and GeoB 8502-2 (cf. Wien et al., accpt.), and the four study cores from the Mauritania Slide Complex showing downcore elemental profiles on **a** Ca, **b** Si, **c** Al, **d** Fe and **e** K. Reference cores are plotted against age, study cores against depth. Note the well-correlated elemental pattern of the turbidite units T 1-GeoB 8522 and T 1-GeoB 8523 which proves them to result from the same turbidite event. The diagonal cross pattern on top of both turbidite layers denotes the transition zone between turbidite and pelagite

The Mauritania Slide Complex is covered by pelagic sediments which predominantly accumulated during the present-day interglacial period (OIS 1). At sites GeoB 8522 and GeoB 8523, slide and pelagites are separated from each other by a turbidite layer (T 1-GeoB 8522, T 1-GeoB 8523), the well correlated elemental pattern of which proves it to derive from the same turbidite event (cf. figure 3). Particular attention was paid to the onset of the pelagic sedimentation above the mass flow deposits at sites GeoB 8520, GeoB 8522 and

GeoB 8523 and thus, to the question of whether deposition of the slide took place synchronously in one phase or in a series of different phases (figure 5). Although XRF data furnish detailed information on the pelagites, correlation proved to be complicated because the elemental patterns essentially plot as one peak (Ca) or depletion (K, Si, Al) only. The geochemical data support two different possibilities for the mode of slide emplacement which will be considered in the following subsections.

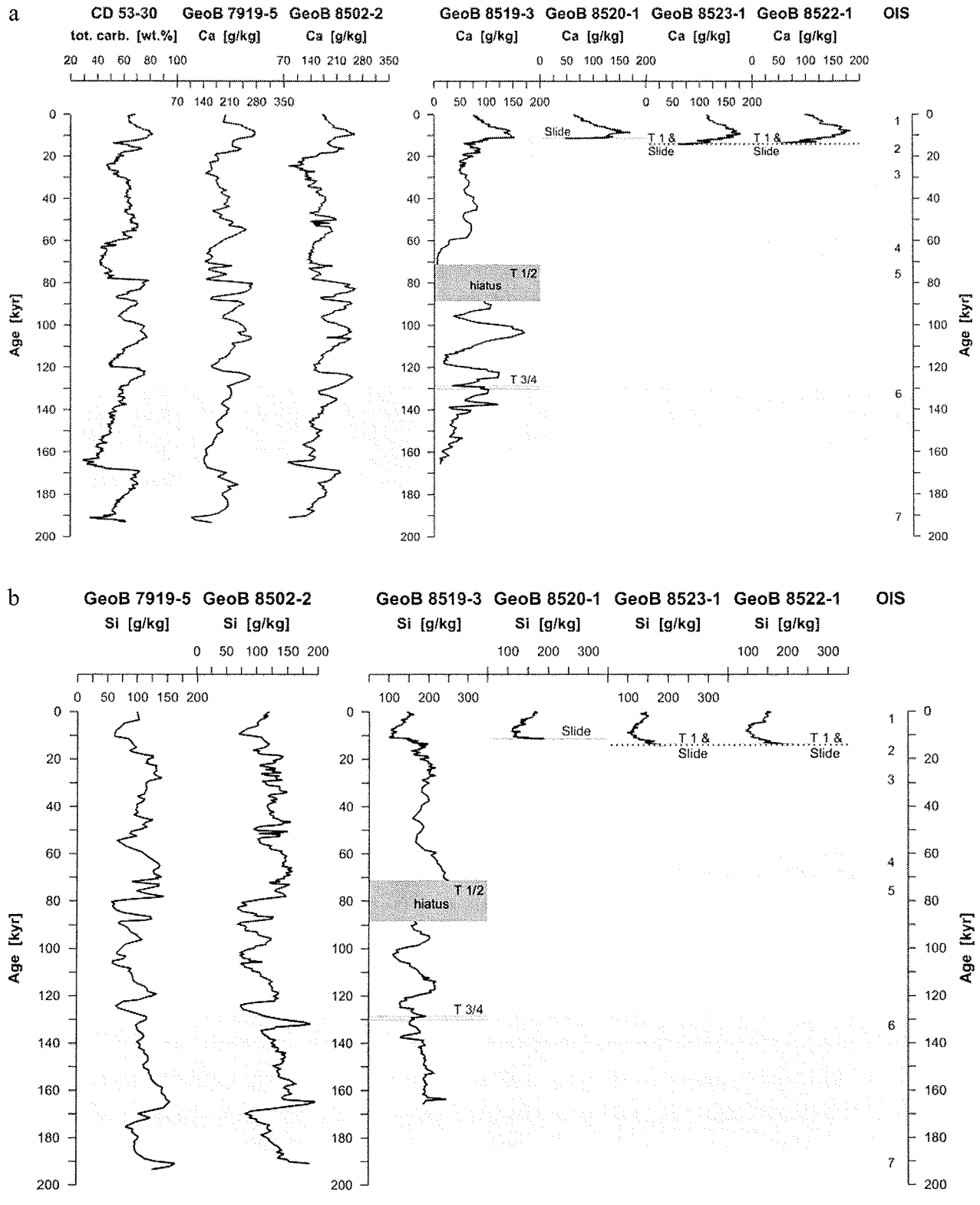

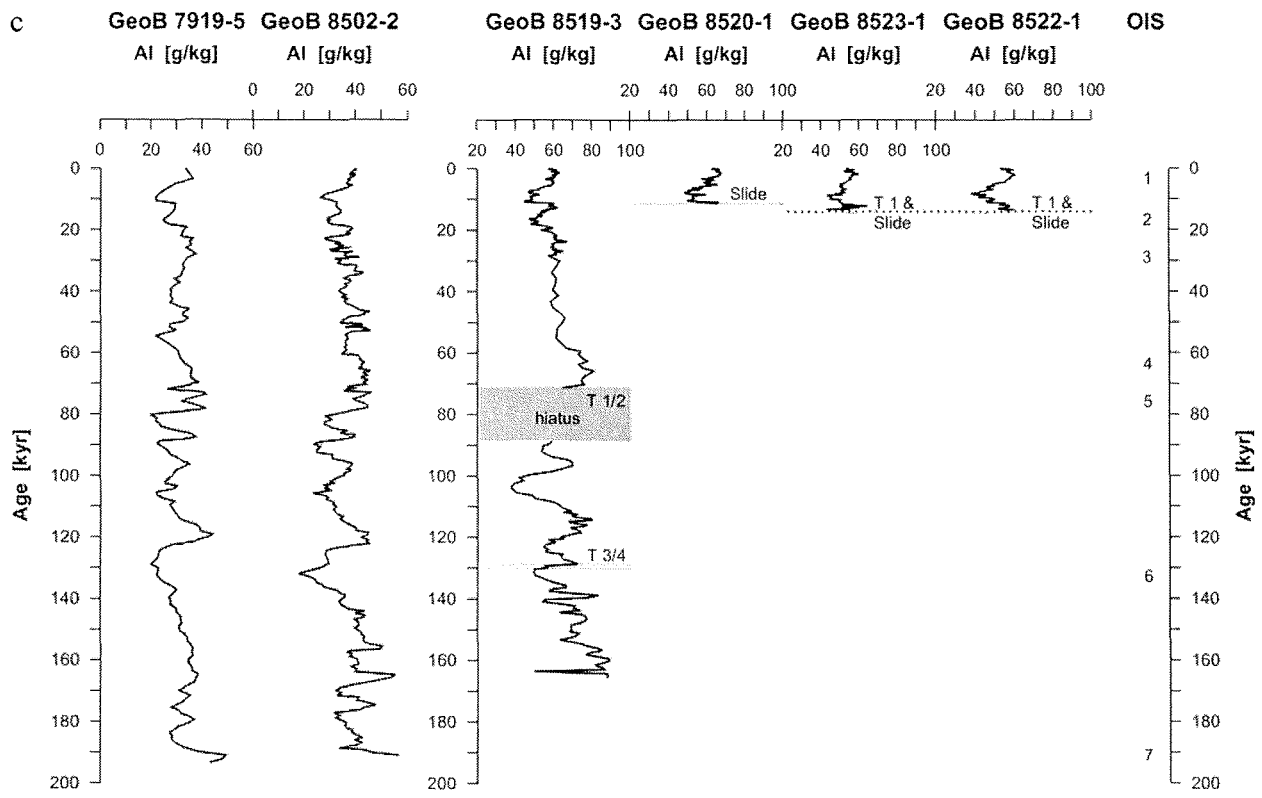
c
GeoB 7919-5
Al [g/kg]
GeoB 8502-2
Al [g/kg]
GeoB 8519-3
Al [g/kg]
GeoB 8520-1
Al [g/kg]
GeoB 8523-1
Al [g/kg]
GeoB 8522-1
Al [g/kg]
OIS
Slide
T 1 &
Slide
T 1 &
Slide
T 1/2
hiatus
T 3/4
Age [kyr]
Age [kyr]

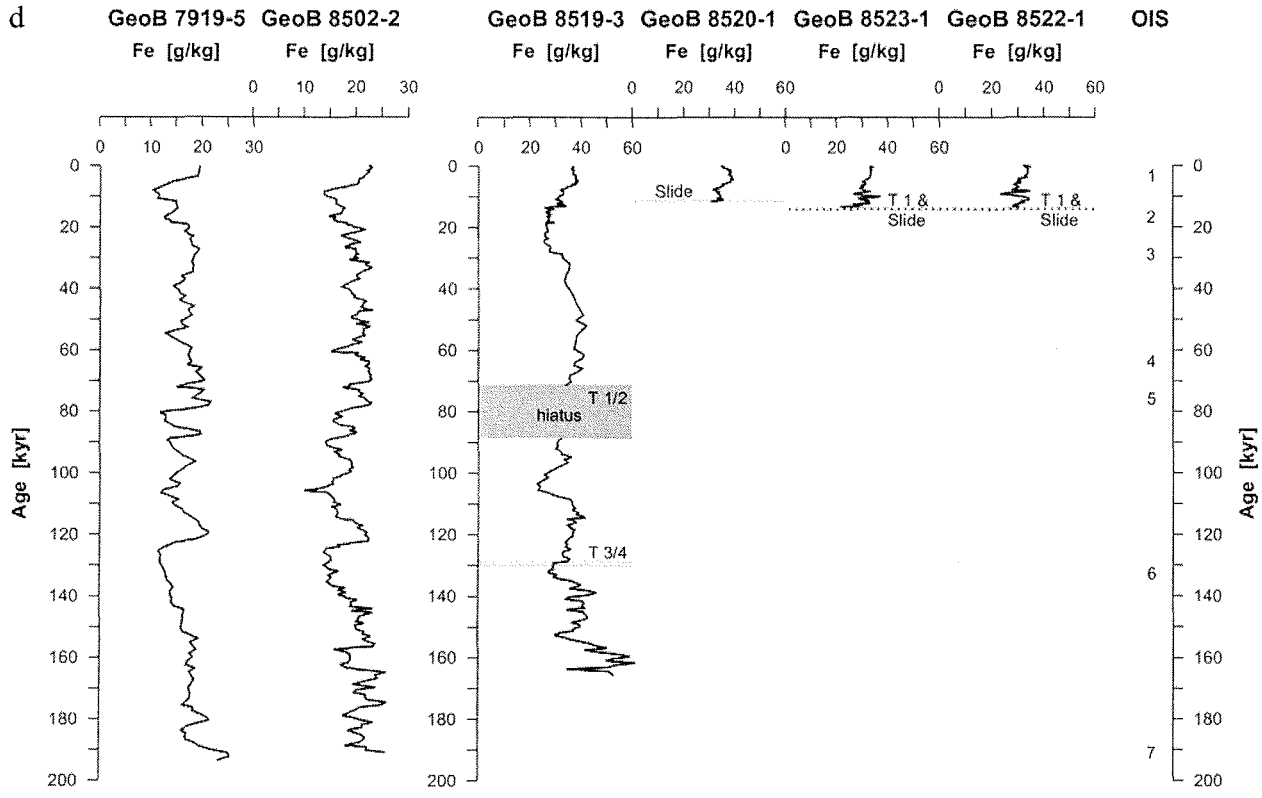
d
GeoB 7919-5
Fe [g/kg]
GeoB 8502-2
Fe [g/kg]
GeoB 8519-3
Fe [g/kg]
GeoB 8520-1
Fe [g/kg]
GeoB 8523-1
Fe [g/kg]
GeoB 8522-1
Fe [g/kg]
OIS
Slide
T 1 &
Slide
T 1 &
Slide
T 1/2
hiatus
T 3/4
Age [kyr]
Age [kyr]

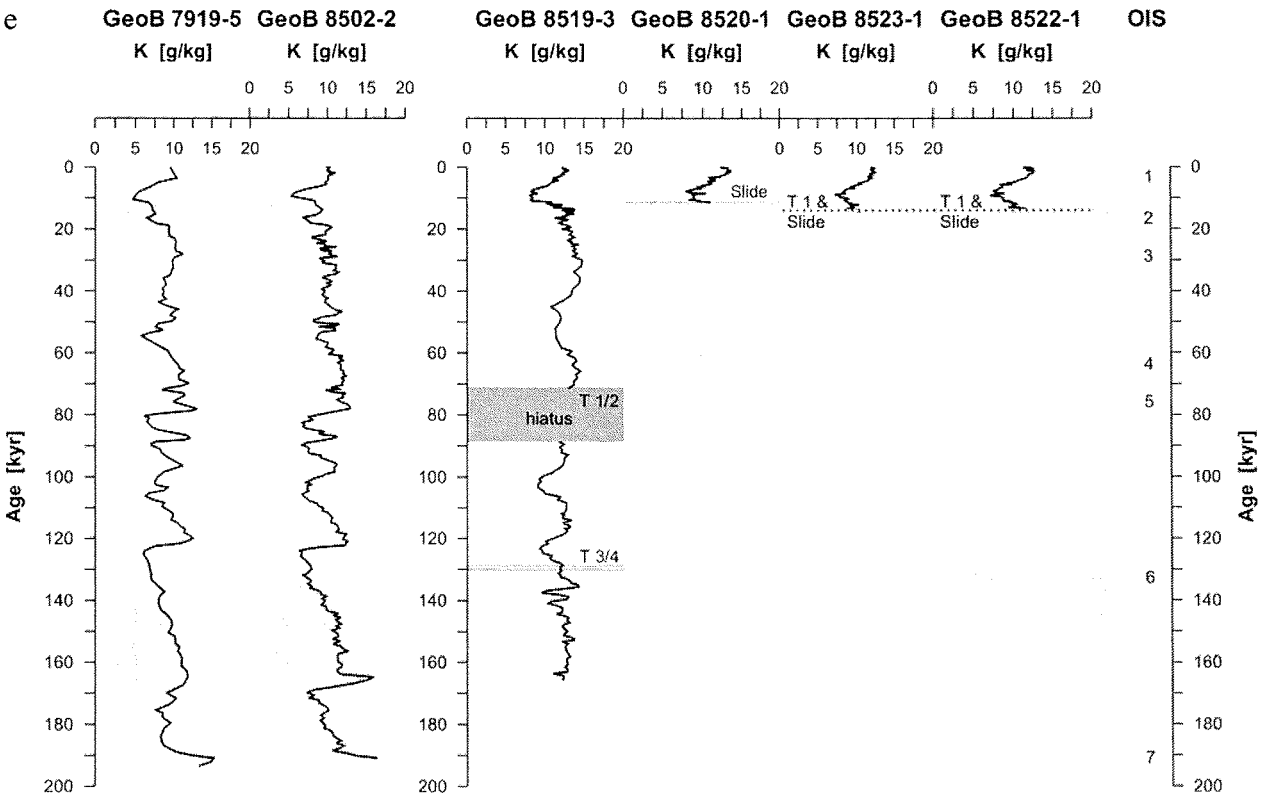

Fig. 4: Correlation of **a** Ca, **b** Si, **c** Al, **d** Fe and **e** K downcore profiles between the four study cores from the Mauritania Slide Complex and the reference cores CD 53-30 (Matthewson et al., 1995; only **a**), GeoB 7919-5 and GeoB 8502-2 (cf. Wien et al., accpt.). The diagonal cross pattern in GeoB 8523-1 and GeoB 8522-1 indicates the age range (13.7–14.3 kyr) during which turbidite emplacement occurred at one certain time

Table 3: Core number, label, depth and emplacement time of the mass flow deposits in four gravity cores from the Mauritania Slide Complex

Core no.	Slide; turbidite	Slide/turbidite depth (cm)	Slide/turbidite emplacement time (kyr)
GeoB 8519-3	T 1	210 – 225	71
	T 2	225 – 260	> 71
	T 3	476 – 483	129
	T 4	492 – 494	130
GeoB 8520-1	Slide	49 – 766	11.4
GeoB 8522-1	T 1	(?45) 50 – 95	certain time between 13.7 – 14.3
	Slide	95 – 387	time-equivalent with or older than T 1-GeoB 8522
GeoB 8523-1	T 1	(?45) 50 – 125	certain time between 13.7 – 14.3
	Slide	125 – 278.5	time-equivalent with or older than T 1-GeoB 8523

5.2.1 Multi-phase event?

Our data indicate emplacement of the Mauritania Slide Complex to be a multi-phase event at the transition from glacial OIS 2 to interglacial OIS 1 (cf. figure 5). Assuming the onset of the pelagites immediately following slide/turbidite emplacement, it can be inferred that slide depositon occurred at ≈ 11.4 kyr at site GeoB 8520, and that turbidite deposition occurred at a certain time between ≈ 13.0–14.3 kyr at site GeoB 8523 and at a certain time between ≈ 13.7–

14.3 kyr at site GeoB 8522. The age ranges for the turbidite event at both northwestern sites result from the not exactly identified boundary between turbidite and overlying pelagites (cf. `4.1 Distinction between pelagic and mass flow deposits´). As the turbidite units in both cores result from the same event (cf. figure 3), we suggest the discrepancy in the youngest possible ages (i.e. 13.0 kyr at site GeoB 8523 vs. 13.7 kyr at site GeoB 8522) to result from the indistinct character of this boundary which induced us to overrate the turbidite unit in T 1-GeoB 8523. We therefore presume the age of 13.7 kyr to be the youngest possible age for turbidite emplacement at both sites and exclude the age of 13.0 kyr from further discussion.

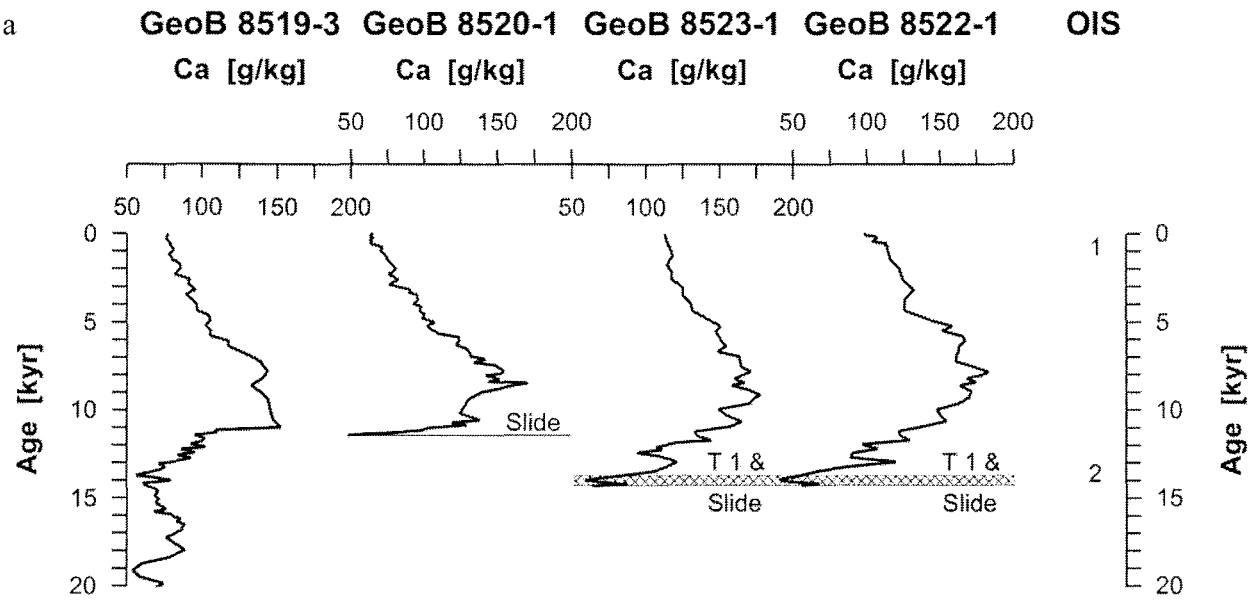

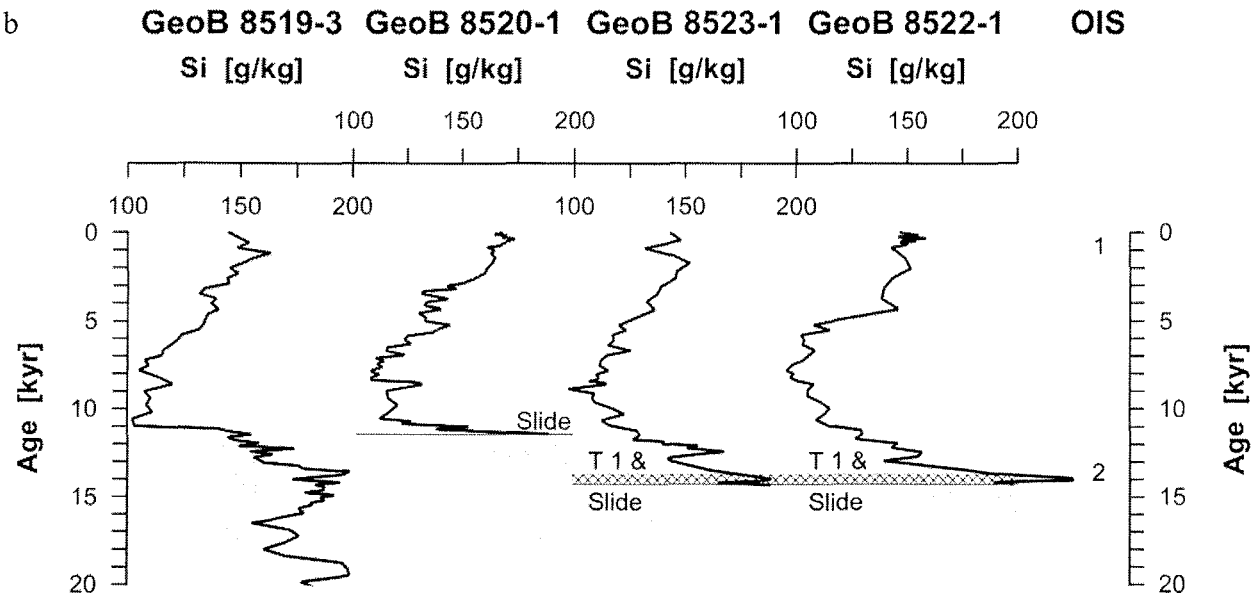

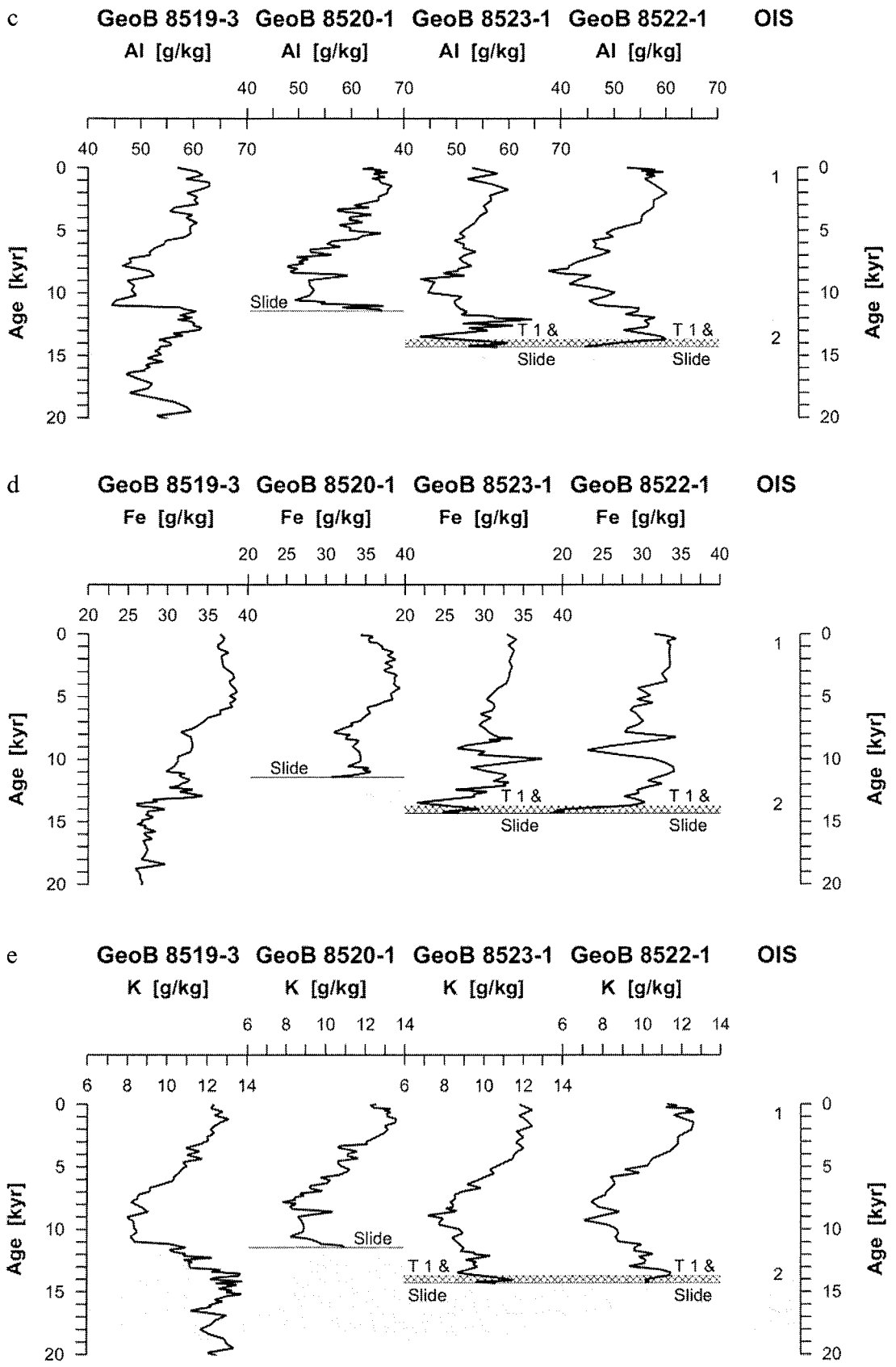

Fig. 5: Reduced dataset back to only 20 kyr showing the correlation of **a** Ca, **b** Si, **c** Al, **d** Fe and **e** K downcore profiles between the topmost pelagic units of the four study cores from the Mauritania Slide Complex. The diagonal cross pattern in GeoB 8523-1 and GeoB 8522-1 indicates the age range (13.7–14.3 kyr) during which turbidite emplacement occurred at one certain time

5.2.2 One-phase event?

Alternatively, our correlation may be slightly imprecise owing to a lack of significant correlateable features in the downcore elemental records of the pelagites which cover the Mauritania Slide Complex. In this case it can be inferred that the ages for an onset of the pelagites above the mass flow deposits at the southeastern (GeoB 8520) and the northwestern (GeoB 8522, GeoB 8523) sites are rough estimations which should be approximated to only one certain age between 11.4 and 14.3 kyr. Emplacement of the Mauritania Slide Complex may then be suggested to have occurred in one single phase. In the following, however, we will continue to use the different age data which result from our correlation.

Fitting of age models to the pelagic units underlying the slide at sites GeoB 8520 and GeoB 8523 proved to be much more complicated due to a lack of significant features in the elemental profiles which would resemble the patterns of the reference cores. This may possibly result from a distortion of the underlying sediments during the depositional event. We will introduce no correlation and, for that reason, skip further discussion of these data.

6 Discussion

6.1 Emplacement times of the mass flow deposits

The results of the present study are a confirmation of the traditional view of mass flow emplacement especially during sea-level low stands in glacial periods (cf. Shanmugam and Moiola, 1982; Vail et al., 1991; Einsele, 1996) and at stage boundaries between different climatic regimes (cf. Weaver and Kuijpers, 1983; Weaver and Rothwell, 1987; Simm et al., 1991). Turbidites on the levee of the Mauritania Canyon were deposited at stage boundaries as has also been reported for several turbidites on the Madeira Abyssal Plain (Rothwell et al., 1992; Weaver et al., 1992), the Agadir Basin (Wynn et al., 2002), the Seine Abyssal Plain (Davies, 1997) and the Cap Timiris Canyon (Wien et al., accpt.).

Emplacement of the Cape Blanc Debris Flow at ≈ 155 kyr occurred during the Late Saalian glaciation (≈ 160–140 kyr; OIS 6) when sea-level was lowered to approximately -150 m relative to the present (Chappell and Shackleton, 1986). Hence, possible mechanisms for initiation of this mass gravity flow may be the collapse of an oversteepened slope caused by enhanced sediment transport to the shelf edge (e.g. Vail et al., 1991; Einsele et al., 1996) or high sediment accumulation owing to increased upwelling during the glacial period (Weaver et al., 2000) or a combination of both.

Deposition of the Mauritania Slide Complex took place at the end of the last glacial period in this area. During this time, significant climatic changes were associated with a rapid sea-level rise

which started at the peak glacial maximum about 18 kyr ago at approximately -120 m relative to the present and since then, has continued to its present-day level (Shackleton, 1987; Lambeck and Chappell, 2001). Emplacement of the Mauritania Slide Complex is roughly time-equivalent to several other large-scale submarine slope instabilities which occurred around the Pleistocene/Holocene transition (12 kyr), for instance the Turbidite *Mb* on the Madeira Abyssal Plain (12 kyr; Rothwell et al., 1992; Weaver et al., 1992) and the Turbidite *AB2* in the Agadir Basin (12 kyr; Wynn et al., 2002), the Canary Debris Flow (≈ 15 kyr; Masson, 1994; Masson, 1996), the Andøya Slide (10 kyr; Laberg et al., 2000; Taylor et al., 2003; Haflidason et al., 2004) and Fugløy Bank Slide on the Norwegian margin (?10 kyr; Taylor et al., 2003; Haflidason et al., 2004), failures on the Ulleung Basin slope in the Japan Sea (last glacial period until Pleistocene/Holocene boundary; Lee et al., 1996) and the Gebra Slide in the Antarctic (13.5–6.5 kyr; Imbo et al., 2003).

6.2 Emplacement of the Mauritania Slide Complex

6.2.1 Mode of emplacement

The above presented geochemical data give no conclusive evidence whether emplacement of the Mauritania Slide Complex results from one single-phase event or at least two events spaced ≈ 2.3–2.9 kyr in time. An interpretation which may reasonably link the two different ages for slide emplacement to a one-phase event is that the deviation results from a diachronous onset of post-slide sedimentation in the different parts of the slide. This may be due to local differences in the bottom water circulation owing to the slide topography. Stronger currents and possible erosion may have delayed the onset of post-slide sedimentation in the southeastern part of the slide (cf. Laberg et al., 2002).

A multi-phase event, by contrast, may explain the irregular shape of the Mauritania Slide Complex. Our data suggest that an older event in the northwestern part of the complex (sites GeoB 8522 and GeoB 8523) has formed the main slide body, whereas a younger event in the southeastern part (site GeoB 8520) seems to result from a subsequent collapse which formed the small protruding tongue (cf. Krastel et al., subm.).

6.2.2 Co-genesis of slide and turbidite?

Debris flows and slides on continental slopes sometimes are the precursors of turbidity currents (e.g. Simm et al., 1991; Mulder and Cochonat, 1996; Talling et al., 2004). Hence the succession of slide and turbidite deposits at sites GeoB 8522 and GeoB 8523 may be significant in terms of a genetic link between them. Assuming both events to be co-genetic and therefore time-equivalent, emplacement occurred at a certain time between ≈ 13.7–14.3 kyr. However, by the available dataset we cannot rule out the possibility of slide and turbidity current being two separate, consecutive events. Supposing this case, the age range of ≈ 13.7–14.3 kyr only applies

to turbidite emplacement whereas transport of the slide can only be stated to have occurred somewhat earlier.

7 Conclusions

Age models for the emplacement of debris flow, slide and turbidite deposits on the NW African continental margin were constructed using element stratigraphy based on shipboard XRF geochemical analysis. The results of this study are in agreement with other findings which show the NW African continental margin has been very unstable over the last Quaternary cycles. Transport events are often linked to times of severe climatic changes as they occur at stage boundaries. And even though we cannot – by the available dataset – determine the exact trigger mechanisms for these transport events, it appears that the transport processes are often controlled by climate-related sea-level changes.

To unravel the depositional history of the Mauritania Slide Complex more accurately, further investigations should focus on sediment cores derived from other parts of the slide deposit. Additional seismo-acoustic and sedimentological data are essential to verify the results presented in this study.

8 Acknowledgements

We gratefully acknowledge the assistance with the laboratory work of Karsten Enneking, Simone Pannike, Luzie Schnieders and all other participants of RV Meteor cruise M 58-1, and the help of Johanna Littek with the subsequent laboratory work at Bremen University. We likewise owe thanks to the Captain and crew members of RV Meteor cruise M 58-1. X-ray radiograph data were provided by the sedimentology working group at Bremen University. Discussions with Till J.J. Hanebuth greatly improved the quality of the manuscript. Funded by the Deutsche Forschungsgemeinschaft as part of the DFG-Research Center 'Ocean Margins' of the University of Bremen.

3 SUMMARY AND GENERAL CONCLUSIONS

This research arose out of our interest in the timing of gravity-driven sediment transport processes on the NW African continental margin, especially with respect to climate-related sea-level variations over the Quaternary glacial/interglacial cycles. Within this context, it was first aimed at the development and application of an onboard XRF technique for quick high-resolution geochemical analysis of gravity cores in order to fit age models by element stratigraphy. Element stratigraphy is based on the core-to-core correlation of elemental data on the pelagic units in newly recovered cores with age dated reference cores and allows an age assessment of the sediments. The results of this thesis demonstrate both, the quality of the high-resolution shipboard XRF analyses, and the suitability of the acquired core data for integration in age models from dated reference cores. Initially, the newly developed XRF technique was tested on stratigraphically undisturbed cores from the Southern Cape Basin. The geochemical data allowed age control back to several 100 kyr and provided valuable information on palaeoclimate, palaeoenvironment and palaeoceanography during the Quaternary in this region.

Element stratigraphy was then applied to stratigraphically disturbed cores recovered from the NW African continental margin where the pelagic sediments are interrupted by deposits which result from gravity-driven mass transport. Three different types of mass flow deposits were in the scope of this research, i.e. turbidites in the Cap Timiris Canyon off Mauritania and in the Mauritania Canyon, the Mauritania Slide Complex and the Cape Blanc Debris Flow. Turbidite activity in the Cap Timiris Canyon was hindcast to 245 kyr and shown to be generally linked to oxygen isotope stage boundaries and to glacial periods. The most recent turbidites in this canyon are seemingly coupled to the last deglaciation and the rapid Holocene sea-level rise. In the Mauritania Canyon, turbidites are also associated with oxygen isotope stage boundaries. Emplacement of the Mauritania Slide Complex occurred in several phases during the rapid sea-level rise at the Pleistocene/Holocene boundary, whereas the Cape Blanc Debris Flow was deposited during the Late Saalian glaciation. In agreement with other studies, these findings indicate that the NW African continental margin has undergone periods of overall increased mass wasting activity, and that the timing of the different transport processes appears to be strongly controlled by climate-related sea-level changes. The age assessment of the transport events and an understanding of their timing and controls adds to endeavours aimed at the formulation of mass balances and thus, contributes to the understanding of mass transport in this area.

In conclusion, element stratigraphy based on shipboard XRF analysis is shown to be a very promising approach to reconstruct the geological history of a study area. The elemental data provide a tool to date sediment columns as well as various events which leave their signature in the downcore profile, and they can also be qualitatively and quantitatively linked for instance

with marine productivity, terrigenous input, water mass chemistry, atmospheric circulation and ocean currents. As geochemical data are available within a day after recovering a sediment core, they can guide onsite decisions for mapping and more detailed sampling and, moreover, form a key element of post-cruise studies and perspectives.

While the present approach has shown shipboard application of the XRF technique to produce reliable geochemical data on sediment cores, future goals may be directed towards a simplification of the sample preparation technique in order to increase the sample throughput. This will allow core investigation at a higher resolution, possibly 2- or 1-cm, or enable analysis of a larger suite of cores within the same time-frame. The XRF technique may thus supply an enhanced dataset which may serve for highly accurate age determination as well as very detailed characterisation of the study area.

4 REFERENCES

Abrantes F (2000) 200 000 yr diatom records from Atlantic upwelling sites reveal maximum productivity during LGM and a shift in phytoplankton community structure at 185 000 yr. Earth Planet Sci Lett 176:7-16

Archer DE (1996) A data-driven model of the global calcite lysocline. Global Biochem Cycles 10:511-526

Babonneau N, Savoye B, Cremer M, Klein B (2002) Morphology and architecture of the present canyon and channel system of the Zaire deep-sea fan. Mar Petrol Geol 19:445-467

Barker PF, Camerlenghi A, Acton GD, Shipboard Scientific Party (1999) Antarctic glacial history and sea-level change. Proc ODP, Initial Reports 178. http://www-odp.tamu.edu/publications/178_IR/178TOC.HTM

Berger WH (1970) Planktonic foraminifera: selective solution and the lysocline. Mar Geol 8:111-138

Berger WH (1977) Deep-sea carbonate and the deglaciation preservation spike in pteropods and foraminifera. Nature 269:301-304

Berger WH, Wefer G (1996) Central themes of South Atlantic circulation. In: Wefer G, Berger WH, Siedler G, Webb D (eds) The South Atlantic: present and past circulation. Springer, Berlin Heidelberg New York, pp 1-11

Berger WH, Bonneau M-C, Parker FL (1982) Foraminifera on the deep-sea floor: lysocline and dissolution rate. Oceanol Acta 5:249-258

Berger WH, Lange CB, Wefer G (2002) Upwelling history of the Benguela-Namibia system: a synthesis of Leg 175 results. In: Wefer G, Berger WH, Richter C (eds) Proc ODP Sci Results 175.

Berger WH, Smetacek VS, Wefer G (1989) Ocean productivity and paleoproductivity - an overview. In: Berger WH, Smetacek VS, Wefer G (eds) Productivity of the ocean: present and past. Wiley-Interscience, New York, pp 1-34

Bertrand P, Cruise Participants (1997) Les rapports de campagne à la mer à bord du Marion Dufresne – Campagne NAUSICAA-IMAGES II-MD105 du 20/10/96 au 25/11/96. Institut Français pour la Recherche et la Technologie Polaires Brest-Iroise, Rep 97-1

Bertrand P, Giraudeau J, Malaize B, Martinez P, Gallinari M, Pedersen TF, Pierre C, Vénec-Peyré MT (2002) Occurrence of an exceptional carbonate dissolution episode during early glacial isotope stage 6 in the southeastern Atlantic. Mar Geol 180:235-248

Bertrand P, Shimmield G, Martinez P, Grousset F, Jorissen F, Paterne M, Pujol C, Bouloubassi I, Buat-Ménard P, Peypouquet J-P, Beaufortd L, Sicre M-A, Lallier-Vergès E, Foster JM, Ternois Y, other participants of the Sedorqua program (1996) The glacial ocean productivity hypothesis: the importance of regional temporal and spatial studies. Mar Geol 130:1-9

Bleil U, Cruise Participants (2004) Report and preliminary results of Meteor cruise M 58-2 Las Palmas - Las Palmas (Canary Islands, Spain), 15.05.-08.06.2003. Ber Fachber Geowissen Bremen 227

Boeckel B (2003) Late Quaternary coccolith assemblages from the south-eastern South Atlantic Ocean: implications for the palaeoceanographic evolution of the Benguela and Agulhas Current systems during the past 250 kyr. In: Present and past coccolith assemblages in the South Atlantic: implications for species ecology, carbonate contribution and palaeoceanographic applicability. PhD Thesis, University of Bremen, Ber Fachber Geowissen Bremen 211, pp 59-84

Bouma AH (1962) Sedimentology of some flysch deposits, a graphic approach to facies interpretation. Elsevier, Amsterdam, 168 pp

Bouma AH (2000) Coarse-grained and fine-grained turbidite systems as end member models: applicability and dangers. Mar Petrol Geol 17:137-143

Bouma AH, Normark WR, Barnes NE (1985) Submarine fans and related turbidite systems. Springer, Berlin Heidelberg New York, 351 pp

Boyd AJ, Nelson G (1998) Variability of the Benguela Current off the Cape Peninsula, South Africa. S Afr J Mar Sci 19:27-40

Brantley S, Glicken H (1986) Volcanic debris avalanches: earthquakes and volcanoes. Washington: USGS Cascades Volcano Observatory, Vancouver

Brown SJ, Elderfield H (1996) Variations in Mg/Ca and Sr/Ca ratios of planktonic foraminifera caused by postdepositional dissolution: evidence of shallow Mg-dependent dissolution. Paleoceanography 11:543-551

Bugge T, Belderson RH, Kenyon NH (1988) The Storegga Slide. Phil Trans Royal Soc London Ser A, 325:357-388

Chappell J, Shackleton NJ (1986) Oxygen isotopes and sea level. Nature 324(6093):137-140

Chen M-T, Chang Y-P, Chang C-C, Wang L-W, Wang C-H, Yu E-F (2002) Late Quaternary sea-surface temperature variations in the southeast Atlantic: a planktic foraminifer faunal record of the past 600 000 yr (IMAGES II MD962085). Mar Geol 180:163-181

Christie DM, Pedersen RB, Miller DJ, Shipboard Scientific Party (2001) Mantle reservoirs and migration associated with Australian-Antarctic rifting. Proc ODP, Initial Reports 187

Coffin MF, Frey FA, Wallace PJ, Shipboard Scientific Party (2000) Kerguelen Plateau-broken ridge: a large igneous province. Proc ODP, Initial Reports 183. http://www-odp.tamu.edu/publications/183_IR/183ir.htm

Crawford RJM (1998) Response of African penguins to regime changes of sardine and anchovy in the Benguela system. S Afr J Mar Sci 19:355-364

Davies TL, Van Niel B, Kidd RB, Weaver PPE (1997) High-resolution stratigraphy and turbidite processes in the Seine Abyssal Plain, northwest Africa. Geo-Mar Lett 17(2):147-153

de Villiers S (1999) Seawater strontium and Sr/Ca variability in the Atlantic and Pacific oceans. Earth Planet Sci Lett 171:623-634

de Villiers S, Shen GT, Nelson BK (1994) The Sr/Ca-temperature relationship in coralline aragonite: influence of variability in $(Sr/Ca)_{seawater}$ and skeletal growth parameters. Geochim Cosmochim Acta 58:197-208

Demarcq H, Barlow RG, Shillington FA (2003) Climatology and variability of sea surface temperature and surface chlorophyll in the Benguela and Agulhas ecosystems as observed by satellite imagery. Afr J Mar Sci 25:363-372

deMenocal P, Ortiz J, Guilderson T, Adkins J, Sarnthein M, Baker L, Yarusinsky M (2000) Abrupt onset and termination of the African Humid Period: rapid climate responses to gradual insolation forcing. Quat Sci Rev 19(1-5):347-361

Detrick RS, Honnorez J, Bryan WB, Juteau T, Shipboard Scientific Party (1988) Mid-Atlantic Ridge. In: Littleton RM, Stewart NJ (eds) Proc ODP, Initial Reports 106. Ocean Drilling Program, College Station, TX

Dick HJB, Natland JH, Miller DJ, Shipboard Scientific Party (1999) Return to Hole 735B. Proc ODP, Initial Reports 176. http://www-odp.tamu.edu/publications/176_IR/176TOC.HTM

Dickens GR (2001) Sulfate profiles and barium fronts in sediment on the Blake Ridge: present and past methane fluxes through a large gas hydrate reservoir. Geochim Cosmochim Acta 65:529-543

Diester-Haass L, Chamley H (1982) Oligocene and post-Oligocene history of sedimentation and climate off Northwest Africa (DSDP Site 369). In: von Rad U, Hinz K, Sarnthein M, Seibold E (eds) Geology of the Northwest African continental margin. Springer, Berlin Heidelberg New York, pp 529-544

Dietrich G, Kalle K, Krauss W, Siedler G (1992) Allgemeine Meereskunde: Eine Einführung in die Ozeanographie. Gebrüder Borntraeger, Berlin, 593 pp

Dott RH (1983) Episodic sedimentation - how normal is average? How rare is rare? Does it matter? J Sediment Petrol 53:5-23

Drago M (2002) A coupled debris flow-turbidity current model. Ocean Engineering 29(14):1769-1780

Droz L, Marsset T, Ondreas H, Lopez M, Savoye B, Spy-Anderson FL (2003) Architecture of an active mud-rich turbidite system: The Zaire Fan (Congo-Angola margin southeast Atlantic): results from ZaiAngo 1 and 2 cruises. AAPG Bull 87(7):1145-1168

Einsele G (1996) Event deposits: the role of sediment supply and relative sea-level changes - overview. Sediment Geol 104(1-4):11-37

Einsele G (2000) Sedimentary basins: evolution, facies, and sediment budget. Springer, Berlin Heidelberg New York, 792 pp

Einsele G, Chough SK, Shiki T (1996) Depositional events and their records - an introduction. Sediment Geol 104(1-4):1-9

Elderfield H (1990) Tracers of ocean paleoproductivity and paleochemistry: an introduction. Paleoceanography 5:711-717

Elderfield H, Cooper M, Ganssen G (2000) Sr/Ca in multiple species of planktonic foraminifera: implications for reconstructions of seawater Sr/Ca. Geochem Geophys Geosyst 1:1999GC000031

Embley RW (1976) New evidence for the occurrence of debris flow deposits in the deep sea. Geology 4:371-374

Embley RW (1980) The role of mass transport in the distribution and character of deep-ocean sediments with special reference to the North Atlantic. Mar Geol 38(1-3):23-50

Embley RW (1982) Anatomy of some Atlantic margin sediment slides and some comments on ages and mechanisms. In: Saxov S, Neiuwenhuis JK (eds) Marine slides and other mass movements. Plenum Press, New York, pp 189-214

Emiliani C (1955) Pleistocene temperatures. J Geol 63:538-578

Evans D, King EL, Kenyon NH, Brett C, Wallis D (1996) Evidence for long-term instability in the Storegga Slide region off western Norway. Mar Geol 130(3-4):281-292

Flores J-A, Gersonde R, Sierro FJ (1999) Pleistocene fluctuations in the Agulhas Current retroflection based on the calcareous plankton record. Mar Micropaleontol 37(1):1-22

Froehlich PN, Bender ML, Luedtke NA, Heath GR, de Vries T (1982) The marine phosphorous cycle. Amer J Sci 282:474-511

Fütterer DK (1983) The modern upwelling record off northwest Africa. In: Thiede J, Suess E (eds) Coastal upwelling: its sedimentary record, Part B. Sedimentary records of ancient coastal upwelling. Plenum Press, London, pp 105-121

Gammelsrød T, Bartholomae CH, Boyer DC, Filipe VLL, O'Toole MJ (1998) Intrusion of warm surface water along the Angolan-Namibian coast in February-March 1995: the 1995 Benguela Niño. S Afr J Mar Sci 19:41-56

Gee MJR, Masson DG, Watts AB, Allen PA (1999) The Saharan debris flow: an insight into the mechanics of long runout submarine debris flows. Sedimentology 46(2):317-335

Gee MJR, Masson DG, Watts AB, Mitchell NC (2001) Passage of debris flows and turbidity currents through a topographic constriction: seafloor erosion and deflection of flow pathways. Sedimentology 48(6):1389-1409

Gee MJR, Watts AB, Masson DG, Mitchell NC (2001) Landslides and the evolution of El Hierro in the Canary Islands. Mar Geol 177(3-4):271-293

Gingele FX, Schmiedl G (1999) Comparison of independent proxies in the reconstruction of deep-water circulation in the south-east Atlantic off Namibia. S Afr J Mar Sci 21:181-190

Giraudeau J (1993) Planktonic foraminiferal assemblages in surface sediments from the southwest African continental margin. Mar Geol 110:47-62

Giraudeau J, Rogers J (1994) Phytoplankton biomass and sea-surface temperature estimates from sea-bed distribution of nanofossils and planktonic foraminifera in the Benguela upwelling system. Micropalaeontology 40:275-285

Gordon AL (2003) The brawniest retroflection. Nature 421:904-905

Govindaraju K (1994) 1994 compilation of working values and descriptions for 383 geostandards. Geostand Newslett 18:1-158

Griffiths MH (2003) Stock structure of snoek *Thyrsites atun* in the Benguela: a new hypothesis. Afr J Mar Sci 25:383-386 http://www-odp.tamu.edu/publications/175_SR/synth/synth.htm

Haese RR (2000) The reactivity of iron. In: Schulz HD, Zabel M (eds) Marine geochemistry. Springer, Berlin Heidelberg New York, pp 233-261

Haflidason H, Sejrup HP, Nygard A, Mienert J, Bryn P, Lien R, Forsberg CF, Berg K, Masson D (2004) The Storegga Slide: architecture, geometry and slide development. Mar Geol 213(1-4):201-234

Heezen BC, Ericson DB, Ewing M (1954) Further evidence for a turbidity current following the 1929 Grand Banks earthquake. Deep Sea Res 1(4):193-202

Heezen BC, Ewing WM (1955) Orleansville earthquake and turbidity currents. AAPG Bull 39(12):2505-2514

Heezen BC, Ewing WM (1952) Turbidity currents and submarine slumps, and the 1929 Grand Banks (Newfoundland) earthquake. Amer J Sci 250(12):849-873

Heckel J, Haschke M, Brumme M, Schindler R (1992) Principles and applications of energy-dispersive X-ray fluorescence analysis with polarized radiation. JAAS 7:281-286

Henrich R, Hanebuth TJJ, Krastel S, Wynn RB (subm.) Architecture and sediment dynamics of the Mauritania Slide Complex. submitted to Sedimentology

Hensen C, Zabel M, Pfeifer K, Schwenk T, Kasten S, Riedinger N, Schulz HD, Boetius A (2003) Control of sulfate pore-water profiles by sedimentary events and the significance of anaerobic oxidation of methane for the burial of sulfur in marine sediments. Geochim Cosmochim Acta 67(14):2631-2647

Herzig PM, Plüger WL (1988) Exploration for hydrothermal activity near the Rodriguez Triple Junction, Indian Ocean. Can Mineral 26:721-736

Heuer V (2003) Early diagenesis at the sulphate/methane transition: (re)distribution of barium and other trace elements in sediments on the continental slope off Namibia, southeast Atlantic. In: Spurenelemente in Sedimenten des Südatlantik. Primärer Eintrag und frühdiagenetische Überprägung. PhD Thesis, University of Bremen, Ber Fachber Geowissen Bremen 209:54-76

Holz, C (2005) Climate-induced variability of fluvial and aeolian sediment supply and gravity-driven sediment transport off Northwest Africa. PhD Thesis, University of Bremen, 116 pp, http://elib.suub.uni-bremen.de/publications/dissertations/E-Diss1205_Diss_Holz.pdf

Hungr O, Evans SG (2004) Entrainment of debris in rock avalanches: an analysis of a long run-out mechanism. Geol Soc Amer Bull 116(9-10):1240-1252

Imbo Y, De Batist M, Canals M, Prieto MJ, Baraza J (2003) The Gebra Slide: a submarine slide on the Trinity Peninsula Margin, Antarctica. Mar Geol 193(3-4):235-252

Imbrie J, Hays JD, Martinson DG, McIntyre A, Mix AC, Morley JJ, Pisias NG, Prell WL, Shackleton NJ (1984) The orbital theory of Pleistocene climate: support from a revised chronology of the marine $\delta^{18}O$ record. In: Berger AL, Imbrie J, Hays J, Kukla G, Saltzman B (eds) Milankovitch and climate. Reidel, Dordrecht, pp 269-305

Imbrie J, McIntyre A, Mix AC (1989) Oceanic response to orbital forcing in the late Quaternary: observational and experimental strategies. In: Berger A, Schneider SH, Duplessy J-C (eds) Climate and geosciences, a challenge for science and society in the 21st century. Kluwer, Dordrecht, pp 121-164

Jacobi RD (1976) Sediment slides on the northwestern continental margin of Africa. Mar Geol 22(3):157-173

Jansen JHF, Van der Gaast SJ, Koster B, Vaars AJ (1998) CORTEX, a shipboard XRF-scanner for element analyses in split sediment cores. Mar Geol 151:143-153

Kastens KA, Mascle J, Auroux C, Shipboard Scientific Party (1987) Tyrrhenian Sea. In: Stewart NJ (ed) Proc ODP, Initial Reports 107. Ocean Drilling Program, College Station, TX

Kennett JP (1982) Marine geology. Prentice-Hall, Englewood Cliffs, New Jersey, 813 pp

Khripounoff A, Vangriesheim A, Babonneau N, Crassous P, Dennielou B, Savoye B (2003) Direct observation of intense turbidity current activity in the Zaire submarine valley at 4000 m water depth. Mar Geol 194(3-4):151-158

Kidd RB, Hunter PM, Simm RW (1987) Turbidity current and debris-flow pathways to the Cape Verde Basin: status of long-range side-scan sonar (GLORIA) surveys. In: Weaver PPE, Thomson J (eds) Geology and geochemistry of abyssal plains. Blackwell; Geol Soc London Spec Publ, Oxford, pp 33-48

Kidd RB, Simm RW, Searle RC (1985) Sonar acoustic facies and sediment distribution on an area of deep ocean floor. Mar Petrol Geol 2:210-221

Krastel S, Schmincke H-U, Jacobs CL, Rihm R, Le Bas TP, Alibés B (2001) Submarine landslides around the Canary Islands. J Geophys Res 106(B3):3977-3997

Krastel S, Hanebuth TJJ, Antobreh AA, Henrich R, Holz C, Kölling M, Schulz HD, Wien K, Wynn RB (2004) Cap Timiris Canyon: a newly discovered channel system offshore of Mauritania. EOS 85(42):417–432

Krastel S, Wynn RB, Hanebuth TJJ, Henrich R, Holz C, Meggers H, Kuhlmann H, Georgiopoulou A, Schulz HD (subm.) Seafloor mapping of sedimentary features offshore Mauritania, NW Africa: implications on their geohazard potential. In review at Norwegian Journal of Geology

Kuhlmann H, Freudenthal T, Helmke P, Meggers H (2004) Reconstruction of paleoceanography off NW Africa during the last 40,000 years: influence of local and regional factors on sediment accumulation. Mar Geol 207(1-4):209-224

Laberg JS, Vorren TO (2000) The Traenadjupet Slide, offshore Norway – morphology, evacuation and triggering mechanisms. Mar Geol 171(1-4):95-114

Laberg JS, Vorren TO, Dowdeswell JA, Kenyon NH, Taylor J (2000) The Andøya Slide and the Andøya Canyon, north-eastern Norwegian-Greenland Sea. Mar Geol 162(2-4):259-275

Laberg JS, Vorren TO, Mienert J, Bryn P, Lien R (2002) The Trænadjupet Slide: a large slope failure affecting the continental margin of Norway 4,000 years ago. Geo-Mar Lett 22(1):19-24

Lambeck K, Chappell J (2001) Sea level change through the last glacial cycle. Science 292(5517):679-686

Lancaster N, Kocurek G, Singhvi A, Pandey V, Deynoux M, Ghienne J-F, Lo K (2002) Late Pleistocene and Holocene dune activity and wind regimes in the western Sahara Desert of Mauritania. Geology 30(11):991-994

Lee HJ, Chough SK, Yoon SH (1996) Slope-stability change from late Pleistocene to Holocene in the Ulleung Basin, East Sea (Japan Sea). Sediment Geol 104(1-4):39-51

Lee HJ, Schwab WC, Edwards BD, Kayen RE (1991) Quantitative controls on submarine slope failure morphology. Mar Geotechnol 10:143-157

Lohmann GP (1995) A model for variation in the chemistry of planktonic foraminifera due to secondary calcification and selective dissolution. Paleoceanography 10:445-458

Lopez M (2001) Architecture and depositional pattern of the Quaternary deep-sea fan of the Amazon. Mar Petrol Geol 18(4):479-486

Lutjeharms JRE (1996) The exchange of water between the South Indian and South Atlantic oceans. In: Wefer G, Berger WH, Siedler G, Webb D (eds) The South Atlantic: present and past circulation. Springer, Berlin Heidelberg New York, pp 125-162

Lutjeharms JRE, Webb DJ, de Cuevas BA, Thompson SR (1995) Large-scale modelling of the south-east Atlantic upwelling system. S Afr J Mar Sci 16:205-225

Martin P, Lea D, Mashiotta T, Papenfuss T, Sarnthein M (1999) Variation of foraminiferal Sr/Ca over Quaternary glacial-interglacial cycles: evidence for changes in mean ocean Sr/Ca? Geochem Geophys Geosyst 1:1999GC000006

Martinez P, Bertrand P, Shimmield GB, Cochrane K, Jorissen FJ, Foster J, Dignan M (1999) Upwelling intensity and ocean productivity changes off Cape Blanc (northwest Africa) during the last 70,000 years: geochemical and micropalaeontological evidence. Mar Geol 158(1-4):57-74

Martinson DG, Pisias NG, Hays JD, Imbrie J, Moore TCJ, Shackleton NJ (1987) Age dating and the orbital theory of the ice ages: development of a high-resolution 0 to 300,000-year chronostratigraphy. Quat Res 27:1-29

Masson DG (1994) Late Quaternary turbidity current pathways to the Madeira Abyssal Plain and some constrains on turbidity current mechanisms. Basin Res 6:17-33

Masson DG (1996) Catastrophic collapse of the volcanic island of Hierro 15 ka ago and the history of landslides in the Canary Islands. Geology 24(3):231-234

Masson DG, Canals M, Alonso B, Urgeles R, Huhnerbach V (1998) The Canary Debris Flow: source area morphology and failure mechanisms. Sedimentology 45(2):411-432

Masson DG, Huggett QJ, Brunsden D (1993) The surface texture of the Saharan Debris Flow deposit and some speculations on submarine debris flow processes. Sedimentology 40:583-598

Masson DG, Van Niel B, Weaver PPE (1997) Flow processes and sediment deformation in the Canary Debris Flow on the NW African Continental Rise. Sediment Geol 110(3-4):163-179

Matthewson AP, Shimmield GB, Kroon D, Fallick AE (1995) A 300 kyr high-resolution aridity record of the North African continent. Paleoceanography 10(3), 677-692

McHugh CMG, Damuth JE, Mountain GS (2002) Cenozoic mass-transport facies and their correlation with relative sea-level change, New Jersey continental margin. Mar Geol 184(3-4):295-334

McIntyre A, Ruddiman WF, Karlin K, Mix AC (1989) Surface water response of the equatorial Atlantic Ocean to orbital forcing. Paleoceanography 4:19-55

McManus J, Berelson WM, Klinkhammer GP, Johnson KS, Coale KH, Anderson RF, Kumar N, Burdige DJ, Hammond DE, Brumsack HJ (1998) Geochemistry of barium in marine sediments: implications for its use as a paleoproxy. Geochim Cosmochim Acta 62:3453-3473

McManus J, Berelson WM, Klinkhammer GP, Kilgore TE, Hammond DE (1994) Remobilization of barium in continental margin sediments. Geochim Cosmochim Acta 58:4899-4907

Meggers H, Cruise Participants (2003) Report and preliminary results of Meteor cruise M 53-1, Limassol - Las Palmas - Mindelo, 30.03.-03.05.2002. Ber Fachber Geowissen Bremen No. 214

Mienert J, Berndt C, Laberg JS, Vorren TO (2003) Slope instability of continental margins. In: Wefer G, Billet D, Hebbeln D, Jørgensen BB, Schlüter M, Weering TCEV (eds) Ocean margin systems. Springer, Berlin Heidelberg New York, pp 179-193

Mitchell-Innes BA, Richardson AJ, Painting SJ (1999) Seasonal changes in phytoplankton biomass on the western Agulhas Bank, South Africa. S Afr J Mar Sci 21:217-233

Moore JG, Clague DA, Holcomb RT, Lipman PW, Normark WR, Torresan ME (1989) Prodigious submarine landslides on the Hawaiian ridge. J Geophys Res 94(B12):17465-17484

Moreno A, Nave S, Kuhlmann H, Canals M, Targarona J, Freudenthal T, Abrantes F (2002) Productivity response in the North Canary Basin to climate changes during the last 250000 yr: a multi-proxy approach. Earth Planet Sci Lett 196(3-4):147-159

Mulder T, Cochonat P (1996) Classification of offshore mass movements. J Sediment Res 66(1):43-57

Nelson G, Boyd AJ, Agenbag JJ, Duncombe Rae CM (1998) An upwelling filament north-west of Cape Town, South Africa. S Afr J Mar Sci 19:75-88

Nichols GJ (1999) Sedimentology and stratigraphy. Blackwell Science, Oxford, 355 pp

Paillard D, Labeyrie L, Yiou P (1996) Macintosh program performs time-series analysis. EOS Trans AGU 77:379

Peakall J, McCaffrey B, Kneller B (2000) A process model for the evolution, morphology, and architecture of sinuous submarine channels. J Sediment Res 70(3):434-448

Pearce TJ, Jarvis I (1995) High-resolution chemostratigraphy of Quaternary distal turbidites: a case study of new methods for the analysis and correlation of barren sequences. In: Dunay RE, Hailwood EA (eds) Non-biostratigraphical methods of dating and correlation. Geol Soc Spec Publ No. 89, London, pp 107-143

Peeters FJC, Acheson R, Brummer G-JA, de Ruijter WPM, Schneider RR, Ganssen GM, Ufkes E, Kroon D (2004) Vigorous exchange between the Indian and Atlantic oceans at the end of the past five glacial periods. Nature 430:661-665

Peterson LC, Haug GH, Hughen KA, Röhl U (2000) Rapid changes in the hydrologic cycle of the tropical Atlantic during the last glacial. Science 290(5498):1947-1951

Pettigrew TL, Casey JF, Miller DJ, Shipboard Scientific Party (1999) Hammer drilling and NERO. Proc ODP, Initial Reports 179. http://www-odp.tamu.edu/publications/179_IR/179TOC.HTM

Pickering KT, Hiscott RN, Hein FJ (1989) Deep-marine environments: clastic sedimentation and tectonics. Unwin-Hyman, London, 420 pp

Piper DJW, Cochonat P, Morrison ML (1999) The sequence of events around the epicentre of the 1929 Grand Banks earthquake: initiation of debris flows and turbidity current inferred from sidescan sonar. Sedimentology 46(1):79–97

Pisias NG, Martinson DG, Moore JTC, Shackleton NJ, Prell W, Hays J, Boden G (1984) High resolution stratigraphic correlation of benthic oxygen isotopic records spanning the last 300,000 years. Mar Geol 56:119-136

Plüger WL, Herzig PM, Becker K-P (1988) Geothermale Metallogenese Indischer Ozean. Fahrtber SO-52, GEMINO-3, Forschungsber RWTH Aachen BMFT (03 R 378 A):193

Posamentier HW, Jervey MT, Vail PR (1988) Eustatic controls on clastic deposition (I) - conceptual framework. In: Wilgus CK, Hastings BS, Kendall CGSC, Posamentier HW, Ross CA, van

Wagoner JC (eds) Sea-level changes: an integrated approach. Spec Publ Soc Econ Paleontol Mineral, Tulsa, pp 109-124

Posamentier HW, Vail PR (1988) Eustatic controls on clastic deposition (II) - sequence and systems tract models. In: Wilgus CK, Hastings BS, Kendall CGSC, Posamentier HW, Ross CA, van Wagoner JC (eds) Sea-level changes: an integrated approach. Spec Publ Soc Econ Paleontol Mineral, Tulsa, pp 125-154

Pye K (1987) Aeolian dust and dust deposits. Academic Press, London, 334 pp

Rau AJ, Rogers J, Lutjeharms JRE, Giraudeau J, Lee-Thorp JA, Chen M-T, Waelbroeck C (2002) A 450-kyr record of hydrological conditions on the western Agulhas Bank Slope, south of Africa. Mar Geol 180:183-201

Reeder MS, Rothwell RG, Stow DAV (2000) Influence of sea level and basin physiography on emplacement of the late Pleistocene Herodotus Basin Megaturbidite, SE Mediterranean Sea. Mar Petrol Geol 17(2):199-218

Röhl U, Abrams LJ (2000) High-resolution, downhole, and nondestructive core measurements from Sites 999 and 1001 in the Caribbean Sea: application to the Late Paleocene Thermal Maximum. In: Leckie RM, Sigurdsson H, Acton GD, Draper G (eds) Proc ODP Sci Results 165:191-203

Rothwell RG, Pearce TJ, Weaver PPE (1992) Late Quaternary evolution of the Madeira Abyssal Plain, Canary Basin, NE Atlantic. Basin Res 4:103-131

Rothwell RG, Reeder MS, Anastasakis G, Stow DAV, Thomson J, Kahler G (2000) Low sea-level stand emplacement of megaturbidites in the western and eastern Mediterranean Sea. Sediment Geol 135(1-4):75-88

Rothwell RG, Thomson J, Kahler G (1998) Low-sea-level emplacement of a very large Late Pleistocene 'megaturbidite' in the western Mediterranean Sea. Nature 392(6674):377-380

Ruddiman W, Sarnthein M, Baldauf J, Shipboard Scientific Party (1988). Eastern tropical Atlantic. Proc. ODP, Initial Reports, 108. Ocean Drilling Program, College Station, TX.

Rust U, Wienecke F (1973) Bathymetrische und geomorphologische Bearbeitung von submarinen "Einschnitten" im Seegebiet vor Westafrika: Ein methodischer Versuch. Münchener Geographische Abhandlungen 9:53-66

Sarnthein M, Thiede J, Pflaumann U (1982) Atmospheric and ocean circulation patterns off Northwest Africa during the past 25 million years. In: von Rad U, Hinz K, Sarnthein M, Seibold E (eds) Geology of the Northwest African continental margin. Springer, Berlin Heidelberg New York, pp 545-604

Schemainda R, Nehring D, Schulz S (1975) Ozeanologische Untersuchungen zum Produktionspotential der nordwestafrikanischen Wasserauftriebsregion. Geodätische und Geophysikalische Veröffentlichungen 16:1–88

Schiebel R (2002) Planktic foraminiferal sedimentation and the marine calcite budget. Global Biogeochem Cycl 16:10.1029/2001GB001459

Schlanger SO (1988) Strontium storage and release during deposition and diagenesis of marine carbonates related to sea-level variations. In: Lerman A, Meybeck M (eds) Physical and chemical weathering in geochemical cycles. Kluwer, Dordrecht, pp 323-339

Schmiedl G, Mackensen A (1997) Late Quaternary paleoproductivity and deep water circulation in the eastern South Atlantic Ocean: evidence from benthic foraminifera. Palaeogeogr Palaeoclimatol Palaeoecol 130:43-80

Schneider RR, Cruise Participants (2003) Report and preliminary results of Meteor cruise M 57-1, Cape Town - Walvis Bay, 20.01.-08.02.2003. Ber Fachber Geowissen Bremen 216

Schneider RR, Schulz HD, Hensen C (2000) Marine carbonates: their formation and destruction. In: Schulz HD, Zabel M (eds) Marine geochemistry. Springer, Berlin Heidelberg New York, pp 283-307

Schramm R, Heckel J (1998) Fast analysis of traces and major elements with ED(P)XRF using polarized X-rays: TURBOQUANT. J Phys IV Fr 8 P5:335-342

Schulz HD, Cruise Participants (1996) Report and preliminary results of Meteor cruise M 34-2, Walvis Bay - Walvis Bay, 29.01.1996-18.02.1996. Ber Fachber Geowissen Bremen 78

Schulz HD, Cruise Participants (2003) Report and preliminary results of Meteor cruise M 58-1, Dakar - Las Palmas, 15.04.-12.05.2003. Ber Fachber Geowissen Bremen 215

Schulz HN, Schulz HD (2005) Large sulfur bacteria and the formation of phosphorite. Science 307(5708):416-418

Schwab WC, Lee HJ, Twichell DC, Locat J, Nelson CH, McArthur WG, Kenyon NH (1996) Sediment mass-flow processes on a depositional lobe, outer Mississippi Fan. J Sediment Res 66(5):916-927

Seibold E, Hinz K (1974) Continental slope construction and destruction, West Africa. In: Burk CA, Drake CL (eds) The geology of continental margins. Springer, Berlin Heidelberg New York, pp 179-196

Sekiya S, Kikuchi Y (1889) The eruption of Bandai-san: Tokyo, Japan. Imperial University, Journal of the College of Science 3:91-172

Shackleton NJ (1987) Oxygen isotopes, ice volume and sea level. Quat Sci Rev 6(3-4):183-190

Shackleton NJ, Opdyke ND (1973) Oxygen isotope and palaeomagnetic stratigraphy of equatorial Pacific core V28-238: oxygen isotope temperatures and ice volumes on a 10^5 year and 10^6 year scale. Quat Res 3:39-55

Shanmugam G, Moiola RJ (1982) Eustatic control of turbidites and winnowed turbidites. Geology 10:231-235

Shanmugam G, Moiola RJ (1984) Eustatic control of calciclastic turbidites. Mar Geol 56(1-4):273-278

Shannon LV, Nelson G (1996) The Benguela: large features and processes and system variability. In: Wefer G, Berger WH, Siedler G, Webb D (eds) The South Atlantic: present and past circulation. Springer, Berlin Heidelberg New York, pp 163-210

Shen C-C, Hastings DW, Lee T, Chiu C-H, Lee M-Y, Wei K-Y, Edwards RL (2001) High precision glacial-interglacial benthic foraminiferal Sr/Ca records from the eastern equatorial Atlantic Ocean and Caribbean Sea. Earth Planet Sci Lett 190:197-209

Siebert L (1984) Large volcanic debris avalanches: characteristics of source areas, deposits, and associated eruptions. J Volcanol Geotherm Res 22(3-4):163-197

Siebert L, Beget JE, Glicken H (1995) The 1883 and late-prehistoric eruptions of Augustine volcano, Alaska. J Volcanol Geotherm Res 66(1-4):367-395

Simm RW, Kidd RB (1983) Submarine debris flow deposits detected by long-range side-scan sonar 1,000-kilometers from source. Geo-Mar Lett 3:13-16

Simm RW, Weaver PPE, Kidd RB, Jones EJW (1991) Late Quaternary mass movement on the lower continental rise and abyssal plain off Western Sahara. Sedimentology 38:27-40

Skogen MD (1999) A biophysical model applied to the Benguela upwelling system. S Afr J Mar Sci 21:235-249

Skogen MD, Shannon LJ, Stiansen JE (2003) Drift patterns of anchovy *Engraulis capensis* larvae in the southern Benguela, and their possible importance for recruitment. Afr J Mar Sci 25:37-47

Spectro Xepos (2000) Spectro Xepos Manual, Dokumentation Spectro Xepos Version 04/2000. Spectro Analytical Instruments, Kleve, Germany, info@spectro.com

Spieß V, Cruise Participants (1993) Report and preliminary results of Meteor cruise M 23-1, Cape Town - Rio de Janeiro, 04.02.1993-25.02.1993. Ber Fachber Geowissen Bremen 42

Stallard MO, Apitz SE, Dooley CA (1995) X-ray fluorescence spectrometry for field analysis of metals in marine sediments. Mar Pollut Bull 31:297-305

Steinke TD, Ward CJ (2003) Use of plastic drift cards as indicators of possible dispersal of propagules of the mangrove *Avicennia marina* by ocean currents. Afr J Mar Sci 25:169-176

Stoll HM, Schrag DP (1996) Evidence for glacial control of rapid sea level changes in the early Cretaceous. Science 272:1771-1774

Stoll HM, Schrag DP (1998) Effects of Quaternary sea level cycles on strontium in seawater. Geochim Cosmochim Acta 62:1107-1118

Stoll HM, Schrag DP (2000) Coccolith Sr/Ca as a new indicator of coccolithophorid calcification and growth rate. Geochem Geophys Geosyst 1:1999GC000015

Stoll HM, Schrag DP, Clemens SC (1999) Are seawater Sr/Ca variations preserved in Quaternary foraminifera? Geochim Cosmochim Acta 63:3535-3547

Stoll HM, Ziveri P, Geisen M, Probert I, Young JR (2002) Potential and limitations of Sr/Ca ratios in coccolith carbonate: new perspectives from cultures and monospecific samples from sediments. Philos Trans R Soc Lond A 360:719-747

Stow DAV, Shanmugam G (1980) Sequence of structures in fine-grained turbidites: Comparison of recent deep-sea and ancient flysch sediments. Sediment Geol 25(1-2):23-42

Stow DAV, Howell DG, Nelson CH (1984) Sedimentary, tectonic and sea-level controls on submarine fans and slope-apron turbidite systems. Geo-Mar Lett 3:57-64

Stow DAV, Mayall M (2000) Deep-water sedimentary systems: new models for the 21st century. Mar Petrol Geol 17(2):125-135

Talling PJ, Amy LA, Wynn RB, Peakall J, Robinson M (2004) Beds comprising debrite sandwiched within co-genetic turbidite: origin and widespread occurrence in distal depositional environments. Sedimentology 51(1):163-194

Taylor J, Dowdeswell JA, Kenyon NH (2003) Morphology and acoustic character of the Middle and Lower North Sea Fan. In: Mienert J, Weaver PPE (eds) European margin sediment dynamics: side-scan sonar and seismic images. Springer, Berlin Heidelberg New York, pp 71- 75

Tetzlaff G, Wolter K (1980) Meteorological patterns and the transport of mineral dust from the North African continent. Paleoecol Africa 12:31-42

Thomson J, Weaver PPE (1994) An AMS radiocarbon method to determine the emplacement time of recent deep-sea turbidites. Sediment Geol 89(1-2):1-7

Torres ME, Brumsack HJ, Bohrmann G, Emeis KC (1996) Barite fronts in continental margin sediments: a new look at barium remobilization in the zone of sulfate reduction and formation of heavy barites in diagenetic fronts. Chem Geol 127:125-139

Urgeles R, Canals M, Baraza J, Alonso B, Masson DG (1997) The most recent megaslides on the Canary Islands: the El Golfo Debris Avalanche and the Canary Debris Flow, west El Hierro Island. J Geophys Res 102:20305-20323

Urgeles R, Masson DG, Canals M, Watts AB, Le Bas TL, Mitchell NC (1999) Recurrent large-scale landsliding on the west flank of La Palma, Canary Islands. J Geophys Res 104(B11):25331-25348

Vail PR, Audemard F, Bowman SA, Eisner PN, Perez-Cruz C (1991) The stratigraphic signatures of tectonics, eustasy and sedimentology – an overview. In: Einsele G, Ricken W, Seilacher A (eds) Cycles and events in stratigraphy. Springer, Berlin Heidelberg New York, pp 617-659

Voight B, Janda RJ, Glicken H, Douglass PM (1983) Nature and mechanics of the Mount St. Helens rockslide-avalanche of 18 May 1980. Geotechnique 33(3):243-273

von Breymann MTK, Emeis KC, Suess E (1992) Water depth and diagenetic constraints on the use of barium as a paleoproductivity indicator. In: Summerhayes CP, Prell WL, Emeis KC (eds) Upwelling systems: evolution since the Early Miocene. Geol Soc London Spec Publ, pp 273-284

Vörösmarty CJ, Fekete BM, Meybeck M, Lammers RB (2000) Global systems of rivers: its role in organizing continental land mass and defining land-to-ocean linkages. Global Biogeochem Cycles 14(2):599-621

Watts A, Masson D (2001) New sonar evidence for recent catastrophic collapses of the north flank of Tenerife, Canary Islands. Bull Volcanol 63(1):8-19

Weaver PPE (1994) Determination of turbidity current erosional characteristics from reworked coccolith assemblages, Canary Basin, north-east Atlantic. Sedimentology 41:1025-1038

Weaver PPE, Kuijpers A (1983) Climatic control of turbidite deposition on the Madeira Abyssal Plain. Nature 306(5941):360-363

Weaver PPE, Rothwell RG (1987) Sedimentation on the Madeira Abyssal Plain over the last 300.000 years. In: Weaver PPE, Thomson J (eds) Geology and geochemistry of abyssal plains. Geol Soc London Spec Publ, pp 71-86

Weaver PPE, Rothwell RG, Ebbing J, Gunn D, Hunter PM (1992) Correlation, frequency of emplacement and source directions of megaturbidites on the Madeira Abyssal Plain. Mar Geol 109(1-2):1-20

Weaver PPE, Thomson J (1993) Calculating erosion by deep-sea turbidity currents during initiation and flow. Nature 364:136-138

Weaver PPE, Wynn RB, Kenyon NH, Evans J (2000) Continental margin sedimentation, with special reference to the north-east Atlantic margin. Sedimentology 47(s1):239-256

Weber ME, Wiedicke MH, Kudrass HR, Hubscher C, Erlenkeuser H (1997) Active growth of the Bengal Fan during sea-level rise and highstand. Geology 25(4):315-318

Weber ME, Wiedicke-Hombach M, Kudrass HR, Erlenkeuser H (2003) Bengal Fan sediment transport activity and response to climate forcing inferred from sediment physical properties. Sediment Geol 155(3-4):361-381

Wefer G, Fischer G (1993) Seasonal patterns of vertical particle flux in equatorial and coastal upwelling areas of the eastern Atlantic. Deep Sea Res I 40(8):1613-1645

Wien K, Wissmann D, Kölling M, Schulz HD (2005) Fast application of X-ray fluorescence spectrometry aboard ship: how good is the new portable Spectro Xepos analyser? Geo-Mar Lett 25(4):248-264

Wien K, Holz C, Kölling M, Schulz HD (accepted for publication) Age models for pelagites and turbidites from the Cap Timiris Canyon off Mauritania, Mar Petrol Geol

Wynn RB, Masson DG, Stow DAV, Weaver PPE (2000) The Northwest African slope apron: a modern analogue for deep-water systems with complex seafloor topography. Mar Petrol Geol 17(2):253-265

Wynn RB, Masson DG, Stow DAV, Weaver PPE (2000) Turbidity current sediment waves on the submarine slopes of the western Canary Islands. Mar Geol 163(1-4):185-198

Wynn RB, Weaver PPE, Masson DG, Stow DAV (2002) Turbidite depositional architecture across three interconnected deep-water basins on the north-west African margin. Sedimentology 49(4):669-695

Zabel M, Schulz HD (2001) Importance of submarine landslides for non-steady state conditions in pore water systems - lower Zaire (Congo) deep-sea fan. Mar Geol 176(1-4):87-99

Publications of this series:

No. 1 **Wefer, G., E. Suess and cruise participants**
Bericht über die POLARSTERN-Fahrt ANT IV/2, Rio de Janeiro - Punta Arenas, 6.11. - 1.12.1985.
60 pages, Bremen, 1986.

No. 2 **Hoffmann, G.**
Holozänstratigraphie und Küstenlinienverlagerung an der andalusischen Mittelmeerküste.
173 pages, Bremen, 1988. (out of print)

No. 3 **Wefer, G. and cruise participants**
Bericht über die METEOR-Fahrt M 6/6, Libreville - Las Palmas, 18.2. - 23.3.1988.
97 pages, Bremen, 1988.

No. 4 **Wefer, G., G.F. Lutze, T.J. Müller, O. Pfannkuche, W. Schenke, G. Siedler, W. Zenk**
Kurzbericht über die METEOR-Expedition No. 6, Hamburg - Hamburg, 28.10.1987 - 19.5.1988.
29 pages, Bremen, 1988. (out of print)

No. 5 **Fischer, G.**
Stabile Kohlenstoff-Isotope in partikulärer organischer Substanz aus dem Südpolarmeer (Atlantischer Sektor). 161 pages, Bremen, 1989.

No. 6 **Berger, W.H. and G. Wefer**
Partikelfluß und Kohlenstoffkreislauf im Ozean.
Bericht und Kurzfassungen über den Workshop vom 3.-4. Juli 1989 in Bremen.
57 pages, Bremen, 1989.

No. 7 **Wefer, G. and cruise participants**
Bericht über die METEOR - Fahrt M 9/4, Dakar - Santa Cruz, 19.2. - 16.3.1989.
103 pages, Bremen, 1989.

No. 8 **Kölling, M.**
Modellierung geochemischer Prozesse im Sickerwasser und Grundwasser.
135 pages, Bremen, 1990.

No. 9 **Heinze, P.-M.**
Das Auftriebsgeschehen vor Peru im Spätquartär. 204 pages, Bremen, 1990. (out of print)

No. 10 **Willems, H., G. Wefer, M. Rinski, B. Donner, H.-J. Bellmann, L. Eißmann, A. Müller, B.W. Flemming, H.-C. Höfle, J. Merkt, H. Streif, G. Hertweck, H. Kuntze, J. Schwaar, W. Schäfer, M.-G. Schulz, F. Grube, B. Menke**
Beiträge zur Geologie und Paläontologie Norddeutschlands: Exkursionsführer.
202 pages, Bremen, 1990.

No. 11 **Wefer, G. and cruise participants**
Bericht über die METEOR-Fahrt M 12/1, Kapstadt - Funchal, 13.3.1990 - 14.4.1990.
66 pages, Bremen, 1990.

No. 12 **Dahmke, A., H.D. Schulz, A. Kölling, F. Kracht, A. Lücke**
Schwermetallspuren und geochemische Gleichgewichte zwischen Porenlösung und Sediment im Wesermündungsgebiet. BMFT-Projekt MFU 0562, Abschlußbericht. 121 pages, Bremen, 1991.

No. 13 **Rostek, F.**
Physikalische Strukturen von Tiefseesedimenten des Südatlantiks und ihre Erfassung in Echolotregistrierungen. 209 pages, Bremen, 1991.

No. 14 **Baumann, M.**
Die Ablagerung von Tschernobyl-Radiocäsium in der Norwegischen See und in der Nordsee.
133 pages, Bremen, 1991. (out of print)

No. 15 **Kölling, A.**
Frühdiagenetische Prozesse und Stoff-Flüsse in marinen und ästuarinen Sedimenten.
140 pages, Bremen, 1991.

No. 16 **SFB 261 (ed.)**
1. Kolloquium des Sonderforschungsbereichs 261 der Universität Bremen (14.Juni 1991):
Der Südatlantik im Spätquartär: Rekonstruktion von Stoffhaushalt und Stromsystemen.
Kurzfassungen der Vorträge und Poster. 66 pages, Bremen, 1991.

No. 17 **Pätzold, J. and cruise participants**
Bericht und erste Ergebnisse über die METEOR-Fahrt M 15/2, Rio de Janeiro - Vitoria,
18.1. - 7.2.1991. 46 pages, Bremen, 1993.

No. 18 **Wefer, G. and cruise participants**
Bericht und erste Ergebnisse über die METEOR-Fahrt M 16/1, Pointe Noire - Recife,
27.3. - 25.4.1991. 120 pages, Bremen, 1991.

No. 19 **Schulz, H.D. and cruise participants**
Bericht und erste Ergebnisse über die METEOR-Fahrt M 16/2, Recife - Belem, 28.4. - 20.5.1991.
149 pages, Bremen, 1991.

No. 20 **Berner, H.**
Mechanismen der Sedimentbildung in der Fram-Straße, im Arktischen Ozean und in der Norwegischen See. 167 pages, Bremen, 1991.

No. 21 **Schneider, R.**
Spätquartäre Produktivitätsänderungen im östlichen Angola-Becken: Reaktion auf Variationen im Passat-Monsun-Windsystem und in der Advektion des Benguela-Küstenstroms.
198 pages, Bremen, 1991. (out of print)

No. 22 **Hebbeln, D.**
Spätquartäre Stratigraphie und Paläozeanographie in der Fram-Straße. 174 pages, Bremen, 1991.

No. 23 **Lücke, A.**
Umsetzungsprozesse organischer Substanz während der Frühdiagenese in ästuarinen Sedimenten.
137 pages, Bremen, 1991.

No. 24 **Wefer, G. and cruise participants**
Bericht und erste Ergebnisse der METEOR-Fahrt M 20/1, Bremen - Abidjan, 18.11.- 22.12.1991.
74 pages, Bremen, 1992.

No. 25 **Schulz, H.D. and cruise participants**
Bericht und erste Ergebnisse der METEOR-Fahrt M 20/2, Abidjan - Dakar, 27.12.1991 - 3.2.1992.
173 pages, Bremen, 1992.

No. 26 **Gingele, F.**
Zur klimaabhängigen Bildung biogener und terrigener Sedimente und ihrer Veränderung durch die Frühdiagenese im zentralen und östlichen Südatlantik. 202 pages, Bremen, 1992.

No. 27 **Bickert, T.**
Rekonstruktion der spätquartären Bodenwasserzirkulation im östlichen Südatlantik über stabile Isotope benthischer Foraminiferen. 205 pages, Bremen, 1992. (out of print)

No. 28 **Schmidt, H.**
Der Benguela-Strom im Bereich des Walfisch-Rückens im Spätquartär. 172 pages, Bremen, 1992.

No. 29 **Meinecke, G.**
Spätquartäre Oberflächenwassertemperaturen im östlichen äquatorialen Atlantik.
181 pages, Bremen, 1992.

No. 30 **Bathmann, U., U. Bleil, A. Dahmke, P. Müller, A. Nehrkorn, E.-M. Nöthig, M. Olesch, J. Pätzold, H.D. Schulz, V. Smetacek, V. Spieß, G. Wefer, H. Willems**
Bericht des Graduierten Kollegs. Stoff-Flüsse in marinen Geosystemen.
Berichtszeitraum Oktober 1990 - Dezember 1992. 396 pages, Bremen, 1992.

No. 31 **Damm, E.**
Frühdiagenetische Verteilung von Schwermetallen in Schlicksedimenten der westlichen Ostsee.
115 pages, Bremen, 1992.

No. 32 **Antia, E.E.**
Sedimentology, Morphodynamics and Facies Association of a mesotidal Barrier Island Shoreface (Spiekeroog, Southern North Sea). 370 pages, Bremen, 1993.

No. 33 **Duinker, J. and G. Wefer (ed.)**
Bericht über den 1. JGOFS-Workshop. 1./2. Dezember 1992 in Bremen. 83 pages, Bremen, 1993.

No. 34 **Kasten, S.**
Die Verteilung von Schwermetallen in den Sedimenten eines stadtbremischen Hafenbeckens.
103 pages, Bremen, 1993.

No. 35 **Spieß, V.**
Digitale Sedimentographie. Neue Wege zu einer hochauflösenden Akustostratigraphie.
199 pages, Bremen, 1993.

No. 36 **Schinzel, U.**
Laborversuche zu frühdiagenetischen Reaktionen von Eisen (III) - Oxidhydraten in marinen Sedimenten.189 pages, Bremen, 1993.

No. 37 **Sieger, R.**
CoTAM - ein Modell zur Modellierung des Schwermetalltransports in Grundwasserleitern.
56 pages, Bremen, 1993. (out of print)

No. 38 **Willems, H. (ed.)**
Geoscientific Investigations in the Tethyan Himalayas. 183 pages, Bremen, 1993.

No. 39 **Hamer, K.**
Entwicklung von Laborversuchen als Grundlage für die Modellierung des Transportverhaltens von Arsenat, Blei, Cadmium und Kupfer in wassergesättigten Säulen. 147 pages, Bremen, 1993.

No. 40 **Sieger, R.**
Modellierung des Stofftransports in porösen Medien unter Ankopplung kinetisch gesteuerter Sorptions- und Redoxprozesse sowie thermischer Gleichgewichte. 158 pages, Bremen, 1993.

No. 41 **Thießen, W.**
Magnetische Eigenschaften von Sedimenten des östlichen Südatlantiks und ihre paläozeanographische Relevanz. 170 pages, Bremen, 1993.

No. 42 **Spieß, V. and cruise participants**
Report and preliminary results of METEOR-Cruise M 23/1, Kapstadt - Rio de Janeiro, 4.-25.2.1993. 139 pages, Bremen, 1994.

No. 43 **Bleil, U. and cruise participants**
Report and preliminary results of METEOR-Cruise M 23/2, Rio de Janeiro - Recife, 27.2.-19.3.1993 133 pages, Bremen, 1994.

No. 44 **Wefer, G. and cruise participants**
Report and preliminary results of METEOR-Cruise M 23/3, Recife - Las Palmas, 21.3. - 12.4.1993 71 pages, Bremen, 1994.

No. 45 **Giese, M. and G. Wefer (ed.)**
Bericht über den 2. JGOFS-Workshop. 18../19. November 1993 in Bremen.
93 pages, Bremen, 1994.

No. 46 **Balzer, W. and cruise participants**
Report and preliminary results of METEOR-Cruise M 22/1, Hamburg - Recife, 22.9. - 21.10.1992. 24 pages, Bremen, 1994.

No. 47 **Stax, R.**
Zyklische Sedimentation von organischem Kohlenstoff in der Japan See: Anzeiger für Änderungen von Paläoozeanographie und Paläoklima im Spätkänozoikum.
150 pages, Bremen, 1994.

No. 48 **Skowronek, F.**
Frühdiagenetische Stoff-Flüsse gelöster Schwermetalle an der Oberfläche von Sedimenten des Weser Ästuares. 107 pages, Bremen, 1994.

No. 49 **Dersch-Hansmann, M.**
Zur Klimaentwicklung in Ostasien während der letzten 5 Millionen Jahre:
Terrigener Sedimenteintrag in die Japan See (ODP Ausfahrt 128). 149 pages, Bremen, 1994.

No. 50 **Zabel, M.**
Frühdiagenetische Stoff-Flüsse in Oberflächen-Sedimenten des äquatorialen und östlichen Südatlantik. 129 pages, Bremen, 1994.

No. 51 **Bleil, U. and cruise participants**
Report and preliminary results of SONNE-Cruise SO 86, Buenos Aires - Capetown, 22.4. - 31.5.93 116 pages, Bremen, 1994.

No. 52 **Symposium: The South Atlantic: Present and Past Circulation.**
Bremen, Germany, 15 - 19 August 1994. Abstracts. 167 pages, Bremen, 1994.

No. 53 **Kretzmann, U.B.**
^{57}Fe-Mössbauer-Spektroskopie an Sedimenten - Möglichkeiten und Grenzen.
183 pages, Bremen, 1994.

No. 54 **Bachmann, M.**
Die Karbonatrampe von Organyà im oberen Oberapt und unteren Unteralb (NE-Spanien, Prov. Lerida): Fazies, Zyklo- und Sequenzstratigraphie. 147 pages, Bremen, 1994. (out of print)

No. 55 **Kemle-von Mücke, S.**
Oberflächenwasserstruktur und -zirkulation des Südostatlantiks im Spätquartär.
151 pages, Bremen, 1994.

No. 56 **Petermann, H.**
Magnetotaktische Bakterien und ihre Magnetosome in Oberflächensedimenten des Südatlantiks.
134 pages, Bremen, 1994.

No. 57 **Mulitza, S.**
Spätquartäre Variationen der oberflächennahen Hydrographie im westlichen äquatorialen Atlantik.
97 pages, Bremen, 1994.

No. 58 **Segl, M. and cruise participants**
Report and preliminary results of METEOR-Cruise M 29/1, Buenos-Aires - Montevideo, 17.6. - 13.7.1994
94 pages, Bremen, 1994.

No. 59 **Bleil, U. and cruise participants**
Report and preliminary results of METEOR-Cruise M 29/2, Montevideo - Rio de Janiero 15.7. - 8.8.1994. 153 pages, Bremen, 1994.

No. 60 **Henrich, R. and cruise participants**
Report and preliminary results of METEOR-Cruise M 29/3, Rio de Janeiro - Las Palmas 11.8. - 5.9.1994. Bremen, 1994. (out of print)

No. 61 **Sagemann, J.**
Saisonale Variationen von Porenwasserprofilen, Nährstoff-Flüssen und Reaktionen in intertidalen Sedimenten des Weser-Ästuars. 110 pages, Bremen, 1994. (out of print)

No. 62 **Giese, M. and G. Wefer**
Bericht über den 3. JGOFS-Workshop. 5./6. Dezember 1994 in Bremen.
84 pages, Bremen, 1995.

No. 63 **Mann, U.**
Genese kretazischer Schwarzschiefer in Kolumbien: Globale vs. regionale/lokale Prozesse.
153 pages, Bremen, 1995. (out of print)

No. 64 **Willems, H., Wan X., Yin J., Dongdui L., Liu G., S. Dürr, K.-U. Gräfe**
The Mesozoic development of the N-Indian passive margin and of the Xigaze Forearc Basin in southern Tibet, China. – Excursion Guide to IGCP 362 Working-Group Meeting "Integrated Stratigraphy". 113 pages, Bremen, 1995. (out of print)

No. 65 **Hünken, U.**
Liefergebiets - Charakterisierung proterozoischer Goldseifen in Ghana anhand von Fluideinschluß - Untersuchungen. 270 pages, Bremen, 1995.

No. 66 **Nyandwi, N.**
The Nature of the Sediment Distribution Patterns in ther Spiekeroog Backbarrier Area, the East Frisian Islands. 162 pages, Bremen, 1995.

No. 67 **Isenbeck-Schröter, M.**
Transportverhalten von Schwermetallkationen und Oxoanionen in wassergesättigten Sanden. - Laborversuche in Säulen und ihre Modellierung -. 182 pages, Bremen, 1995.

No. 68 **Hebbeln, D. and cruise participants**
Report and preliminary results of SONNE-Cruise SO 102, Valparaiso - Valparaiso, 95.
134 pages, Bremen, 1995.

No. 69 **Willems, H. (Sprecher), U.Bathmann, U. Bleil, T. v. Dobeneck, K. Herterich, B.B. Jorgensen, E.-M. Nöthig, M. Olesch, J. Pätzold, H.D. Schulz, V. Smetacek, V. Speiß. G. Wefer**
Bericht des Graduierten-Kollegs Stoff-Flüsse in marine Geosystemen.
Berichtszeitraum Januar 1993 - Dezember 1995.
45 & 468 pages, Bremen, 1995.

No. 70 **Giese, M. and G. Wefer**
Bericht über den 4. JGOFS-Workshop. 20./21. November 1995 in Bremen. 60 pages, Bremen, 1996. (out of print)

No. 71 **Meggers, H.**
Pliozän-quartäre Karbonatsedimentation und Paläozeanographie des Nordatlantiks und des Europäischen Nordmeeres - Hinweise aus planktischen Foraminiferengemeinschaften.
143 pages, Bremen, 1996. (out of print)

No. 72 **Teske, A.**
Phylogenetische und ökologische Untersuchungen an Bakterien des oxidativen und reduktiven marinen Schwefelkreislaufs mittels ribosomaler RNA. 220 pages, Bremen, 1996. (out of print)

No. 73 **Andersen, N.**
Biogeochemische Charakterisierung von Sinkstoffen und Sedimenten aus ostatlantischen Produktions-Systemen mit Hilfe von Biomarkern. 215 pages, Bremen, 1996.

No. 74 **Treppke, U.**
Saisonalität im Diatomeen- und Silikoflagellatenfluß im östlichen tropischen und subtropischen Atlantik. 200 pages, Bremen, 1996.

No. 75 **Schüring, J.**
Die Verwendung von Steinkohlebergematerialien im Deponiebau im Hinblick auf die Pyritverwitterung und die Eignung als geochemische Barriere. 110 pages, Bremen, 1996.

No. 76 **Pätzold, J. and cruise participants**
Report and preliminary results of VICTOR HENSEN cruise JOPS II, Leg 6, Fortaleza - Recife, 10.3. - 26.3. 1995 and Leg 8, Vítoria - Vítoria, 10.4. - 23.4.1995.
87 pages, Bremen, 1996.

No. 77 **Bleil, U. and cruise participants**
Report and preliminary results of METEOR-Cruise M 34/1, Cape Town - Walvis Bay, 3.-26.1.1996.
129 pages, Bremen, 1996.

No. 78 **Schulz, H.D. and cruise participants**
Report and preliminary results of METEOR-Cruise M 34/2, Walvis Bay - Walvis Bay, 29.1.-18.2.96
133 pages, Bremen, 1996.

No. 79 **Wefer, G. and cruise participants**
Report and preliminary results of METEOR-Cruise M 34/3, Walvis Bay - Recife, 21.2.-17.3.1996.
168 pages, Bremen, 1996.

No. 80 **Fischer, G. and cruise participants**
Report and preliminary results of METEOR-Cruise M 34/4, Recife - Bridgetown, 19.3.-15.4.1996. 105 pages, Bremen, 1996.

No. 81 **Kulbrok, F.**
Biostratigraphie, Fazies und Sequenzstratigraphie einer Karbonatrampe in den Schichten der Oberkreide und des Alttertiärs Nordost-Ägyptens (Eastern Desert, N'Golf von Suez, Sinai). 153 pages, Bremen, 1996.

No. 82 **Kasten, S.**
Early Diagenetic Metal Enrichments in Marine Sediments as Documents of Nonsteady-State Depositional Conditions. Bremen, 1996.

No. 83 **Holmes, M.E.**
Reconstruction of Surface Ocean Nitrate Utilization in the Southeast Atlantic Ocean Based on Stable Nitrogen Isotopes. 113 pages, Bremen, 1996.

No. 84 **Rühlemann, C.**
Akkumulation von Carbonat und organischem Kohlenstoff im tropischen Atlantik: Spätquartäre Produktivitäts-Variationen und ihre Steuerungsmechanismen. 139 pages, Bremen, 1996.

No. 85 **Ratmeyer, V.**
Untersuchungen zum Eintrag und Transport lithogener und organischer partikulärer Substanz im östlichen subtropischen Nordatlantik. 154 pages, Bremen, 1996.

No. 86 **Cepek, M.**
Zeitliche und räumliche Variationen von Coccolithophoriden-Gemeinschaften im subtropischen Ost-Atlantik: Untersuchungen an Plankton, Sinkstoffen und Sedimenten. 156 pages, Bremen, 1996.

No. 87 **Otto, S.**
Die Bedeutung von gelöstem organischen Kohlenstoff (DOC) für den Kohlenstoffffluß im Ozean. 150 pages, Bremen, 1996.

No. 88 **Hensen, C.**
Frühdiagenetische Prozesse und Quantifizierung benthischer Stoff-Flüsse in Oberflächensedimenten des Südatlantiks. 132 pages, Bremen, 1996.

No. 89 **Giese, M. and G. Wefer**
Bericht über den 5. JGOFS-Workshop. 27./28. November 1996 in Bremen. 73 pages, Bremen, 1997.

No. 90 **Wefer, G. and cruise participants**
Report and preliminary results of METEOR-Cruise M 37/1, Lisbon - Las Palmas, 4.-23.12.1996. 79 pages, Bremen, 1997.

No. 91 **Isenbeck-Schröter, M., E. Bedbur, M. Kofod, B. König, T. Schramm & G. Mattheß**
Occurrence of Pesticide Residues in Water - Assessment of the Current Situation in Selected EU Countries. 65 pages, Bremen 1997.

No. 92 **Kühn, M.**
Geochemische Folgereaktionen bei der hydrogeothermalen Energiegewinnung. 129 pages, Bremen 1997.

No. 93 **Determann, S. & K. Herterich**
JGOFS-A6 "Daten und Modelle": Sammlung JGOFS-relevanter Modelle in Deutschland. 26 pages, Bremen, 1997.

No. 94 **Fischer, G. and cruise participants**
Report and preliminary results of METEOR-Cruise M 38/1, Las Palmas - Recife, 25.1.-1.3.1997, with Appendix: Core Descriptions from METEOR Cruise M 37/1. Bremen, 1997.

No. 95 **Bleil, U. and cruise participants**
Report and preliminary results of METEOR-Cruise M 38/2, Recife - Las Palmas, 4.3.-14.4.1997. 126 pages, Bremen, 1997.

No. 96 **Neuer, S. and cruise participants**
Report and preliminary results of VICTOR HENSEN-Cruise 96/1. Bremen, 1997.

No. 97 **Villinger, H. and cruise participants**
Fahrtbericht SO 111, 20.8. - 16.9.1996. 115 pages, Bremen, 1997.

No. 98 **Lüning, S.**
Late Cretaceous - Early Tertiary sequence stratigraphy, paleoecology and geodynamics of Eastern Sinai, Egypt. 218 pages, Bremen, 1997.

No. 99 **Haese, R.R.**
Beschreibung und Quantifizierung frühdiagenetischer Reaktionen des Eisens in Sedimenten des Südatlantiks. 118 pages, Bremen, 1997.

No. 100 **Lührte, R. von**
Verwertung von Bremer Baggergut als Material zur Oberflächenabdichtung von Deponien - Geochemisches Langzeitverhalten und Schwermetall-Mobilität (Cd, Cu, Ni, Pb, Zn). Bremen, 1997.

No. 101 **Ebert, M.**
Der Einfluß des Redoxmilieus auf die Mobilität von Chrom im durchströmten Aquifer. 135 pages, Bremen, 1997.

No. 102 **Krögel, F.**
Einfluß von Viskosität und Dichte des Seewassers auf Transport und Ablagerung von Wattsedimenten (Langeooger Rückseitenwatt, südliche Nordsee). 168 pages, Bremen, 1997.

No. 103 **Kerntopf, B.**
Dinoflagellate Distribution Patterns and Preservation in the Equatorial Atlantic and Offshore North-West Africa. 137 pages, Bremen, 1997.

No. 104 **Breitzke, M.**
Elastische Wellenausbreitung in marinen Sedimenten - Neue Entwicklungen der Ultraschall Sedimentphysik und Sedimentechographie. 298 pages, Bremen, 1997.

No. 105 **Marchant, M.**
Rezente und spätquartäre Sedimentation planktischer Foraminiferen im Peru-Chile Strom. 115 pages, Bremen, 1997.

No. 106 **Habicht, K.S.**
Sulfur isotope fractionation in marine sediments and bacterial cultures. 125 pages, Bremen, 1997.

No. 107 **Hamer, K., R.v. Lührte, G. Becker, T. Felis, S. Keffel, B. Strotmann, C. Waschkowitz, M. Kölling, M. Isenbeck-Schröter, H.D. Schulz**
Endbericht zum Forschungsvorhaben 060 des Landes Bremen: Baggergut der Hafengruppe Bremen-Stadt: Modelluntersuchungen zur Schwermetallmobilität und Möglichkeiten der Verwertung von Hafenschlick aus Bremischen Häfen. 98 pages, Bremen, 1997.

No. 108 **Greeff, O.W.**
Entwicklung und Erprobung eines benthischen Landersystemes zur *in situ*-Bestimmung von Sulfatreduktionsraten mariner Sedimente. 121 pages, Bremen, 1997.

No. 109 **Pätzold, M. und G. Wefer**
Bericht über den 6. JGOFS-Workshop am 4./5.12.1997 in Bremen. Im Anhang: Publikationen zum deutschen Beitrag zur Joint Global Ocean Flux Study (JGOFS), Stand 1/1998. 122 pages, Bremen, 1998.

No. 110 **Landenberger, H.**
CoTReM, ein Multi-Komponenten Transport- und Reaktions-Modell. 142 pages, Bremen, 1998.

No. 111 **Villinger, H. und Fahrtteilnehmer**
Fahrtbericht SO 124, 4.10. - 16.10.199. 90 pages, Bremen, 1997.

No. 112 **Gietl, R.**
Biostratigraphie und Sedimentationsmuster einer nordostägyptischen Karbonatrampe unter Berücksichtigung der Alveolinen-Faunen. 142 pages, Bremen, 1998.

No. 113 **Ziebis, W.**
The Impact of the Thalassinidean Shrimp *Callianassa truncata* on the Geochemistry of permeable, coastal Sediments. 158 pages, Bremen 1998.

No. 114 **Schulz, H.D. and cruise participants**
Report and preliminary results of METEOR-Cruise M 41/1, Málaga - Libreville, 13.2.-15.3.1998. Bremen, 1998.

No. 115 **Völker, D.J.**
Untersuchungen an strömungsbeeinflußten Sedimentationsmustern im Südozean. Interpretation sedimentechographischer Daten und numerische Modellierung. 152 pages, Bremen, 1998.

No. 116 **Schlünz, B.**
Riverine Organic Carbon Input into the Ocean in Relation to Late Quaternary Climate Change. 136 pages, Bremen, 1998.

No. 117 **Kuhnert, H.**
Aufzeichnug des Klimas vor Westaustralien in stabilen Isotopen in Korallenskeletten. 109 pages, Bremen, 1998.

No. 118 **Kirst, G.**
Rekonstruktion von Oberflächenwassertemperaturen im östlichen Südatlantik anhand von Alkenonen. 130 pages, Bremen, 1998.

No. 119 **Dürkoop, A.**
Der Brasil-Strom im Spätquartär: Rekonstruktion der oberflächennahen Hydrographie während der letzten 400 000 Jahre. 121 pages, Bremen, 1998.

No. 120 **Lamy, F.**
Spätquartäre Variationen des terrigenen Sedimenteintrags entlang des chilenischen Kontinentalhangs als Abbild von Klimavariabilität im Milanković- und Sub-Milanković-Zeitbereich. 141 pages, Bremen, 1998.

No. 121 **Neuer, S. and cruise participants**
Report and preliminary results of POSEIDON-Cruise Pos 237/2, Vigo – Las Palmas, 18.3.-31.3.1998. 39 pages, Bremen, 1998

No. 122 **Romero, O.E.**
Marine planktonic diatoms from the tropical and equatorial Atlantic: temporal flux patterns and the sediment record. 205 pages, Bremen, 1998.

No. 123 **Spiess, V. und Fahrtteilnehmer**
Report and preliminary results of RV SONNE Cruise 125, Cochin – Chittagong, 17.10.-17.11.1997. 128 pages, Bremen, 1998.

No. 124 **Arz, H.W.**
Dokumentation von kurzfristigen Klimaschwankungen des Spätquartärs in Sedimenten des westlichen äquatorialen Atlantiks. 96 pages, Bremen, 1998.

No. 125 **Wolff, T.**
Mixed layer characteristics in the equatorial Atlantic during the late Quaternary as deduced from planktonic foraminifera. 132 pages, Bremen, 1998.

No. 126 **Dittert, N.**
Late Quaternary Planktic Foraminifera Assemblages in the South Atlantic Ocean: Quantitative Determination and Preservational Aspects. 165 pages, Bremen, 1998.

No. 127 **Höll, C.**
Kalkige und organisch-wandige Dinoflagellaten-Zysten in Spätquartären Sedimenten des tropischen Atlantiks und ihre palökologische Auswertbarkeit. 121 pages, Bremen, 1998.

No. 128 **Hencke, J.**
Redoxreaktionen im Grundwasser: Etablierung und Verlagerung von Reaktionsfronten und ihre Bedeutung für die Spurenelement-Mobilität. 122 pages, Bremen 1998.

No. 129 **Pätzold, J. and cruise participants**
Report and preliminary results of METEOR-Cruise M 41/3, Vítoria, Brasil – Salvador de Bahia, Brasil, 18.4. - 15.5.1998. Bremen, 1999.

No. 130 **Fischer, G. and cruise participants**
Report and preliminary results of METEOR-Cruise M 41/4, Salvador de Bahia, Brasil – Las Palmas, Spain, 18.5. – 13.6.1998. Bremen, 1999.

No. 131 **Schlünz, B. und G. Wefer**
Bericht über den 7. JGOFS-Workshop am 3. und 4.12.1998 in Bremen. Im Anhang: Publikationen zum deutschen Beitrag zur Joint Global Ocean Flux Study (JGOFS), Stand 1/ 1999. 100 pages, Bremen, 1999.

No. 132 **Wefer, G. and cruise participants**
Report and preliminary results of METEOR-Cruise M 42/4, Las Palmas - Las Palmas - Viena do Castelo; 26.09.1998 - 26.10.1998. 104 pages, Bremen, 1999.

No. 133 **Felis, T.**
Climate and ocean variability reconstructed from stable isotope records of modern subtropical corals (Northern Red Sea). 111 pages, Bremen, 1999.

No. 134 **Draschba , S.**
North Atlantic climate variability recorded in reef corals from Bermuda. 108 pages, Bremen, 1999.

No. 135 **Schmieder, F.**
Magnetic Cyclostratigraphy of South Atlantic Sediments. 82 pages, Bremen, 1999.

No. 136 **Rieß, W.**
In situ measurements of respiration and mineralisation processes – Interaction between fauna and geochemical fluxes at active interfaces. 68 pages, Bremen, 1999.

No. 137 **Devey, C.W. and cruise participants**
Report and shipboard results from METEOR-cruise M 41/2, Libreville – Vitoria, 18.3. – 15.4.98. 59 pages, Bremen, 1999.

No. 138 **Wenzhöfer, F.**
Biogeochemical processes at the sediment water interface and quantification of metabolically driven calcite dissolution in deep sea sediments. 103 pages, Bremen, 1999.

No. 139 **Klump, J.**
Biogenic barite as a proxy of paleoproductivity variations in the Southern Peru-Chile Current. 107 pages, Bremen, 1999.

No. 140 **Huber, R.**
Carbonate sedimentation in the northern Northatlantic since the late pliocene. 103 pages, Bremen, 1999.

No. 141 **Schulz, H.**
Nitrate-storing sulfur bacteria in sediments of coastal upwelling. 94 pages, Bremen, 1999.

No. 142 **Mai, S.**
Die Sedimentverteilung im Wattenmeer: ein Simulationsmodell. 114 pages, Bremen, 1999.

No. 143 **Neuer, S. and cruise participants**
Report and preliminary results of Poseidon Cruise 248, Las Palmas - Las Palmas, 15.2.-26.2.1999.
45 pages, Bremen, 1999.

No. 144 **Weber, A.**
Schwefelkreislauf in marinen Sedimenten und Messung von *in situ* Sulfatreduktionsraten.
122 pages, Bremen, 1999.

No. 145 **Hadeler, A.**
Sorptionsreaktionen im Grundwasser: Unterschiedliche Aspekte bei der Modellierung des Transportverhaltens von Zink. 122 pages, 1999.

No. 146 **Dierßen, H.**
Zum Kreislauf ausgewählter Spurenmetalle im Südatlantik: Vertikaltransport und Wechselwirkung zwischen Partikeln und Lösung. 167 pages, Bremen, 1999.

No. 147 **Zühlsdorff, L.**
High resolution multi-frequency seismic surveys at the Eastern Juan de Fuca Ridge Flank and the Cascadia Margin – Evidence for thermally and tectonically driven fluid upflow in marine sediments. 118 pages, Bremen 1999.

No. 148 **Kinkel, H.**
Living and late Quaternary Coccolithophores in the equatorial Atlantic Ocean: response of distribution and productivity patterns to changing surface water circulation. 183 pages, Bremen, 2000.

No. 149 **Pätzold, J. and cruise participants**
Report and preliminary results of METEOR Cruise M 44/3, Aqaba (Jordan) - Safaga (Egypt) – Dubá (Saudi Arabia) – Suez (Egypt) - Haifa (Israel), 12.3.-26.3.-2.4.-4.4.1999. 135 pages, Bremen, 2000.

No. 150 **Schlünz, B. and G. Wefer**
Bericht über den 8. JGOFS-Workshop am 2. und 3.12.1999 in Bremen. Im Anhang:
Publikationen zum deutschen Beitrag zur Joint Global Ocean Flux Study (JGOFS), Stand 1/ 2000.
95 pages, Bremen, 2000.

No. 151 **Schnack, K.**
Biostratigraphie und fazielle Entwicklung in der Oberkreide und im Alttertiär im Bereich der Kharga Schwelle, Westliche Wüste, SW-Ägypten. 142 pages, Bremen, 2000.

No. 152 **Karwath, B.**
Ecological studies on living and fossil calcareous dinoflagellates of the equatorial and tropical Atlantic Ocean. 175 pages, Bremen, 2000.

No. 153 **Moustafa, Y.**
Paleoclimatic reconstructions of the Northern Red Sea during the Holocene inferred from stable isotope records of modern and fossil corals and molluscs. 102 pages, Bremen, 2000.

No. 154 **Villinger, H. and cruise participants**
Report and preliminary results of SONNE-cruise 145-1 Balboa – Talcahuana, 21.12.1999 – 28.01.2000.
147 pages, Bremen, 2000.

No. 155 **Rusch, A.**
Dynamik der Feinfraktion im Oberflächenhorizont permeabler Schelfsedimente. 102 pages, Bremen, 2000.

No. 156 **Moos, C.**
Reconstruction of upwelling intensity and paleo-nutrient gradients in the northwest Arabian Sea derived from stable carbon and oxygen isotopes of planktic foraminifera. 103 pages, Bremen, 2000.

No. 157 **Xu, W.**
Mass physical sediment properties and trends in a Wadden Sea tidal basin. 127 pages, Bremen, 2000.

No. 158 **Meinecke, G. and cruise participants**
Report and preliminary results of METEOR Cruise M 45/1, Malaga (Spain) - Lissabon (Portugal),
19.05. - 08.06.1999. 39 pages, Bremen, 2000.

No. 159 **Vink, A.**
Reconstruction of recent and late Quaternary surface water masses of the western subtropical Atlantic Ocean based on calcareous and organic-walled dinoflagellate cysts. 160 pages, Bremen, 2000.

No. 160 **Willems, H. (Sprecher), U. Bleil, R. Henrich, K. Herterich, B.B. Jørgensen, H.-J. Kuß, M. Olesch, H.D. Schulz,V. Spieß, G. Wefer**
Abschlußbericht des Graduierten-Kollegs Stoff-Flüsse in marine Geosystemen.
Zusammenfassung und Berichtszeitraum Januar 1996 - Dezember 2000. 340 pages, Bremen, 2000.

No. 161 **Sprengel, C.**
Untersuchungen zur Sedimentation und Ökologie von Coccolithophoriden im Bereich der Kanarischen Inseln: Saisonale Flussmuster und Karbonatexport. 165 pages, Bremen, 2000.

No. 162 **Donner, B. and G. Wefer**
Bericht über den JGOFS-Workshop am 18.-21.9.2000 in Bremen:
Biogeochemical Cycles: German Contributions to the International Joint Global Ocean Flux Study.
87 pages, Bremen, 2000.

No. 163 **Neuer, S. and cruise participants**
Report and preliminary results of Meteor Cruise M 45/5, Bremen – Las Palmas, October 1 – November 3, 1999. 93 pages, Bremen, 2000.

No. 164 **Devey, C. and cruise participants**
Report and preliminary results of Sonne Cruise SO 145/2, Talcahuano (Chile) - Arica (Chile), February 4 – February 29, 2000. 63 pages, Bremen, 2000.

No. 165 **Freudenthal, T.**
Reconstruction of productivity gradients in the Canary Islands region off Morocco by means of sinking particles and sediments. 147 pages, Bremen, 2000.

No. 166 **Adler, M.**
Modeling of one-dimensional transport in porous media with respect to simultaneous geochemical reactions in CoTReM. 147 pages, Bremen, 2000.

No. 167 **Santamarina Cuneo, P.**
Fluxes of suspended particulate matter through a tidal inlet of the East Frisian Wadden Sea (southern North Sea). 91 pages, Bremen, 2000.

No. 168 **Benthien, A.**
Effects of CO_2 and nutrient concentration on the stable carbon isotope composition of C37:2 alkenones in sediments of the South Atlantic Ocean. 104 pages, Bremen, 2001.

No. 169 **Lavik, G.**
Nitrogen isotopes of sinking matter and sediments in the South Atlantic. 140 pages, Bremen, 2001.

No. 170 **Budziak, D.**
Late Quaternary monsoonal climate and related variations in paleoproductivity and alkenone-derived sea-surface temperatures in the western Arabian Sea. 114 pages, Bremen, 2001.

No. 171 **Gerhardt, S.**
Late Quaternary water mass variability derived from the pteropod preservation state in sediments of the western South Atlantic Ocean and the Caribbean Sea. 109 pages, Bremen, 2001.

No. 172 **Bleil, U. and cruise participants**
Report and preliminary results of Meteor Cruise M 46/3, Montevideo (Uruguay) – Mar del Plata (Argentina), January 4 – February 7, 2000. Bremen, 2001.

No. 173 **Wefer, G. and cruise participants**
Report and preliminary results of Meteor Cruise M 46/4, Mar del Plata (Argentina) – Salvador da Bahia (Brazil), February 10 – March 13, 2000. With partial results of METEOR cruise M 46/2. 136 pages, Bremen, 2001.

No. 174 **Schulz, H.D. and cruise participants**
Report and preliminary results of Meteor Cruise M 46/2, Recife (Brazil) – Montevideo (Uruguay), December 2 – December 29, 1999. 107 pages, Bremen, 2001.

No. 175 **Schmidt, A.**
Magnetic mineral fluxes in the Quaternary South Atlantic: Implications for the paleoenvironment.
97 pages, Bremen, 2001.

No. 176 **Bruhns, P.**
Crystal chemical characterization of heavy metal incorporation in brick burning processes.
93 pages, Bremen, 2001.

No. 177 **Karius, V.**
Baggergut der Hafengruppe Bremen-Stadt in der Ziegelherstellung. 131 pages, Bremen, 2001.

No. 178 **Adegbie, A. T.**
Reconstruction of paleoenvironmental conditions in Equatorial Atlantic and the Gulf of Guinea Basins for the last 245,000 years. 113 pages, Bremen, 2001.

No. 179 **Spieß, V. and cruise participants**
Report and preliminary results of R/V Sonne Cruise SO 149, Victoria - Victoria, 16.8. - 16.9.2000.
100 pages, Bremen, 2001.

No. 180 **Kim, J.-H.**
Reconstruction of past sea-surface temperatures in the eastern South Atlantic and the eastern South Pacific across Termination I based on the Alkenone Method. 114 pages, Bremen, 2001.

No. 181 **von Lom-Keil, H.**
Sedimentary waves on the Namibian continental margin and in the Argentine Basin – Bottom flow reconstructions based on high resolution echosounder data. 126 pages, Bremen, 2001.

No. 182 **Hebbeln, D. and cruise participants**
PUCK: Report and preliminary results of R/V Sonne Cruise SO 156, Valparaiso (Chile) - Talcahuano (Chile), March 29 - May 14, 2001. 195 pages, Bremen, 2001.

No. 183 **Wendler, J.**
Reconstruction of astronomically-forced cyclic and abrupt paleoecological changes in the Upper Cretaceous Boreal Realm based on calcareous dinoflagellate cysts. 149 pages, Bremen, 2001.

No. 184 **Volbers, A.**
Planktic foraminifera as paleoceanographic indicators: production, preservation, and reconstruction of upwelling intensity. Implications from late Quaternary South Atlantic sediments. 122 pages, Bremen, 2001.

No. 185 **Bleil, U. and cruise participants**
Report and preliminary results of R/V METEOR Cruise M 49/3, Montevideo (Uruguay) - Salvador (Brasil), March 9 - April 1, 2001. 99 pages, Bremen, 2001.

No. 186 **Scheibner, C.**
Architecture of a carbonate platform-to-basin transition on a structural high (Campanian-early Eocene, Eastern Desert, Egypt) – classical and modelling approaches combined. 173 pages, Bremen, 2001.

No. 187 **Schneider, S.**
Quartäre Schwankungen in Strömungsintensität und Produktivität als Abbild der Wassermassen-Variabilität im äquatorialen Atlantik (ODP Sites 959 und 663): Ergebnisse aus Siltkorn-Analysen. 134 pages, Bremen, 2001.

No. 188 **Uliana, E.**
Late Quaternary biogenic opal sedimentation in diatom assemblages in Kongo Fan sediments. 96 pages, Bremen, 2002.

No. 189 **Esper, O.**
Reconstruction of Recent and Late Quaternary oceanographic conditions in the eastern South Atlantic Ocean based on calcareous- and organic-walled dinoflagellate cysts. 130 pages, Bremen, 2001.

No. 190 **Wendler, I.**
Production and preservation of calcareous dinoflagellate cysts in the modern Arabian Sea. 117 pages, Bremen, 2002.

No. 191 **Bauer, J.**
Late Cenomanian – Santonian carbonate platform evolution of Sinai (Egypt): stratigraphy, facies, and sequence architecture. 178 pages, Bremen, 2002.

No. 192 **Hildebrand-Habel, T.**
Die Entwicklung kalkiger Dinoflagellaten im Südatlantik seit der höheren Oberkreide. 152 pages, Bremen, 2002.

No. 193 **Hecht, H.**
Sauerstoff-Optopoden zur Quantifizierung von Pyritverwitterungsprozessen im Labor- und Langzeit-in-situ-Einsatz. Entwicklung - Anwendung – Modellierung. 130 pages, Bremen, 2002.

No. 194 **Fischer, G. and cruise participants**
Report and Preliminary Results of RV METEOR-Cruise M49/4, Salvador da Bahia – Halifax, 4.4.-5.5.2001. 84 pages, Bremen, 2002.

No. 195 **Gröger, M.**
Deep-water circulation in the western equatorial Atlantic: inferences from carbonate preservation studies and silt grain-size analysis. 95 pages, Bremen, 2002.

No. 196 **Meinecke,G. and cruise participants**
Report of RV POSEIDON Cruise POS 271, Las Palmas - Las Palmas, 19.3.-29.3.2001. 19 pages, Bremen, 2002.

No. 197 **Meggers, H. and cruise participants**
Report of RV POSEIDON Cruise POS 272, Las Palmas - Las Palmas, 1.4.-14.4.2001. 19 pages, Bremen, 2002.

No. 198 **Gräfe, K.-U.**
Stratigraphische Korrelation und Steuerungsfaktoren Sedimentärer Zyklen in ausgewählten Borealen und Tethyalen Becken des Cenoman/Turon (Oberkreide) Europas und Nordwestafrikas. 197 pages, Bremen, 2002.

No. 199 **Jahn, B.**
Mid to Late Pleistocene Variations of Marine Productivity in and Terrigenous Input to the Southeast Atlantic. 97 pages, Bremen, 2002.

No. 200 **Al-Rousan, S.**
Ocean and climate history recorded in stable isotopes of coral and foraminifers from the northern Gulf of Aqaba. 116 pages, Bremen, 2002.

No. 201 **Azouzi, B.**
Regionalisierung hydraulischer und hydrogeochemischer Daten mit geostatistischen Methoden. 108 pages, Bremen, 2002.

No. 202 **Spieß, V. and cruise participants**
Report and preliminary results of METEOR Cruise M 47/3, Libreville (Gabun) - Walvis Bay (Namibia), 01.06 - 03.07.2000. 70 pages, Bremen 2002.

No. 203 **Spieß, V. and cruise participants**
Report and preliminary results of METEOR Cruise M 49/2, Montevideo (Uruguay) - Montevideo, 13.02 - 07.03.2001. 84 pages, Bremen 2002.

No. 204 **Mollenhauer, G.**
Organic carbon accumulation in the South Atlantic Ocean: Sedimentary processes and glacial/interglacial Budgets. 139 pages, Bremen 2002.

No. 205 **Spieß, V. and cruise participants**
Report and preliminary results of METEOR Cruise M49/1, Cape Town (South Africa) - Montevideo (Uruguay), 04.01.2000 - 10.02.2000. 57 pages, Bremen, 2003.

No. 206 **Meier, K.J.S.**
Calcareous dinoflagellates from the Mediterranean Sea: taxonomy, ecology and palaeoenvironmental application. 126 pages, Bremen, 2003.

No. 207 **Rakic, S.**
Untersuchungen zur Polymorphie und Kristallchemie von Silikaten der Zusammensetzung $Me_2Si_2O_5$ (Me:Na, K). 139 pages, Bremen, 2003.

No. 208 **Pfeifer, K.**
Auswirkungen frühdiagenetischer Prozesse auf Calcit- und Barytgehalte in marinen Oberflächen-sedimenten. 110 pages, Bremen, 2003.

No. 209 **Heuer, V.**
Spurenelemente in Sedimenten des Südatlantik. Primärer Eintrag und frühdiagenetische Überprägung. 136 pages, Bremen, 2003.

No. 210 **Streng, M.**
Phylogenetic Aspects and Taxonomy of Calcareous Dinoflagellates. 157 pages, Bremen 2003.

No. 211 **Boeckel, B.**
Present and past coccolith assemblages in the South Atlantic: implications for species ecology, carbonate contribution and palaeoceanographic applicability. 157 pages, Bremen, 2003.

No. 212 **Precht, E.**
Advective interfacial exchange in permeable sediments driven by surface gravity waves and its ecological consequences. 131 pages, Bremen, 2003.

No. 213 **Frenz, M.**
Grain-size composition of Quaternary South Atlantic sediments and its paleoceanographic significance. 123 pages, Bremen, 2003.

No. 214 **Meggers, H. and cruise participants**
Report and preliminary results of METEOR Cruise M 53/1, Limassol - Las Palmas – Mindelo, 30.03.2002 - 03.05.2002. 81 pages, Bremen, 2003.

No. 215 **Schulz, H.D. and cruise participants**
Report and preliminary results of METEOR Cruise M 58/1, Dakar – Las Palmas, 15.04..2003 - 12.05.2003. Bremen, 2003.

No. 216 **Schneider, R. and cruise participants**
Report and preliminary results of METEOR Cruise M 57/1, Cape Town – Walvis Bay, 20.01. – 08.02.2003. 123 pages, Bremen, 2003.

No. 217 **Kallmeyer, J.**
Sulfate reduction in the deep Biosphere. 157 pages, Bremen, 2003.

No. 218 **Røy, H.**
Dynamic Structure and Function of the Diffusive Boundary Layer at the Seafloor. 149 pages, Bremen, 2003.

No. 219 **Pätzold, J., C. Hübscher and cruise participants**
Report and preliminary results of METEOR Cruise M 52/2&3, Istanbul – Limassol – Limassol, 04.02. – 27.03.2002. Bremen, 2003.

No. 220 **Zabel, M. and cruise participants**
Report and preliminary results of METEOR Cruise M 57/2, Walvis Bay – Walvis Bay, 11.02. – 12.03.2003. 136 pages, Bremen 2003.

No. 221 **Salem, M.**
Geophysical investigations of submarine prolongations of alluvial fans on the western side of the Gulf of Aqaba-Red Sea. 100 pages, Bremen, 2003.

No. 222 **Tilch, E.**
Oszillation von Wattflächen und deren fossiles Erhaltungspotential (Spiekerooger Rückseitenwatt, südliche Nordsee). 137 pages, Bremen, 2003.

No. 223 **Frisch, U. and F. Kockel**
Der Bremen-Knoten im Strukturnetz Nordwest-Deutschlands. Stratigraphie, Paläogeographie, Strukturgeologie. 379 pages, Bremen, 2004.

No. 224 **Kolonic, S.**
Mechanisms and biogeochemical implications of Cenomanian/Turonian black shale formation in North Africa: An integrated geochemical, millennial-scale study from the Tarfaya-LaAyoune Basin in SW Morocco. 174 pages, Bremen, 2004. Report online available only.

No. 225 **Panteleit, B.**
Geochemische Prozesse in der Salz- Süßwasser Übergangszone. 106 pages, Bremen, 2004.

No. 226 **Seiter, K.**
Regionalisierung und Quantifizierung benthischer Mineralisationsprozesse. 135 pages, Bremen, 2004.

No. 227 **Bleil, U. and cruise participants**
Report and preliminary results of METEOR Cruise M 58/2, Las Palmas – Las Palmas (Canary Islands, Spain), 15.05. – 08.06.2003. 123 pages, Bremen, 2004.

No. 228 **Kopf, A. and cruise participants**
Report and preliminary results of SONNE Cruise SO175, Miami - Bremerhaven, 12.11 - 30.12.2003. 218 pages, Bremen, 2004.

No. 229 **Fabian, M.**
Near Surface Tilt and Pore Pressure Changes Induced by Pumping in Multi-Layered Poroelastic Half-Spaces.
121 pages, Bremen, 2004.

No. 230 **Segl, M. , and cruise participants**
Report and preliminary results of POSEIDON cruise 304 Galway – Lisbon, 5. – 22. Oct. 2004, 27 pages, Bremen 2004

No. 231 **Meinecke, G. and cruise participants**
Report and preliminary results of POSEIDON Cruise 296, 42 pages, Bremen 2005.

No. 232 **Meinecke, G. and cruise participants**
Report and preliminary results of POSEIDON Cruise 310, 49 pages, Bremen 2005.

No. 233 **Meinecke, G. and cruise participants**
Report and preliminary results of METEOR Cruise 58/3, Bremen 2005.

No. 234 **Feseker, T.**
Numerical Studies on Groundwater Flow in Coastal Aquifers. 219 pages. Bremen 2004.

No. 235 **Sahling, H. and cruise participants**
Report and preliminary results of R/V POSEIDON Cruise P317/4, Istanbul-Istanbul , 16 October - 4 November 2004. 92 pages, Bremen 2004.

No. 236 **Meinecke, G. und Fahrtteilnehmer**
Report and preliminary results of POSEIDON Cruise 305, Las Palmas (Spain) - Lisbon (Portugal), October 28th – November 6th, 2003. 43 pages, Bremen 2005.

No. 237 **Ruhland, G. and cruise participants**
Report and preliminary results of POSEIDON Cruise 319, Las Palmas (Spain) - Las Palmas (Spain), December 6th – December 17th, 2004. 50 pages, Bremen 2005.

No. 238 **Chang, T.S.**
Dynamics of fine-grained sediments and stratigraphic evolution of a back-barrier tidal basin of the German Wadden Sea (southern North Sea). 102 pages, Bremen 2005.

No. 239 **Lager, T.**
Predicting the source strength of recycling materials within the scope of a seepage water prognosis by means of standardized laboratory methods. 141 pages, Bremen 2005.

No. 240 **Meinecke, G.**
DOLAN - Operationelle Datenübertragung im Ozean und Laterales Akustisches Netzwerk in der Tiefsee. Abschlußbericht. 42 pages, Bremen 2005.

No. 241 **Guasti, E.**
Early Paleogene environmental turnover in the southern Tethys as recorded by foraminiferal and organic-walled dinoflagellate cysts assemblages. 203 pages, Bremen 2005.

No. 242 **Riedinger, N.**
Preservation and diagenetic overprint of geochemical and geophysical signals in ocean margin sediments related to depositional dynamics. 91 pages, Bremen 2005.

No. 243 **Ruhland, G. and cruise participants**
Report and preliminary results of POSEIDON cruise 320, Las Palmas (Spain) - Las Palmas (Spain), March 08th - March 18th, 2005. 57 pages, Bremen 2005.

No. 244 **Inthorn, M.**
Lateral particle transport in nepheloid layers – a key factor for organic matter distribution and quality in the Benguela high-productivity area. 127 pages, Bremen, 2006.

No. 245 **Aspetsberger, F.**
Benthic carbon turnover in continental slope and deep sea sediments: importance of organic matter quality at

different time scales. 136 pages, Bremen, 2006.

No. 246 **Hebbeln, D. and cruise participants**
Report and preliminary results of RV SONNE Cruise SO-184, PABESIA, Durban (South Africa) – Cilacap (Indonesia) – Darwin (Australia), July 08th - September 13th, 2005. 142 pages, Bremen 2006.

No. 247 **Ratmeyer, V. and cruise participants**
Report and preliminary results of RV METEOR Cruise M61/3. Development of Carbonate Mounds on the Celtic Continental Margin, Northeast Atlantic. Cork (Ireland) – Ponta Delgada (Portugal), 04.06. – 21.06.2004. 64 pages, Bremen 2006.

No. 248 **Wien, K.**
Element Stratigraphy and Age Models for Pelagites and Gravity Mass Flow Deposits based on Shipboard XRF Analysis. 100 pages, Bremen 2006.